Aus der Klinik und Poliklinik für Nuklearmedizin
Klinik der Ludwig-Maximilians-Universität München
Vorstand: Prof. Dr. Peter Bartenstein

Etablierung einer standardisierten Analyse longitudinaler Aβ PET Scans zur effektiven Evaluation der BACE-Inhibition im transgenen Alzheimer-Mausmodell

Dissertation

zum Erwerb des Doktorgrades der Medizin
an der Medizinischen Fakultät der Ludwig-Maximilians-Universität zu München

vorgelegt von
Felix Overhoff,
geb. in Köln
Jahr 2021

Mit Genehmigung der Medizinischen Fakultät der Universität München

Berichterstatter:	Prof. Dr. Axel Rominger
Mitberichterstatter:	Prof. Dr. Jochen Herms
	Prof. Dr. Nikolaus Plesnila
Dekan:	Prof. Dr. med. dent. Reinhard Hickel
Tag der mündlichen Prüfung:	29.04.2021

Die vorliegende kumulative Dissertation umfasst zwei bereits publizierte Manuskripte:

Overhoff F, Brendel M, Jaworska A, Korzhova V, Delker A, Probst F, Focke C, Gildehaus FJ, Carlsen J, Baumann K, Haass C, Bartenstein P, Herms J, Rominger A (2016)
Automated spatial brain normalization and hindbrain white matter reference tissue give improved [(18)F]-florbetaben PET quantitation in Alzheimer's model mice
Front Neurosci. 2016 Feb 29;10:45. doi: 10.3389/fnins.2016.00045. eCollection 2016.

Brendel M, Jaworska A, Overhoff F, Blume T, Probst F, Gildehaus FJ, Bartenstein P, Haass C, Bohrmann B, Herms J, Willem M, Rominger A (2018)
Efficacy of chronic BACE1 inhibition in PS2APP mice depends on the regional Aβ deposition rate and plaque burden at treatment initiation.
Theranostics. 2018 Sep 9;8(18):4957-4968. doi: 10.7150/thno.27868. eCollection 2018.

Kumulative Dissertation gemäß § 4a der Promotionsordnung

Inhalt:

1. Einführung
    1. Die Amyloid-Hypothese der Genese des Morbus Alzheimers
    2. Therapeutische Ansätze mit Fokus auf das BACE1
    3. Die Positronen-Emissions-Tomographie im PS2APP Kleintiermodell des Morbus Alzheimer
2. Inhalte der Promotionsthematik
    1. Etablierung einer untersucherunabhängigen [18F]-Florbetaben PET Quantifizierung im Mausmodell
    2. Die Effektivität der chronischen BACE1 Hemmung beruht auf dem Ausmaß und der Region der Aβ Ablagerungen bei Therapiebeginn
3. Zusammenfassung
4. Summary
5. Literaturverzeichnis
6. Publikationen
7. Danksagung
8. Lebenslauf
9. Eidesstattliche Versicherung

Abkürzungsverzeichnis:

Aβ - Amyloid β

APP - Amyloid precursor protein

sAPPα - Soluble alpha-amyloid precursor protein

sAPPβ - Soluble beta-amyloid precursor protein

AICD - Amyloid intracellular domain

CTF η - C-terminales Fragment eta

CTF 83 - C-terminales Fragment C83

CTF 99 - C-terminales Fragment C99

BACE1 - Beta-site amyloid precursor protein-cleaving enzyme 1/ Beta Sekretase

NFTs - Neurofibrillary tangles

Sez6 - Seizure-related gene 6

FDG - Fluordesoxyglukose

FBB - [18F]-Florbetaben

PET - Positronen-Emissions-Tomographie

MRT - Magnetresonanztomographie

SUV - Standardized uptake value

SUVR - Standardized uptake value ratios

PSEN – Presenilin

PEN 2 – Presenilin enhancer 2

APH – Anterior pharynx defective 1

PS 2 - Humanes Presenilin 2

BL – Baseline

FU - Follow up

TER - Terminal

CBL - Zerebellum

REF - Referenzregionen

WM - Weiße Substanz

BST - Hirnstamm

GLM - Gesamtes Gehirn

TG-VEH - Transgene PS2APP Placebo Mäuse

TG-BSI - Transgene PS2APP BACE1 Inhibitor Mäuse

WT-VEH - Wildtyp C57BL/6 Placebo Mäuse

WT-BSI - Wildtyp C57BL/6 BACE1 Inhibitor Mäuse

R - Pearsons Koeffizient der Korrelation

κ – Fleiss Kappa

VOI - Volume of interest

DEA - Diethanolamine

ECL - Enhanced chemiluminescence

HRP - Horseradish peroxidase

MANOVA- Multivariate analysis of variance

MANCOVA - Multivariate analysis of covariance

NMDA - N-Methyl-D-Aspartat

PBS - Phosphate buffered saline

PVDF - Polyvinylidendifluorid

SD - Standard deviation

SDS-PAGE - Sodium dodecyl sulfate polyacrylamide gel electrophoresis

1. Einführung

Mit der zunehmenden Alterung der westlichen Bevölkerung im Rahmen des demographischen Wandels gewinnen primär mit dem Alter einhergehende Erkrankungen zunehmend an sozialer und ökonomischer Bedeutung. (Winblad *et al*, 2016) Dementielle Erkrankungen zeigen in diesem Zusammenhang eine besonders ausgeprägte Beeinträchtigung der oben genannten Aspekte. Da der Morbus Alzheimer mit 50-70% die häufigste Demenzerkrankung darstellt und zu 95 % auf eine mit dem Alter einhergehende senile Form beruht, nimmt diese Erkrankung in diesem Zusammenhang eine besondere Stellung ein.

Entsprechend der progredienten gesamtgesellschaftlichen Bedeutung besteht ein erheblicher Bedarf an therapeutischen und präventiven Strategien zur Eindämmung der Konsequenzen dieser Entwicklung. Hierbei scheint es besonders wichtig zu sein, frühe Zeichen der Erkrankung rechtzeitig zu erkennen, um eine zeitnahe Intervention zu ermöglichen. Dies ist von Bedeutung, da sich gezeigt hat, dass der bereits abgelaufene Verlust von Neuronen nicht mehr reversibel ist. Konsequenterweise können therapeutische Strategien primär einen weiteren Progress der Erkrankung verhindern, die bereits eingetretene dementielle Entwicklung allerdings nur geringfügig beeinflussen.

1.1 Genese und Folgen der Amyloid-Pathologie

Im Wesentlichen basieren die meisten Hypothesen zur Genese des Morbus Alzheimers primär auf zwei pathohistologischen Beobachtungen, die in einem nicht gänzlich geklärten Zusammenhang zu einander stehen. (Duyckaerts *et al*, 2009) So zeigen sich bei betroffenen Personen in der Histologie zum einen extrazelluläre Ablagerung des Proteins Amyloid β (Aβ), zum anderen intrazelluläre Ablagerungen des Motorproteins Tau. Diese in der Regel physiologischen Proteine liegen bei Alzheimer Patienten in einer abnormen, fibrillären Form vor.

Hardy und Higgins beschrieben 1992 erstmals die entscheidende Rolle der Ablagerungen des Proteins Aβ in der Genese des Morbus Alzheimer. (Hardy & Higgins, 1992) So führt eine Veränderung des Gleichgewichtes zwischen Produktion und Abbau des Aβ zur Einleitung der neurodegenerativen Prozesse. (Querfurth & LaFerla, 2010; Selkoe & Hardy, 2016) Aβ entsteht durch proteolytische Spaltung des transmembranösen Amyloid Precursor Proteins (APP). Die APP

Prozessierungskaskaden können abhängig vom Endprodukt prinzipiell in zwei Gruppen unterteilt werden, eine Aβ-produzierende und eine ohne Aβ-Produktion.
An diesen Kaskaden sind vier bisher bekannte Proteasen beteiligt.
1) Die α Sekretase: Mit Adam 9, 10, 17 aus der Gruppe der Disintegrin und Metalloproteasen wurden bisher drei Enzyme mit α Sekretase Aktivität identifiziert. Allerdings scheint lediglich Adam 10 eine relevante Rolle in der APP-Prozessierung zu spielen. (Kuhn *et al*, 2010)
2) Die β Sekretase: Unterteilt in die transmembranöse Aspartatprotease beta-site amyloid precursor protein-cleaving enzyme 1 (BACE1) und beta-site amyloid precursor protein-cleaving enzyme 2 (BACE2). (Hussain *et al*, 1999; Sinha *et al*, 1999)
3) Die γ Sekretase: Ein Multiproteinkomplex bestehend aus der katalysierenden Domäne Presenilin, sowie den weiteren Untereinheiten Nicastrin, Presenilin enhancer 2 (PEN-2) und dem anterior pharynx defective 1 (APH-1). Insgesamt konnten bisher vier Varianten dieser Komplexe mit den zwei unterschiedlichen PSEN und den zwei APH1 Untereinheiten beschrieben werden. (De Strooper, 2003; Edbauer *et al*, 2003)
4) Die η Sekretase: Eine membrangebundene Matrixmetalloprotease. (Willem *et al*, 2015)
In der Gruppe der nicht Aβ-produzierenden Kaskaden können abhängig von den beteiligten Enzymen zwei Prozessierungswege mit unterschiedlichen Produkten unterschieden werden. Zum einen spaltet das Enzym α Sekretase das APP an der Aminosäure 83 vom C-Terminus in die lösliche Ektodomäne soluble alpha-amyloid precursor protein (sAPPα) und das in der Membran verbleibende C-terminale Fragment 83 (CTF83). Da diese Spaltung in der Aβ-Region stattfindet, kann es nicht zu einer Aβ-Formation kommen. (LaFerla *et al*, 2007) Das sAPPα zeigt neben einer neuroprotektiven Funktion eine positive Wirkung auf Lern- und Erinnerungsvermögen, sowie der strukturellen Integrität der Neuronen. (Endres & Deller, 2017) Darüber hinaus hat sAPPα eine BACE-hemmende Wirkung. (Peters-Libeu *et al*, 2015) Das verbliebene CTF83 wird zusätzlich an seiner transmembranösen Domäne durch das Enzym γ Sekretase in ein extrazelluläres Fragment p3 und eine Amyloid intracellular domain (AICD) gespalten.
Ein weiterer nicht Aβ-produzierender Weg ist die primäre APP-Spaltung durch die η Sekretase. Hierbei entsteht das C-terminale Fragment eta (CTFη), das im Anschluss durch die α oder β Sekretase in die löslichen Spaltprodukte Aη-α, bzw. Aη-β prozessiert wird. Besonders Aη-α führt in höheren Konzentrationen zu einer

Hypoaktivität und Beeinträchtigung der Langzeitpotenzierung im Hippocampus. (Willem *et al.*, 2015)

Beim Aβ-produzierenden Weg kommt es zu einer kompetitiven, primären Spaltung des extrazellulären Teils des APP durch das Enzym BACE. Diese spaltet das APP an der Aminosäure 99 vom C-Terminus in das lösliche N-terminale sAPPβ und ein C-terminale Fragment 99 (CTF 99). Das sAPPβ wird durch einen aktuell noch nicht beschriebenen Prozess weiter gespalten und gibt ein Fragment frei, das sogenannte N-APP. Dieses kann wiederum an den Death receptor 6 der Neuronen binden und darüber proapoptotische Prozesse auslösen. (Nikolaev *et al*, 2009) Die erste Aminosäure des CTF99 stellt die erste Aminosäure des Aβ dar und wird zwischen der 38 und 43 Aminosäure an seiner transmembranösen Domäne durch die γ Sekretase gespalten. Durch diesen Prozess entstehen zu 90 % an der 40. Aminosäure gespaltene Proteine (Aβ 1-40) und zu 10% an der 42. Aminosäure gespaltene Proteine (Aβ 1-42). Alternativ kann das C99 Fragment von einer α Sekretase weiter zu CTF83 gespalten werden und somit die Produktion von Aβ unterbrochen werden. (Kuhn *et al.*, 2010)

Aβ neigt zur Formation von Aggregaten verschiedener Länge. Dabei kommt es neben der monomären Form zur Entstehung von löslichen Oligomeren. Im weiteren Verlauf können sich diese unterschiedlichen Formen ansammeln und als unlösliche fibrilläre Plaques extrazellulär um die Neurone ablagern. Nach aktuellen Erkenntnissen sind die Oligomere, besonders solche mit einem niedrigen molekularen Gewicht, die ausschlaggebende pathologische Form bei der Alzheimererkrankung. (Ferreira & Klein, 2011; Yang *et al*, 2017a) Entsprechend sind mit hoher Wahrscheinlichkeit nicht die Plaques an sich, sondern das Verhältnis von Plaques zu Oligomeren entscheidend. (Selkoe & Hardy, 2016) In diesem Zusammenhang ist vor allem das Aβ 1-42 von Bedeutung, da es neben der deutlich ausgeprägten Tendenz zur Aggregation, hydrophober und entsprechend schlechter löslich ist. (Selkoe, 2001) Darüber hinaus konnte eine stärkere neurotoxische Wirkung nachgewiesen werden. (Dahlgren *et al*, 2002; Jan *et al*, 2008)

Das Aβ führt initial über eine Veränderung des Gleichgewichtes der Neurotransmitter Glutamat/GABA zu Gunsten des exzitatorischen Glutamats zu einer Hyperaktivität der Neuronen. Da sich die Amyloid-Plaques bevorzugt in Regionen erhöhter Aktivität bilden, kommt es in Arealen mit ohnehin schon hoher Amyloid-Konzentration zur weiteren Bildung und Ansammlung von Aβ. Im weiteren Verlauf stellt sich dann ein

Übergewicht des inhibitorischen GABAs mit entsprechender Hypoaktivität ein. Abschließend führen diese Prozesse zum Zelluntergang. (Busche *et al*, 2016)
Ein weiterer potentieller Effekt des Aβ ist das Auslösen von posttranslationalen Veränderungen des Proteins Tau, wobei die genaue Beziehung noch nicht ausreichend geklärt ist. Man geht davon aus, dass sich die Veränderungen primär in Form von Hyperphosphorylierung und Acetylierung und die darauffolgende Aggregation in sogenannte neurofibrillary tangles (NFT) äußert. Diese Aggregate lagern sich dann intrazellulär in den Dendriten, entgegen der physiologischen axonalen Lokalisation des Proteins Tau, ab. (Forner *et al*, 2017)

1.2 Therapeutische Ansätze mit Fokus auf das BACE1

Die aktuellen Leitlinien der deutschen Neurologischen Gesellschaft empfehlen lediglich eine symptomatische Pharmakotherapie mit den Acetylcholinesterase-Hemmern Donepezil, Galantamin, Rivastigmin bei leichter bis mittelschwerer Demenz und dem nicht kompetitiven NMDA- Antagonisten Memantin bei moderater bis schwerer Demenz. (Deuschl G, 2016) Weitere nicht direkt Amyloid bezogene experimentelle therapeutische Ansätze sind die Behandlung der initialen Hyperaktivität der Neurone mit dem Antikonvulsivum Levetiracetam oder GABA-Agonisten und die Immunisierung gegen Tau. (Bakker *et al*, 2015; Busche *et al.*, 2016; Dai *et al*, 2017)
Im Rahmen der kausalen Therapie besteht theoretisch die Möglichkeit an den zwei Stellschrauben des Amyloidstoffwechsels zu intervenieren. Zum einen kann die Amyloidproduktion vermindert und zum anderen der -abbau gesteigert werden.
Eine Methode, den Abbau des Amyloids zu steigern ist die aktive oder passive Immunisierung, wobei die aktive Immunisierung mittels monoklonaler Antikörper die primär verfolgte Variante ist. Während die erste Generation der monoklonalen Antikörper bei Patienten mit milder, beziehungsweise moderater Demenz weitestgehend gescheitert ist, stehen aktuell belastbare Ergebnisse einer neuen Generation Antikörper noch aus. (Abushouk *et al*, 2017; Doody *et al*, 2014; Sevigny *et al*, 2016) Im Angesicht des Scheiterns zahlreicher Interventionen in den Amyloid-Stoffwechsel bei Patienten mit milder bis moderate Demenz, verlagert sich der Fokus zunehmend auf eine präventive pharmakologische Therapie. (Abbott & Dolgin, 2016; The Lancet, 2017)
Zur Verminderung der Genese des Amyloids wird in die Prozessierung des Proteins APP eingegriffen. Mögliche Angriffspunkte sind hierbei die α, β und γ Sekretase. Die

Aktivierung der α Sekretase könnte die kompetitive APP-Prozessierung zunehmend zu Gunsten des nicht Amyloid produzierenden Weges verlagern. Darüber hinaus könnte die vermehrte Produktion des neuroprotektiven Spaltproduktes sAPPα sich positiv auf die kognitiven Defizite auswirken. (Lichtenthaler, 2011)

Initiale Versuche, die γ Sekretase komplett zu hemmen, sind auf Grund mangelnder Wirkung bei einem ausgeprägten Nebenwirkungsprofil gescheitert. Letzteres beruht hierbei primär auf der Hemmung des Notch Signalwegs. (Coric *et al*, 2015; Doody *et al*, 2013) Folglich gerät die Modulation der γ Sekretase zunehmend in den Fokus. Dadurch soll die Produktion kürzerer Aβ Fragmente stimuliert und eine Affektion des Notch Signalwegs vermieden werden. (Selkoe & Hardy, 2016) Einige Vertreter dieser Gruppe sind zurzeit in der Erprobung. (Blain *et al*, 2016; Brendel *et al*, 2015d; Hawkins *et al*, 2011; Imbimbo *et al*, 2007; Imbimbo *et al*, 2009; Kounnas *et al*, 2010; Loureiro *et al*, 2013; Mitani *et al*, 2014; Murakami *et al*, 2016; Rogers *et al*, 2012; Scannevin *et al*, 2016; Soares *et al*, 2016; Van Broeck *et al*, 2011; Wagner *et al*, 2017)

BACE1 stellt eine weitere Zielstruktur in der Aβ Genese dar. Durch die Blockade kommt es zu einer Verschiebung der APP-Prozessierung zu Gunsten der nicht Aβ-produzierenden Wege. Dabei zeigt allerdings besonders die Zunahme des Spaltproduktes der η Sekretase Aη-α einen negativen Effekt auf die kognitive Leistung. (Willem *et al.*, 2015) Ein weiteres Problem der BACE1 Hemmung ist die Wirkung auf andere physiologische Substrate des Enzyms. Identifizierte Substrate sind Neuregulin 1, die Sez6 Familie und die Familie der L1 adhesions Moleküle. Eine Hemmung der Prozessierung dieser Substrate durch Hemmung von BACE1 führt entsprechend zu einer Einschränkung ihrer physiologischen Wirkung auf die Regulation der Myelinisierung, der Migration und Ausbildung von Neuronen, sowie der synaptischen Plastizität. (Munro *et al*, 2016) Eine weitere potenzielle Ursache relevanter Nebenwirkungen ist die simultane Hemmung des Homologs BACE2. Da das Enzym an der Regulation der B-Zellen im Pankreas und an der Formation von Melanosomen beteiligt ist, kann es zu Auswirkungen auf das Glukose-Gleichgewicht, beziehungsweise auf die Pigmentierung kommen. (Barao *et al*, 2016; Yang *et al*, 2017b) Zurzeit befinden sich mehrere BACE-Inhibitoren in unterschiedlichen Entwicklungsstadien. Neben neuen präklinisch effektiven Inhibitoren haben einige Substanzen schon den Einzug in klinische Studien geschafft. (Deleye *et al*, 2017; Neumann *et al*, 2015) Die am weitesten vorangeschrittene Substanz Verubecestat wurde in Phase 3 allerdings auf Grund einer eingeschränkten Effektivität bei Patienten

mit milder und moderater Form eingestellt. Eine Versuchsreihe im Prodromalstadium scheiterte ebenfalls. (Egan *et al*, 2018; Egan *et al*, 2019; Hawkes, 2017) Weitere Substanzen befinden sich aktuell in den Phasen 1-3.

Zur Steigerung der Effektivität und Verminderung der Toxizität der einzelnen Ansatzpunkte könnte besonders eine Kombination eines produktionshemmenden und eines abbausteigernden Wirkstoffes sinnvoll sein. Die überlegene Wirkung einer solchen Therapie konnte im präklinischen Modell schon nachgewiesen werden. (Jacobsen *et al*, 2014)

1.3 Die Positronen-Emissions-Tomographie im PS2APP Kleintiermodell des Morbus Alzheimer

Mit der zunehmenden Bedeutung präventiver Interventionen rücken Strategien zur Früherkennung, beziehungsweise Identifizierung gefährdeter Personen in den Fokus. Hierzu bieten sich, neben dem Nachweis der gängigen Biomarker Aβ 1-42 und Tau im Liquor, bildgebende Verfahren an. Dabei kommen funktionelle und morphologische Modalitäten, sowie eine Kombination beider zur Anwendung.

Während bei der MRT der Substanzverlust im Vordergrund steht, können mit der Positronen-Emissions-Tomographie **(**PET) und entsprechenden Tracern verschiedene Stoffwechselprozesse bzw. Ablagerungen dargestellt werden. Mögliche Ziele für die Tracer sind Amyloid, Tau, der Glucose-Stoffwechsel und die mikrogliale Aktivität. Neben dem bereits etablierten FDG PET zur Detektion von Stoffwechselveränderungen haben zuletzt auch die Tracer Florbetaben (FBB), Flutemetamol und Florbetapir zur Darstellung des zerebralen Amyloids Einzug in die nationalen Leitlinien erhalten. (Deuschl G, 2016) In den entsprechenden Zulassungsstudien konnte eine hohe Sensitivität und Spezifität in Korrelation zum histopathologischen Goldstandard nachgewiesen werden. (Clark *et al*, 2011; Sabri *et al*, 2015; Wolk *et al*, 2011) Eine entscheidende Frage zur adäquaten Analyse der akquirierten Daten ist die Intensitätsskalierung mit Normalisierung zur injizierten Gesamtdosis oder zur Aufnahme eines Tracers in einer Referenzregion. Diesbezüglich wurde bei einem Großteil der Studien eine Skalierung mit Normalisierung zum Zerebellum genutzt. (Barthel *et al*, 2011; Clark *et al.*, 2011; Vandenberghe *et al*, 2010) Aktuellere Studien konnten zuletzt allerdings eine longitudinale Stabilisierung der Standardized uptake value ratios (SUVR) durch eine Normalisierung zur weißen

Substanz des Hirnstamms nachweisen. (Brendel *et al*, 2015a; Chen *et al*, 2015; Landau *et al*, 2015)

Präklinische Studien zur Amyloid-Akkumulation im Kleintiermodell nehmen eine signifikante Stellung in Bezug auf das Verständnis des Morbus Alzheimers und der Evaluation potenzieller Therapien ein. (Johnson *et al*, 2013) Studien an transgenen Mäusen konnten das effektive longitudinale Monitoring der Amyloid-Akkumulation im zeitlichen Verlauf bereits adäquat in Korrelation zum histopathologischen Goldstandard darstellen. (Rominger *et al*, 2013) In diesen Studien kamen verschiedene transgene Mausmodelle zum Einsatz. Zur Evaluation dieser verschiedenen Modelle konnte, unter Einsatz des Amyloid Tracers FBB, die Überlegenheit der PS2APP Mutation im direkten Vergleich mit den Mutationen APP (swex), PS1G384A, APP/PS1dE9 und APP (swe) in Bezug auf die konstante longitudinale Anreicherung von Aβ dargestellt werden. (Brendel *et al*, 2015b) Die transgene B6.PS2APP ist ein Homozygot für die humane Presenilin (PS) 2, N141I Mutation und die humane APP Mutation K670N, M671L. Das Modell wird durch Koinjektion der beiden Transgene in eine C57Bl/6 Zygote geschaffen. (Richards *et al*, 2003) In diesem Modell lassen sich erste Amyloid-Ablagerungen in Cortex und Hippocampus bereits im Alter von 5-6 Monaten beobachten. (Ozmen *et al*, 2009)

2. Inhalte der Promotionsarbeit

Das Ziel dieser Promotionsarbeit war es zunächst eine optimale und standardisierte Analyse der Positron-Emissions-Tomographie in einem transgenen Kleintiermodell der Amyloid-Anreicherung zu etablieren. Auf Basis dieser Ergebnisse erfolgte im Anschluss eine multimodale Interventionsstudie mit dem BACE-Inhibitor RO5508887.

2.1 Etablierung einer untersucherunabhängigen [18F]-Florbetaben PET Quantifizierung im Mausmodell

Vorklinische Studien sind häufig inadäquat verblindet und verfolgen unterschiedliche Analysemethoden, so dass die Vergleichbarkeit unterschiedlicher Studien erschwert ist. (Jucker, 2010) Folglich beschäftigte sich der erste Teil dieser Promotionsarbeit mit der Optimierung und Standardisierung der präklinischen Aβ Bildgebung in der PET. Es erfolgte zum einen die Evaluation eines automatisierten Algorithmus zur räumlichen Normalisierung des Gehirns, zum anderen die Evaluation der Intensitätsskalierung mit Normalisierung zu unterschiedlichen Referenzregionen.

Dazu wurden insgesamt 114 Aβ PET Scans des oben beschriebenen Mausmodells PS2APP mit dem Tracer FBB angefertigt. Darunter waren 37 Mäuse mit einem Baseline Scan (BL) im Alter von 8 Monaten und einem kurzfristigen Folgescan (FU) im Alter von 9,5 Monate, sowie 40 Scans im Alter von 13-16 Monaten (TER).
Die Herstellung des Tracers, die Bildakquisition und die Rekonstruktion erfolgten nach einem standardisierten Protokoll. (Brendel *et al*, 2015c; Rominger *et al.*, 2013; Zhang *et al*, 2005)
Nach initialer Verblindung durch Codierung der Dateien erfolgte zur weiteren Analyse die starre, manuelle Fusion der akquirierten microPET Dateien auf eine zerebrale MRT Vorlage mittels dem PMOD FUSION tool (v.3.4 PMOD Technologies, Zürich). Dieser Prozess wurde durch einen Experten (mehr als 1000 Fusionen), einen fortgeschrittenen Analysten (mehr als 150 Fusionen) und einen unerfahrenen Analysten (Training von vier Stunden über zwei Tage) durchgeführt. Der erfahrene Analyst wiederholte die Fusion zur Abschätzung der Test-Retest Variabilität (%). Zur Berechnung des Standardized uptake value (SUV) wurden alle räumlich normalisierten Bilder des erfahrenen Analysten zur injizierten Dosis intensitätsskaliert und mit dem Gewicht der individuellen Maus multipliziert. Dann wurden die Bilder altersabhängig zur Generation von drei Schablonen gemittelt. Die Fusionen der drei Analysten wurden durch Verwendung einer automatisierten, nicht-linearen Transformation auf alle Schablonen räumlich normalisiert. Diese Normalisierung entfernte, durch Verwendung des Algorithmus in SPM5 als Teil des PMOD FUSION tools, relevante Unterschiede in Größe und Form des Gehirns. Die Einstellungen wurden entsprechend auf die Größe des Gehirns einer Maus angepasst. Diese wurde sowohl mit, als auch ohne Glättung vor dem Prozess durchgeführt. Die errechnete Matrix wurde gespeichert und auf die „rohe“ Bilddatei angewandt, um einen Auflösungsverlust durch wiederholte Prozessierung zu vermeiden.
Zum Vergleich der verschiedenen Erfahrungsstufen wurden das Fleiss Kappa der Ergebnisse der TER-Scans (SUV(CTX) und SUVR(CTX/REF)) zwischen Experten vs. erfahrenen Analysten, erfahrenen vs. unerfahrenen Analysten und Experten vs. unerfahrenen Analysten jeweils vor und nach automatisierter Normalisierung verglichen. Dann erfolgte die Berechnung der Variabilität zwischen den Analysten, die im Anschluss mit der Test-Retest Variabilität des Experten verglichen wurde.
Zur Bewertung des Einflusses der altersspezifischen Schablonen auf die automatisierte Normalisierung wurden die Ergebnisse der finalen Fusion (TER) des

Experten vor Normalisierung mit der finalen Fusion nach Normalisierung auf die TER, FU und BL Schablone verglichen und der Fehler in % berechnet. Hierbei zogen wir die Fusion des Experten als Goldstandard heran.

Zur Evaluation der Intensitätsskalierungen definierten wir, neben der einfachen Berechnung des frontalen kortikalen SUV(CTX), vier Referenzregionen (REF) anhand der MRT und [18F]-FBB Vorlagen.

1. Zerebellum (CBL)
2. Weiße Substanz (WM) inklusive Pons, Pedunculi cerebelli, dem kranialen Hypothalamus und dem kaudalen Thalamus
3. Hirnstamm (BST), ovale Region von Pons bis zum Mittelhirn
4. Das gesamte Gehirn (GLM)

Als Zielregion wurden zwei bilaterale frontale kortikale VOIs definiert und das Verhältnis zur Referenzregion $SUVR_{CTX/REF}$ berechnet. Die longitudinale Stabilität wurde durch Vergleich der SUV_{CTX}, beziehungsweise $SUVR_{CTX/REF}$ zwischen dem initialen Scan und dem im kurzfristigen Intervall von sechs Wochen erfolgten Scan (FU) getestet. Der Pearsons Koeffizient der Korrelation (R) wurde für SUV_{CTX} und $SUVR_{CTX/REF}$ Werte der vier Referenzregionen berechnet. Dies erfolgte unter der Annahme der zuvor beschriebenen linearen Progression der Amyloidablagerungen im PS2APP Mausmodel. (Brendel *et al.*, 2015c) Außerdem berechneten wir, zur Definition der Stabilität, die Varianz in der jeweiligen Gruppe.

Als Goldstandard erfolgte zusätzlich die histologische Bestimmung der kortikalen Amyloid-Last der Tiere nach einem standardisierten Protokoll. (Brendel *et al.*, 2015b) Im Anschluss daran korrelierten wir die histologische Amyloid-Last mit allen Intensitätsskalierungen vor und nach Normalisierung.

Die Applikation des automatischen räumlichen Normalisierungsalgorithmus konnte eine nahezu perfekte Übereinstimmung der Analyse unterschiedlicher Analysten erreichen. (Abbildung 1)

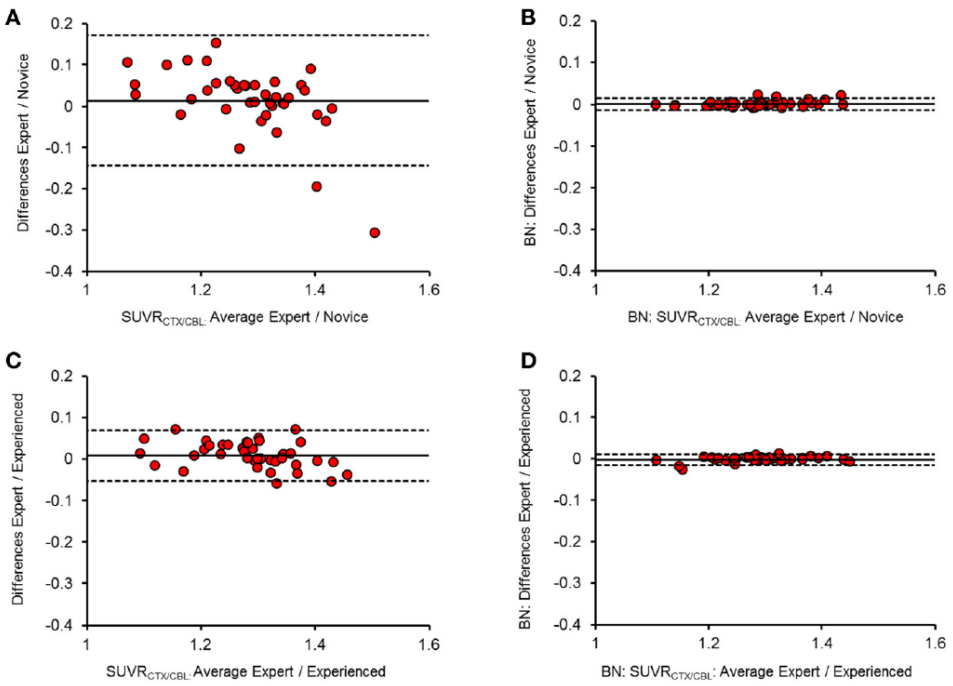

Abbildung 1 (entsprechend Figure 2 im Originalmanuskript): Bland-Altman Diagramm der Übereinstimmung SUVRCTX/CBL vor (A,C) und nach (B,D) automatischer räumlicher Normalisierung. Differenzen (Y-Achse) und Mittelwerte (X-Achse) zwischen den Analysten. Dicke Linie: Mittelwerte der Differenz. Gestrichelte Linie: Mittelwert der Differenz plus 1,96 · Standardabweichung. Vergleich Experte/ unerfahrener Analyst (A, B). Vergleich Experte/ erfahrener Analyst (C,D).

Hierbei blieb die Korrelation mit dem histologischen Goldstandard gleich oder verbesserte sich. Eine nicht mit dem zeitlichen Verlauf der Pathologie übereinstimmende Schablone resultierte in einem systematischen Bias von bis zu 2,9% der SUVR.

Alle Methoden mit Skalierung zu einer Referenzregion (SUVR) schnitten in Bezug auf die longitudinale Stabilität (d >1,21 vs. d=0,23) und die Übereinstimmung mit dem histologischen Goldstandard (R>0.66 vs. R>0.31) besser als die reine Bestimmung der SUV des Kortex ab. Eine Analyse der Skalierung zum GBM auf Voxelebene erbrachte einen physiologisch nicht erklärbaren Abfall der SUVR im Bereich des Rautenhirns. Die entscheidenden Qualitäten einer optimalen Referenzregion definierten wir wie folgt:

1. Vorhandensein einer hohen Korrelation zur Histologie, was durch alle Referenzregionen erfüllt wurde. Allerdings zeigte sich ein Trend zu einer Überlegenheit der WM und des GBM.
2. Abwesenheit einer artifiziellen Anhebung der Varianz in der Gruppe, was durch die Skalierung zum CTX nicht erfüllt wurde.

3. Die Effektgröße der longitudinalen kortikalen Amyloid-Progression in der Ziel-VOI sollte optimal erfasst werden. Dieses Kriterium wurde am besten durch BST und WM erfüllt.
4. Geringer Effekt der Pathologie auf die Referenzregion, was nicht durch die Skalierung zum GBM erfüllt wurde.
5. Minimalen Einfluss einzelner Tiere auf die Schablone. In diesem Bezug waren die Skalierungen zu GBM und CBL unterlegen.

In Zusammenschau aller Qualitäten waren die SUVRs mit Skalierung zur WM den anderen Referenzregionen somit überlegen. Abbildung 1, beziehungsweise Tabelle 4 im originalen Manuskript, listet die einzelnen Vor- und Nachteile der einzelnen Referenzregionen auf.

	Template affection	Variance	Longitudinal effect size	Pathology affection	Histology
SUV_{CTX}	o	–	–	o	–
$SUVR_{CTX/CBL}$	–	+	+	o	+
$SUVR_{CTX/WM}$	o	+	++	o	+(+)
$SUVR_{CTX/BST}$	o	+	++	o	+
$SUVR_{CTX/GLM}$	–	+	+	–	+(+)

Abbildung 2 (entsprechend Table 4 im Originalmanuskript): Signifikante Vorteile (mäßig: +, hellgrün; groß: ++, dunkelgrün) / Nachteile (hell rot) des SUVCTX und der SUVR. O= neutral, (+) = Trend zum Vorteil. Template affection: Auswirkung der Schablonen unterschiedlichen Alters. Pathology affection: Physiologisch nicht erklärbare Veränderungen des Signals. Histology: Übereinstimmung mit der Histologie.

Zusammenfasend konnten demnach folgende Schlüsse gezogen werden:

1. Die automatische räumliche Normalisierung im Mausmodel der zerebralen Amyloid-Akkumulation kann effektiv auf Analysen durch Aß PET mit dem Tracer Florbetaben angewandt werden. Dies gewährleistet eine Pseudoverblindung der Endpunkte durch Elimination der Varianz verschiedener Analysten und trägt somit maßgeblich zur Reproduzierbarkeit der Daten bei.
2. Eine intrazerebrale Referenzregion ohne Expression der Pathologie ist essentiell zur akkuraten Quantifizierung der Amyloid-Last in-vivo durch Aβ PET und dem Tracer FBB. Im Bezug auf die oben genannten Kriterien ist der Gebrauch einer

Referenzregion aus der oben definierten WM den anderen getesteten Regionen überlegen.

Diese Ergebnisse wurden im Rahmen meiner Erstautorenschaft „Automated Spatial Brain Normalization and Hindbrain White Matter Reference Tissue Give Improved [18F]-Florbetaben PET Quantitation in Alzheimer's Model Mice“ im Februar 2016 in der Fachzeitschrift Frontiers in Neuroscience publiziert. Mein Anteil an dieser Publikation bestand in der Durchführung der PET Scans, der Auswertung der Bilddateien, der Analyse der Daten und dem Verfassen des Manuskriptes. Außerdem erfolgte die Betreuung der Versuchstiere durch mich.

2.2 Die Effektivität der chronischen BACE1 Hemmung beruht auf dem Ausmaß und der Region der Aβ Ablagerungen bei Therapiebeginn

Basierend auf den Ergebnissen zur optimalen Analyse longitudinaler Aβ PET Scans unserer Arbeitsgruppe erfolgte eine Publikation zur präklinischen in-vivo Evaluation der zerebralen Amyloid-Last unter Therapie mit dem BACE Inhibitor RO5508887 im Mausmodell PS2APP.

Hierzu wurden 26 weibliche PS2APP (swe) (TG) und 22 weibliche C57BL/6 (WT) Mäuse im Alter von 9,5 Monaten in einen Placeboarm (TG-VEH) und einen Interventionsarm (TG-BSI) randomisiert. Nach initialer Anfertigung eines Baseline [18F]-FBB PET Scans erfolgte die zweimal tägliche orale Applikation von RO5508887 oder einer entsprechenden Placebolösung über einen Zeitraum von 4 Monaten. Nach 10 und nach 18,5 Wochen wurde jeweils ein FU Scan angefertigt. Zur Evaluation des generellen longitudinalen Progresses wurde außerdem ein Scan im Alter von 8 Monaten durchgeführt. Im Anschluss an den finalen Scan wurden die Gehirne der Tiere zur histologischen und biochemischen Analyse entnommen. RO5508887 wurde in einer definierten Dosierung von 100mg/KG/Tag, verteilt auf zwei Einzeldosen, oral verabreicht. Diese Dosierung hatte sich zuvor in einer Evaluationsstudie zur chronischen Therapie mit dem transgenen Mausmodell APPV7171 als geeignet herausgestellt. (Jacobsen *et al.*, 2014)

Die Durchführung und Analyse der [18F]-FBB PET Scans erfolgte, ebenso wie die histochemische Analyse, nach einem zuvor publizierten Protokoll. (Brendel *et al.*, 2015c; Overhoff *et al*, 2016; Rominger *et al.*, 2013)

Jeweils eine Hemisphäre des Kraniums wurde im flüssigen Stickstoff bei -80°C schockgefroren. Lösliche Proteine wurden mittels DEA Puffer, Mempranproteine mittels RIPA Puffer extrahiert. Darunter unlösliches Material wurde in 70%iger Ameisensäure gelöst. Amyloid-Quantifizierung erfolgte nach dem Protokoll des Herstellers MSD®. Die Proteine wurden mittels diskontinuierlicher SDS-PAGE unter Zuhilfenahme eines Tris-Glycin-Puffer und dem Mini-PROTEAN-System (BIORAD) auf aktivierten PVDF-Membranen getrennt. Niedermolekulare Proteine (< 20 kDa) wurden mit dem XCell SureLock Mini-Cell-System (Novex) getrennt. Die Proteine wurden mit dem Tank/Wet Mini Trans-Blot Zellsystem (BIORAD) auf die Membranen übertragen. Übertragene Proteine wurden mittels Immunodetektion und enhanced Chemiluminescence (ECL) nachgewiesen. Die Signale wurden durch Bestrahlung mit einem Röntgenfilm erfasst. Zum Nachweis von Produkten der APP-Prozessierung unter den DEA-löslichen Proteinen verwendeten wir die Antikörpern a22C11 zum Nachweis des APP-N-Terminus, 6A1 zum Nachweis von sAPPβ (swe) und 2D8 zum Nachweis von Aη-α.

Die Behandlung und die serielle PET-Bildgebung erwiesen sich als gut verträglich. Bereits 10 Wochen nach Behandlungsbeginn zeigte die PET eine signifikante Reduktion des Amyloid-Progresses (+6,7% bei BSI vs. +10,3% bei VEH, $p < 0.05$). Dieser Effekt war auch im Verlauf nach 18,5 Wochen Behandlung weiter progredient (+8,4% bei BSI vs. +15,2% bei VEH, $p < 0,001$). Wir fanden eine lineare Beziehung ($R > 0,99$; $p < 0,001$) zwischen der regionalen Amyloid-Progressionsrate bei TG-VEH und des Progresses bei TG-BSI-Mäusen. Hieraus leiteten wir einen Schwellenwert für die regionale Depositionsrate von 3,7%/18,5 Wochen bei TG-VEH ab, unterhalb dessen eine vollständige Blockierung der weiteren Signalzunahme durch Intervention mit RO5508887 erreicht werden konnte. Die Korrelation zwischen Behandlungseffekt und dem Ausmaß des naiven Verlaufs bestätigte sich durch eine Kartierung des %-Behandlungseffekts auf Voxelebene. Die absolute Reduktion der Aβ Deposition unter Behandlung war 7,6 ± 1,7% in hoch akkumulierenden Regionen (≥ 10%) und 4,8 ± 2,0% in niedrig akkumulierenden Regionen (<10%). Der relative Behandlungseffekt war 49 ± 11% in hochakkumulierenden Hirnregionen und 69 ± 28% in Regionen mit geringer Akkumulation. Die vorliegenden Ergebnisse bei TG-VEH-Mäusen deuten auf einen umgekehrten Zusammenhang zwischen der BL Aβ Belastung und dem relativen Anstieg von 9,5 auf 13,5 Monate im Alter hin ($R = -0,53$, $p < 0,05$). TG-BSI-Mäuse zeigten den größten behandlungsbedingten Unterschied zur TG-VEH-Gruppe, wenn

ihr ursprünglicher Aβ-Spiegel niedrig war. Der beschleunigte Anstieg der Placebo Gruppe konnte verhindert werden, was zu einer Umkehrung der Korrelation führte (R = +0,27, p = n. s.).

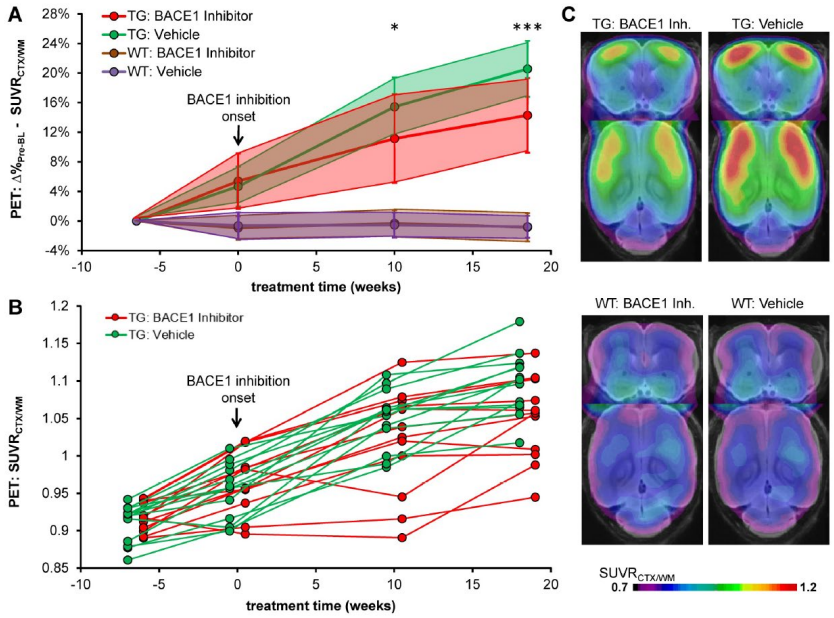

Abbildung 3 (entsprechend Figure 2 im Originalmanuskript): Longitudinale Aβ PET Bildgebung der BACE1-Inhibition. (A) Mittelwert (±SD) des kortikalen Amyloid-Signals im Therapieverlauf für TG-BSI, TG-VEH und WT. (B) Individueller Progress des kortikalen Amyloid-Signals in den TG-Mäusen. (C) Signalintensitäten des frontalen kortikalen Amyloid-Signals in TG und WT Mäuse im terminalen Scan. Koronale und axiale Schnitte zeigen die Gruppenmittelwerte auf einer T1 MRT-Schablone. * p < 0,05; *** p < 0,001

Die Immunhistochemie bestätigte die PET-Befunde durch die direkte Validierung von fibrillärem Aβ und zeigte eine geringere Plaque-Belastung (-9,7%, p < 0,05), sowie Plaque-Dichte (-9,9%, p <0,05) bei BACE1-behandelten TG-Mäusen im Vergleich zur Kontrollgruppe. Ein wesentlicher Effekt wurde bei der Ablagerung von de novo Plaques beobachtet.

Im Rahmen der biochemischen Analysen konnte die Inhibition der Enzymaktivität durch niedrigere sAPPβ (swe) Level bei simultaner Elevation der sAPPα Level und unveränderter Gesamtmenge des sAPP nachgewiesen werden. In Relation zur TG-VEH-Gruppe konnten eine 47% Reduktion von löslichem Aβ40 bzw. eine 61% Reduktion von löslichem Aβ42 nachgewiesen werden. Die unlöslichen Aß40 Level zeigten lediglich eine Tendenz zum Rückgang der Amyloidose (-10, p = 0,45), während die Aß42 Level signifikant gesenkt werden konnten (-40%, p < 0,05).

Zusammenfassend konnten entsprechend vier Aussagen getroffen werden:

1. Die chronische BACE-I-Behandlung hemmt effektiv die fibrilläre Aβ-Deposition
2. Akute und chronische Hemmung des BACE1 senkt die Aβ-Deposition
3. Die Wirksamkeit der chronischen Hemmung des BACE1 hängt von der regionalen Aβ-Depositionsrate ab
4. Die Hemmung von BACE1 ist während des frühen Amyloidaufbaus effektiver

Diese Ergebnisse wurden im Rahmen meiner Co-Autorenschaft „Efficacy of chronic BACE1 inhibition in PS2APP mice depends on the regional Aβ deposition rate and plaque burden at treatment initiation“ im September 2018 in der Fachzeitschrift Theranostics publiziert. Mein Anteil an dieser Publikation bestand in der Durchführung der PET-Scans, der Auswertung der Bilddateien, der Analyse der Daten und dem Erstellen der Grafiken. Außerdem erfolgte die Betreuung und Therapie der Versuchstiere durch mich.

3. Zusammenfassung

Das Ziel des ersten Teils meiner Promotionsarbeit war es eine optimale und standardisierte Analyse der Positron-Emissions-Tomographie in einem transgenen Kleintiermodell der Amyloid-Anreicherung zu etablieren. Hierzu erfolgte die Evaluation einer automatisierten räumlichen Normalisierung und einer Intensitätsskalierung zu verschiedenen Referenzregionen.

Insgesamt wurden 114 Aβ PET Scans des Mausmodells PS2APP mit dem Tracer FBB angefertigt. Darunter waren 37 Mäuse mit einem Baseline Scan (BL) im Alter von 8 Monaten und einem kurzfristigen Folgescan (FU) im Alter von 9,5 Monate, sowie 40 Scans im Alter von 13-16 Monaten (TER). Die so akquirierten microPET Dateien wurden durch eine starre, manuelle Fusion auf eine zerebrale MRT Vorlage durch drei Analysten mit unterschiedlichem Erfahrungsniveau untersucht. Im Anschluss wurden die Bilder durch Verwendung einer automatisierten, nicht-linearen Transformation auf altersabhängige Schablonen räumlich normalisiert und die Übereinstimmung der Analysten mittels Fleiss Kappa ermittelt. Zur Berechnung der zerebralen Amyloid-Last definierten wir, neben dem reinen SUV (CTX), vier Referenzregionen mit den entsprechenden SUVR. Als Referenzregionen bestimmten wir den Hirnstamm (BST), das Zerebellum (CBL), die weiße Substanz (WM) und das gesamte Gehirn (GLM). Die

Ergebnisse wurden anhand der longitudinalen Stabilität und der Übereinstimmung mit dem histologischen Goldstandart verglichen.

Die räumliche Normalisierung resultierte in einer nahezu perfekten Übereinstimmung der Analysen. Die Korrelation zur Histologie blieb konstant oder verbesserte sich (alle $\kappa \geq 0.99$). Alle SUVR waren der reinen SUV (CTX) überlegen ($d \geq 1.21$ vs. $d = 0.23$ und $R \geq 0.66$ vs. $R \geq 0.31$). Eine Analyse der Skalierung zum GBM auf Voxelebene erbrachte einen physiologisch nicht erklärbaren Abfall der SUVR im Bereich des Rautenhirns. Die optimale Referenzregion definierten wir anhand der Korrelation mit der Histologie, der artifizielle Anhebung der Varianz in der Gruppe, der Effektgröße der longitudinalen kortikalen Amyloid-Progression, den Effekt der Pathologie in der Referenzregion und den Einfluss einzelner Tiere. In Zusammenschau der untersuchten Qualitäten war die Intensitätsskalierung zur WM den übrigen SUVR überlegen.

Auf Basis dieser Ergebnisse erfolgte im Anschluss, als zweiter Teil meiner Promotionsarbeit, eine multimodale Interventionsstudie zur Untersuchung der Amyloidose unter Therapie mit dem BACE-Inhibitor RO5508887.

Hierzu wurden 26 weibliche PS2APP (swe) (TG) und 22 weibliche C57BL/6 (WT) Mäuse im Alter von 9,5 Monaten in einen Placeboarm (TG-VEH) und einen Interventionsarm (TG-BSI) randomisiert. Nach initialer Anfertigung eines Baseline [18F]-FBB PET-Scans erfolgte die zweimal tägliche orale Applikation von RO5508887 oder einer entsprechenden Placebolösung über einen Zeitraum von 4 Monaten. Nach 10 und nach 18,5 Wochen wurde jeweils ein FU Scan angefertigt. Im Anschluss an den finalen Scan wurden die Gehirne der Tiere zur histologischen und biochemischen Quantifizierung und Differenzierung entnommen.

Der Amyloid-Progress war 15.3 ± 4.4% in der Placebo Gruppe und 8.4 ± 2.2% in der Therapiegruppe. Durch die Therapie konnte der Anstieg der Amyloidose signifikant reduziert werden ($p<0.001$). Diesen Effekt konnte die histologische Analyse in Bezug auf die Plaque-Belastung (-9,7%, $p < 0,05$) und die Plaque-Dichte (-9,9%, $p <0,05$) bestätigen. Auch die biochemische Analyse zeigte eine Reduktion des löslichen und unlöslichen Aβ40 (-47% und -10%), sowie des löslichen und unlöslichen Aβ42 (-61% und -40%). Die akute BACE-Inhibition konnte durch eine Reduktion des sAPPβ bei Anstieg des sAPPα und unveränderten sAPP nachgewiesen werden. Außerdem stellte sich eine negative Korrelation zwischen dem Ausmaß der Amyloidose bei Therapiebeginn und dem Progress unter Therapie dar. Zusätzlich beobachteten wir

eine weitere inverse Korrelation zwischen der naiven Amyloid-Akkumulation und dem Therapieeffekt. So war die absolute Reduktion der Aβ-Deposition unter Behandlung 7,6 ± 1,7% in hoch akkumulierenden Regionen (≥ 10%) und 4,8 ± 2,0% in niedrig akkumulierenden Regionen (<10%). Der relative Behandlungseffekt war 49 ± 11% in hochakkumulierenden Hirnregionen und 69 ± 28% in Regionen mit geringer naiver Akkumulation. In Regionen mit einem niedrigen, naiven Progress konnte ein Schwellenwert der regionale Depositionsrate von 3,7%/18,5 Wochen bestimmt werden, unterhalb dem eine vollständige Blockierung der weiteren Signalzunahme angenommen werden kann.

Zusammenfassend stellten wir die Überlegenheit einer Analyse von longitudinalen Aβ PET Daten im Mausmodell durch Verwendung einer räumlichen Normalisierung und einer SUVR mit Skalierung zur WM dar. Auf Basis dieser Erkenntnisse konnten wir im Anschluss zeigen, dass der Therapieeffekt einer BACE-Inhibition auf den Progress der zerebralen Amyloidose von der Aβ-Last bei Therapiebeginn abhängig ist.

4) Summary

The objective of this doctoral thesis was to further develop and standardize the analysis of positron emission tomography in a transgenic mouse model of cerebral amyloid accumulation and apply these findings to a multimodal intervention study.

Therefore, the first part of this doctoral thesis aimed to evaluate an automated spatial normalization and an intensity scaling to different reference regions. Therefore, we acquired 114 Aβ PET Scans of the transgenic AD mouse model PS2APP using the Aβ Tracer FBB. Among those were 37 mice with a baseline scan (BL) at 8 month of age and a short term follow up scan (FU) at 9,5 months of age, as well as 40 scans (24 from this and 16 from a previous study) of mice within an age range between 13-16 month (TER). Afterwards, three reader at different training levels performed a rigid fusion of the naive PET Images on a cerebral MRI template. The fusion of the expert was repeated to assess the test-retest variability. The fusions were spatially normalized by an automated, non-linear transformation using age specific templates. The agreement between the readers was determined by Fleiss kappa. To evaluate the intensity scaling, we calculated a target SUV (CTX) using a bilateral frontal cortex VOI and defined four different reference regions based on the MRI and [18F]-FBB templates. The SUV of each reference region was put in relation to the previously mentioned SUV (CTX) for calculation of [18F]-FBB cortex-to-reference SUVR

(CTX/REF). The results were compared on basis of longitudinal stability (Cohen's effect size (d)) and reference to the histopathological quantification (Pearson's R).
Application of an automated spatial normalization resulted in nearly perfect agreement between different reader (κ ≥ 0.99) and at least constant correlation with the histochemical goldstandard. Intensity scaling to a reference region (CTX/REF) improved the longitudinal stability (d > 1, 21 vs. d= 0, 23) and the agreement with the histochemical goldstandard (R> 0.66 vs. R>0.31) compared to SUV (CTX). Voxel-wise analysis of the intensity scaling to the GBM (SUVR CTX/GBM) suggested a physiologically implausible decrease in the hindbrain from BL to FU. The reference regions were evaluated according to the histological correlation, the artificial increase in variance within the group, the effect size of the longitudinal cortical amyloid progression, the effect of the pathology in the reference region and the influence of individual animals. In regard to the evaluated qualities, intensity scaling to the WM was superior to the other reference regions.

In the second part of this doctoral thesis we aimed to apply these findings to a multimodal intervention study using the BACE1 inhibitor RO5508887. Therefore, we randomized 26 female PS2APP (swe) (TG) and 22 female C57BL/6 (WT) mice at the age of 9,5 month either into a treatment or vehicle arm. After an initial [18F]-FBB PET baseline scan we initiated a daily oral treatment with either RO5508887 or vehicle over the course of 4 month. After 10 and 18,5 weeks we acquired a follow up and a terminal scan. Following the terminal scan, we removed the brains and the hemispheres were randomly assigned to histochemical or biochemical analysis.
The first PET scan after 10 weeks of treatment revealed a significant reduction of amyloidosis (+6,7% for BSI vs. +10,3% for VEH, p <0.05) with further reduction after 18,5 weeks (+8,4% for BSI vs. +15,2% for VEH, p <0,001). Histochemical analysis confirmed the PET results for the parameters plaque load (-9.7%, p < 0.05) and plaque density (-9.9%, p < 0.05). In addition, biochemical analysis showed a reduction in the soluble and insoluble Aβ40 (-47% and -10%), as well as the soluble and insoluble Aβ42 (-61% and -40%). The acute BACE inhibition could be demonstrated by lower levels of sAPPβ and increased sAPPα, while total sAPP remained unchanged. Furthermore, we were able to detect a negative correlation between the baseline Aβ deposition and the progress under treatment. We observed an additional inverse correlation between the naïve Aβ accumulation, represented by the control group, and the treatment effect. Absolut reduction of Aβ deposition was 7,6 ± 1,7% in high accumulating regions (≥

10%), while the reduction in low accumulating regions (<10%) was 4,8 ± 2,0%. Relative reduction in high accumulating regions was 49 ± 11%, compared to 69 ± 28% in low accumulating regions. We observed a complete block of further Aβ accumulation in regions with a naïve deposition rate below 3.7% / 18.5 weeks.

In summary, we presented the superiority of applying an automated spatial normalization and calculating a SUVR with intensity scaling to the WM for the analysis of longitudinal preclinical Aβ PET data. Based on these findings, we were able to show an inverse correlation of the baseline Aβ-load and the therapeutic effect of BACE inhibition on Aβ-progression.

5.Literaturverzeichnis

Abbott A, Dolgin E (2016) Failed Alzheimer's trial does not kill leading theory of disease. *Nature* 540: 15-16

Abushouk AI, Elmaraezy A, Aglan A, Salama R, Fouda S, Fouda R, AlSafadi AM (2017) Bapineuzumab for mild to moderate Alzheimer's disease: a meta-analysis of randomized controlled trials. *BMC Neurology* 17: 66

Bakker A, Albert MS, Krauss G, Speck CL, Gallagher M (2015) Response of the medial temporal lobe network in amnestic mild cognitive impairment to therapeutic intervention assessed by fMRI and memory task performance. *Neuroimage Clin* 7: 688-698

Barao S, Moechars D, Lichtenthaler SF, De Strooper B (2016) BACE1 Physiological Functions May Limit Its Use as Therapeutic Target for Alzheimer's Disease. *Trends Neurosci* 39: 158-169

Barthel H, Gertz HJ, Dresel S, Peters O, Bartenstein P, Buerger K, Hiemeyer F, Wittemer-Rump SM, Seibyl J, Reininger C *et al* (2011) Cerebral amyloid-beta PET with florbetaben (18F) in patients with Alzheimer's disease and healthy controls: a multicentre phase 2 diagnostic study. *Lancet Neurol* 10: 424-435

Blain JF, Bursavich MG, Freeman EA, Hrdlicka LA, Hodgdon HE, Chen T, Costa DE, Harrison BA, Kapadnis S, Murphy DA *et al* (2016) Characterization of FRM-36143 as a new gamma-secretase modulator for the potential treatment of familial Alzheimer's disease. *Alzheimers Res Ther* 8: 34

Brendel M, Hogenauer M, Delker A, Sauerbeck J, Bartenstein P, Seibyl J, Rominger A, Alzheimer's Disease Neuroimaging I (2015a) Improved longitudinal [(18)F]-AV45 amyloid PET by white matter reference and VOI-based partial volume effect correction. *Neuroimage* 108: 450-459

Brendel M, Jaworska A, Griessinger E, Rotzer C, Burgold S, Gildehaus FJ, Carlsen J, Cumming P, Baumann K, Haass C *et al* (2015b) Cross-sectional comparison of small animal [18F]-florbetaben amyloid-PET between transgenic AD mouse models. *PLoS One* 10: e0116678

Brendel M, Jaworska A, Herms J, Trambauer J, Rotzer C, Gildehaus FJ, Carlsen J, Cumming P, Bylund J, Luebbers T *et al* (2015c) Amyloid-PET predicts inhibition of de novo plaque formation upon chronic gamma-secretase modulator treatment. *Mol Psychiatry*

Brendel M, Jaworska A, Herms J, Trambauer J, Rotzer C, Gildehaus FJ, Carlsen J, Cumming P, Bylund J, Luebbers T *et al* (2015d) Monitoring of chronic gamma-secretase modulator treatment by serial amyloid-PET. *Mol Psychiatry* 20: 1141

Busche MA, Staufenbiel M, Willem M, Haass C, Förstl H (2016) Mechanismen der Alzheimer-Krankheit. *Der Nervenarzt* 87: 1163-1174

Chen K, Roontiva A, Thiyyagura P, Lee W, Liu X, Ayutyanont N, Protas H, Luo JL, Bauer R, Reschke C *et al* (2015) Improved Power for Characterizing Longitudinal Amyloid-beta PET Changes and Evaluating Amyloid-Modifying Treatments with a Cerebral White Matter Reference Region. *J Nucl Med* 56: 560-566

Clark CM, Schneider JA, Bedell BJ, Beach TG, Bilker WB, Mintun MA, Pontecorvo MJ, Hefti F, Carpenter AP, Flitter ML *et al* (2011) Use of florbetapir-PET for imaging beta-amyloid pathology. *JAMA* 305: 275-283

Coric V, Salloway S, van Dyck CH, Dubois B, Andreasen N, Brody M, Curtis C, Soininen H, Thein S, Shiovitz T *et al* (2015) Targeting Prodromal Alzheimer Disease With Avagacestat: A Randomized Clinical Trial. *JAMA Neurol* 72: 1324-1333

Dahlgren KN, Manelli AM, Stine WB, Jr., Baker LK, Krafft GA, LaDu MJ (2002) Oligomeric and fibrillar species of amyloid-beta peptides differentially affect neuronal viability. *J Biol Chem* 277: 32046-32053

Dai C-l, Tung YC, Liu F, Gong C-X, Iqbal K (2017) Tau passive immunization inhibits not only tau but also Aβ pathology. *Alzheimer's Research & Therapy* 9: 1

De Strooper B (2003) Aph-1, Pen-2, and Nicastrin with Presenilin generate an active gamma-Secretase complex. *Neuron* 38: 9-12

Deleye S, Waldron AM, Verhaeghe J, Bottelbergs A, Wyffels L, Van Broeck B, Langlois X, Schmidt ME, Stroobants S, Staelens S (2017) Evaluation of muPET outcome measures to detect disease modification induced by BACE inhibition in a transgenic mouse model of Alzheimer's disease. *J Nucl Med*

Deuschl G MWea, 2016. S3-Leitlinie Demenzen.

Doody RS, Raman R, Farlow M, Iwatsubo T, Vellas B, Joffe S, Kieburtz K, He F, Sun X, Thomas RG *et al* (2013) A Phase 3 Trial of Semagacestat for Treatment of Alzheimer's Disease. *New England Journal of Medicine* 369: 341-350

Doody RS, Thomas RG, Farlow M, Iwatsubo T, Vellas B, Joffe S, Kieburtz K, Raman R, Sun X, Aisen PS *et al* (2014) Phase 3 Trials of Solanezumab for Mild-to-Moderate Alzheimer's Disease. *New England Journal of Medicine* 370: 311-321

Duyckaerts C, Delatour B, Potier MC (2009) Classification and basic pathology of Alzheimer disease. *Acta Neuropathol* 118: 5-36

Edbauer D, Winkler E, Regula JT, Pesold B, Steiner H, Haass C (2003) Reconstitution of gamma-secretase activity. *Nat Cell Biol* 5: 486-488

Egan MF, Kost J, Tariot PN, Aisen PS, Cummings JL, Vellas B, Sur C, Mukai Y, Voss T, Furtek C *et al* (2018) Randomized Trial of Verubecestat for Mild-to-Moderate Alzheimer's Disease. *N Engl J Med* 378: 1691-1703

Egan MF, Kost J, Voss T, Mukai Y, Aisen PS, Cummings JL, Tariot PN, Vellas B, van Dyck CH, Boada M *et al* (2019) Randomized Trial of Verubecestat for Prodromal Alzheimer's Disease. *N Engl J Med* 380: 1408-1420

Endres K, Deller T (2017) Regulation of Alpha-Secretase ADAM10 In vitro and In vivo: Genetic, Epigenetic, and Protein-Based Mechanisms. *Front Mol Neurosci* 10: 56
Ferreira ST, Klein WL (2011) The Abeta oligomer hypothesis for synapse failure and memory loss in Alzheimer's disease. *Neurobiol Learn Mem* 96: 529-543

Forner S, Baglietto-Vargas D, Martini AC, Trujillo-Estrada L, LaFerla FM (2017) Synaptic Impairment in Alzheimer's Disease: A Dysregulated Symphony. *Trends Neurosci* 40: 347-357

Hardy JA, Higgins GA (1992) Alzheimer's disease: the amyloid cascade hypothesis. *Science* 256: 184-185

Hawkes N (2017) Merck ends trial of potential Alzheimer’s drug verubecestat. *BMJ* 356
Hawkins J, Harrison DC, Ahmed S, Davis RP, Chapman T, Marshall I, Smith B, Mead TL, Medhurst A, Giblin GMP *et al* (2011) Dynamics of Aβ42 Reduction in Plasma, CSF and Brain of Rats Treated with the γ-Secretase Modulator, GSM-10h. *Neurodegenerative Diseases* 8: 455-464

Hussain I, Powell D, Howlett DR, Tew DG, Meek TD, Chapman C, Gloger IS, Murphy KE, Southan CD, Ryan DM *et al* (1999) Identification of a novel aspartic protease (Asp 2) as beta-secretase. *Mol Cell Neurosci* 14: 419-427

Imbimbo BP, Del Giudice E, Colavito D, D'Arrigo A, Dalle Carbonare M, Villetti G, Facchinetti F, Volta R, Pietrini V, Baroc MF *et al* (2007) 1-(3',4'-Dichloro-2-fluoro[1,1'-biphenyl]-4-yl)-cyclopropanecarboxylic acid (CHF5074), a novel gamma-secretase modulator, reduces brain beta-amyloid pathology in a transgenic mouse model of Alzheimer's disease without causing peripheral toxicity. *J Pharmacol Exp Ther* 323: 822-830

Imbimbo BP, Hutter-Paier B, Villetti G, Facchinetti F, Cenacchi V, Volta R, Lanzillotta A, Pizzi M, Windisch M (2009) CHF5074, a novel gamma-secretase modulator, attenuates brain beta-amyloid pathology and learning deficit in a mouse model of Alzheimer's disease. *Br J Pharmacol* 156: 982-993

Jacobsen H, Ozmen L, Caruso A, Narquizian R, Hilpert H, Jacobsen B, Terwel D, Tanghe A, Bohrmann B (2014) Combined treatment with a BACE inhibitor and anti-

Abeta antibody gantenerumab enhances amyloid reduction in APPLondon mice. *J Neurosci* 34: 11621-11630

Jan A, Gokce O, Luthi-Carter R, Lashuel HA (2008) The ratio of monomeric to aggregated forms of Abeta40 and Abeta42 is an important determinant of amyloid-beta aggregation, fibrillogenesis, and toxicity. *J Biol Chem* 283: 28176-28189

Johnson KA, Minoshima S, Bohnen NI, Donohoe KJ, Foster NL, Herscovitch P, Karlawish JH, Rowe CC, Carrillo MC, Hartley DM *et al* (2013) Appropriate use criteria for amyloid PET: a report of the Amyloid Imaging Task Force, the Society of Nuclear Medicine and Molecular Imaging, and the Alzheimer's Association. *J Nucl Med* 54: 476-490

Jucker M (2010) The benefits and limitations of animal models for translational research in neurodegenerative diseases. *Nat Med* 16: 1210-1214

Kounnas MZ, Danks AM, Cheng S, Tyree C, Ackerman E, Zhang X, Ahn K, Nguyen P, Comer D, Mao L *et al* (2010) Modulation of gamma-secretase reduces beta-amyloid deposition in a transgenic mouse model of Alzheimer's disease. *Neuron* 67: 769-780

Kuhn PH, Wang H, Dislich B, Colombo A, Zeitschel U, Ellwart JW, Kremmer E, Rossner S, Lichtenthaler SF (2010) ADAM10 is the physiologically relevant, constitutive alpha-secretase of the amyloid precursor protein in primary neurons. *EMBO J* 29: 3020-3032

LaFerla FM, Green KN, Oddo S (2007) Intracellular amyloid-beta in Alzheimer's disease. *Nat Rev Neurosci* 8: 499-509

Landau SM, Fero A, Baker SL, Koeppe R, Mintun M, Chen K, Reiman EM, Jagust WJ (2015) Measurement of longitudinal beta-amyloid change with 18F-florbetapir PET and standardized uptake value ratios. *J Nucl Med* 56: 567-574

Lichtenthaler SF (2011) alpha-secretase in Alzheimer's disease: molecular identity, regulation and therapeutic potential. *J Neurochem* 116: 10-21

Loureiro RM, Dumin JA, McKee TD, Austin WF, Fuller NO, Hubbs JL, Shen R, Jonker J, Ives J, Bronk BS *et al* (2013) Efficacy of SPI-1865, a novel gamma-secretase modulator, in multiple rodent models. *Alzheimers Res Ther* 5: 19

Mitani Y, Akashiba H, Saita K, Yarimizu J, Uchino H, Okabe M, Asai M, Yamasaki S, Nozawa T, Ishikawa N *et al* (2014) Pharmacological characterization of the novel gamma-secretase modulator AS2715348, a potential therapy for Alzheimer's disease, in rodents and nonhuman primates. *Neuropharmacology* 79: 412-419

Munro KM, Nash A, Pigoni M, Lichtenthaler SF, Gunnersen JM (2016) Functions of the Alzheimer’s Disease Protease BACE1 at the Synapse in the Central Nervous System. *Journal of Molecular Neuroscience* 60: 305-315

Murakami K, Watanabe T, Koike T, Kamata M, Igari T, Kondo S (2016) Pharmacological properties of a novel and potent gamma-secretase modulator as a therapeutic option for the treatment of Alzheimer's disease. *Brain Res* 1633: 73-86

Neumann U, Rueeger H, Machauer R, Veenstra SJ, Lueoend RM, Tintelnot-Blomley M, Laue G, Beltz K, Vogg B, Schmid P *et al* (2015) A novel BACE inhibitor NB-360 shows a superior pharmacological profile and robust reduction of amyloid-beta and neuroinflammation in APP transgenic mice. *Mol Neurodegener* 10: 44

Nikolaev A, McLaughlin T, O'Leary DD, Tessier-Lavigne M (2009) APP binds DR6 to trigger axon pruning and neuron death via distinct caspases. *Nature* 457: 981-989

Overhoff F, Brendel M, Jaworska A, Korzhova V, Delker A, Probst F, Focke C, Gildehaus FJ, Carlsen J, Baumann K *et al* (2016) Automated Spatial Brain Normalization and Hindbrain White Matter Reference Tissue Give Improved [(18)F]-Florbetaben PET Quantitation in Alzheimer's Model Mice. *Front Neurosci* 10: 45

Ozmen L, Albientz A, Czech C, Jacobsen H (2009) Expression of transgenic APP mRNA is the key determinant for beta-amyloid deposition in PS2APP transgenic mice. *Neuro-degenerative diseases* 6: 29-36

Peters-Libeu C, Campagna J, Mitsumori M, Poksay KS, Spilman P, Sabogal A, Bredesen DE, John V (2015) sAbetaPPalpha is a Potent Endogenous Inhibitor of BACE1. *J Alzheimers Dis* 47: 545-555

Querfurth HW, LaFerla FM (2010) Alzheimer's disease. *N Engl J Med* 362: 329-344

Richards JG, Higgins GA, Ouagazzal AM, Ozmen L, Kew JN, Bohrmann B, Malherbe P, Brockhaus M, Loetscher H, Czech C *et al* (2003) PS2APP transgenic mice, coexpressing hPS2mut and hAPPswe, show age-related cognitive deficits associated with discrete brain amyloid deposition and inflammation. *J Neurosci* 23: 8989-9003

Rogers K, Felsenstein KM, Hrdlicka L, Tu Z, Albayya F, Lee W, Hopp S, Miller MJ, Spaulding D, Yang Z *et al* (2012) Modulation of gamma-secretase by EVP-0015962 reduces amyloid deposition and behavioral deficits in Tg2576 mice. *Mol Neurodegener* 7: 61

Rominger A, Brendel M, Burgold S, Keppler K, Baumann K, Xiong G, Mille E, Gildehaus FJ, Carlsen J, Schlichtiger J *et al* (2013) Longitudinal assessment of cerebral beta-amyloid deposition in mice overexpressing Swedish mutant beta-amyloid precursor protein using 18F-florbetaben PET. *J Nucl Med* 54: 1127-1134

Sabri O, Sabbagh MN, Seibyl J, Barthel H, Akatsu H, Ouchi Y, Senda K, Murayama S, Ishii K, Takao M *et al* (2015) Florbetaben PET imaging to detect amyloid beta plaques in Alzheimer's disease: phase 3 study. *Alzheimers Dement* 11: 964-974

Scannevin RH, Chollate S, Brennan MS, Snodgrass-Belt PA, Peng H, Xu L, Jung MY, Bussiere T, Arastu MF, Talreja T *et al* (2016) BIIB042, a novel gamma-secretase modulator, reduces amyloidogenic Abeta isoforms in primates and rodents and plaque pathology in a mouse model of Alzheimer's disease. *Neuropharmacology* 103: 57-68

Selkoe DJ (2001) Alzheimer's disease: genes, proteins, and therapy. *Physiol Rev* 81: 741-766

Selkoe DJ, Hardy J (2016) The amyloid hypothesis of Alzheimer's disease at 25 years. *EMBO Molecular Medicine* 8: 595-608

Sevigny J, Chiao P, Bussiere T, Weinreb PH, Williams L, Maier M, Dunstan R, Salloway S, Chen T, Ling Y *et al* (2016) The antibody aducanumab reduces Abeta plaques in Alzheimer's disease. *Nature* 537: 50-56

Sinha S, Anderson JP, Barbour R, Basi GS, Caccavello R, Davis D, Doan M, Dovey HF, Frigon N, Hong J *et al* (1999) Purification and cloning of amyloid precursor protein beta-secretase from human brain. *Nature* 402: 537-540

Soares HD, Gasior M, Toyn JH, Wang JS, Hong Q, Berisha F, Furlong MT, Raybon J, Lentz KA, Sweeney F *et al* (2016) The gamma-Secretase Modulator, BMS-932481, Modulates Abeta Peptides in the Plasma and Cerebrospinal Fluid of Healthy Volunteers. *J Pharmacol Exp Ther* 358: 138-150

The Lancet N (2017) Solanezumab: too late in mild Alzheimer's disease? *The Lancet Neurology* 16: 97

Van Broeck B, Chen JM, Treton G, Desmidt M, Hopf C, Ramsden N, Karran E, Mercken M, Rowley A (2011) Chronic treatment with a novel gamma-secretase modulator, JNJ-40418677, inhibits amyloid plaque formation in a mouse model of Alzheimer's disease. *Br J Pharmacol* 163: 375-389

Vandenberghe R, Van Laere K, Ivanoiu A, Salmon E, Bastin C, Triau E, Hasselbalch S, Law I, Andersen A, Korner A *et al* (2010) 18F-flutemetamol amyloid imaging in Alzheimer disease and mild cognitive impairment: a phase 2 trial. *Ann Neurol* 68: 319-329

Wagner SL, Rynearson KD, Duddy SK, Zhang C, Nguyen PD, Becker A, Vo U, Masliah D, Monte L, Klee JB *et al* (2017) Pharmacological and Toxicological Properties of the Potent Oral γ-Secretase Modulator BPN-15606. *Journal of Pharmacology and Experimental Therapeutics* 362: 31-44

Willem M, Tahirovic S, Busche MA, Ovsepian SV, Chafai M, Kootar S, Hornburg D, Evans LD, Moore S, Daria A *et al* (2015) eta-Secretase processing of APP inhibits neuronal activity in the hippocampus. *Nature* 526: 443-447

Winblad B, Amouyel P, Andrieu S, Ballard C, Brayne C, Brodaty H, Cedazo-Minguez A, Dubois B, Edvardsson D, Feldman H *et al* (2016) Defeating Alzheimer's disease and other dementias: a priority for European science and society. *Lancet Neurol* 15: 455-532

Wolk DA, Grachev ID, Buckley C, Kazi H, Grady MS, Trojanowski JQ, Hamilton RH, Sherwin P, McLain R, Arnold SE (2011) Association between in vivo fluorine 18-labeled flutemetamol amyloid positron emission tomography imaging and in vivo cerebral cortical histopathology. *Arch Neurol* 68: 1398-1403

Yang T, Li S, Xu H, Walsh DM, Selkoe DJ (2017a) Large Soluble Oligomers of Amyloid beta-Protein from Alzheimer Brain Are Far Less Neuroactive Than the Smaller Oligomers to Which They Dissociate. *J Neurosci* 37: 152-163

Yang T, Li S, Xu H, Walsh DM, Selkoe DJ (2017b) Large Soluble Oligomers of Amyloid β-Protein from Alzheimer Brain Are Far Less Neuroactive Than the Smaller Oligomers to Which They Dissociate. *The Journal of Neuroscience* 37: 152-163

Zhang W, Oya S, Kung MP, Hou C, Maier DL, Kung HF (2005) F-18 stilbenes as PET imaging agents for detecting beta-amyloid plaques in the brain. *J Med Chem* 48: 5980-5988

frontiers in Neuroscience

ORIGINAL RESEARCH
published: 29 February 2016
doi: 10.3389/fnins.2016.00045

Automated Spatial Brain Normalization and Hindbrain White Matter Reference Tissue Give Improved [^{18}F]-Florbetaben PET Quantitation in Alzheimer's Model Mice

*Felix Overhoff[1†], Matthias Brendel[1†], Anna Jaworska[2,3], Viktoria Korzhova[2], Andreas Delker[1], Federico Probst[1], Carola Focke[1], Franz-Josef Gildehaus[1], Janette Carlsen[1], Karlheinz Baumann[4], Christian Haass[2,5,6], Peter Bartenstein[1,5], Jochen Herms[2,5] and Axel Rominger[1,5]**

[1] Department of Nuclear Medicine, Ludwig-Maximilians-University of Munich, Munich, Germany, [2] DZNE-German Center for Neurodegenerative Diseases, Munich, Germany, [3] Laboratory of Neurodegeneration, International Institute of Molecular and Cell Biology, Warsaw, Poland, [4] Roche Pharma Research and Early Development, Neuroscience Discovery, Roche Innovation Center Basel, F. Hoffmann-La Roche Ltd, Basel, Switzerland, [5] Munich Cluster for Systems Neurology (SyNergy), Munich, Germany, [6] Biomedical Center, Ludwig-Maximilians-University of Munich, Munich, Germany

OPEN ACCESS

Edited by:
John Ashburner,
UCL Institute of Neurology, UK

Reviewed by:
Hidenao Fukuyama,
Kyoto University, Japan
Stephen John Sawiak,
University of Cambridge, UK

***Correspondence:**
Axel Rominger
axel.rominger@med.uni-muenchen.de

[†]These authors have contributed equally to this work.

Specialty section:
This article was submitted to Brain Imaging Methods, a section of the journal Frontiers in Neuroscience

Received: 10 November 2015
Accepted: 01 February 2016
Published: 29 February 2016

Citation:
Overhoff F, Brendel M, Jaworska A, Korzhova V, Delker A, Probst F, Focke C, Gildehaus F-J, Carlsen J, Baumann K, Haass C, Bartenstein P, Herms J and Rominger A (2016) Automated Spatial Brain Normalization and Hindbrain White Matter Reference Tissue Give Improved [^{18}F]-Florbetaben PET Quantitation in Alzheimer's Model Mice. Front. Neurosci. 10:45. doi: 10.3389/fnins.2016.00045

Preclinical PET studies of β-amyloid (Aβ) accumulation are of growing importance, but comparisons between research sites require standardized and optimized methods for quantitation. Therefore, we aimed to evaluate systematically the (1) impact of an automated algorithm for spatial brain normalization, and (2) intensity scaling methods of different reference regions for Aβ-PET in a large dataset of transgenic mice. PS2APP mice in a 6 week longitudinal setting ($N = 37$) and another set of PS2APP mice at a histologically assessed narrow range of Aβ burden ($N = 40$) were investigated by [^{18}F]-florbetaben PET. Manual spatial normalization by three readers at different training levels was performed prior to application of an automated brain spatial normalization and inter-reader agreement was assessed by Fleiss Kappa (κ). For this method the impact of templates at different pathology stages was investigated. Four different reference regions on brain uptake normalization were used to calculate frontal cortical standardized uptake value ratios ($SUVR_{CTX/REF}$), relative to raw SUV_{CTX}. Results were compared on the basis of longitudinal stability (Cohen's d), and in reference to gold standard histopathological quantitation (Pearson's R). Application of an automated brain spatial normalization resulted in nearly perfect agreement (all $\kappa \geq 0.99$) between different readers, with constant or improved correlation with histology. Templates based on inappropriate pathology stage resulted in up to 2.9% systematic bias for $SUVR_{CTX/REF}$. All $SUVR_{CTX/REF}$ methods performed better than SUV_{CTX} both with regard to longitudinal stability ($d \geq 1.21$ vs. $d = 0.23$) and histological gold standard agreement ($R \geq 0.66$ vs. $R \geq 0.31$). Voxel-wise analysis suggested a physiologically implausible longitudinal decrease by global mean scaling. The hindbrain white matter reference ($R_{mean} = 0.75$)

was slightly superior to the brainstem (R_{mean} = 0.74) and the cerebellum (R_{mean} = 0.73). Automated brain normalization with reference region templates presents an excellent method to avoid the inter-reader variability in preclinical Aβ-PET scans. Intracerebral reference regions lacking Aβ pathology serve for precise longitudinal *in vivo* quantification of [^{18}F]-florbetaben PET. Hindbrain white matter reference performed best when considering the composite of quality criteria.

Keywords: Alzheimer's disease, β-amyloid, [^{18}F]-florbetaben, small animal PET, reference region, brain normalization

INTRODUCTION

The steadily growing number of patients suffering from Alzheimer's disease (AD) will place a great burden on healthcare systems in the coming decades, baring development of an effective intervention therapy (Schneider, 2013). Molecular imaging of β-amyloid (Aβ) with positron emission tomography (PET) has given new insight into the progression of AD pathology and has entered clinical diagnostic use (Johnson et al., 2013). Furthermore, PET imaging is increasingly used for detecting cerebral amyloidosis in transgenic mouse models of AD (Manook et al., 2012; Rominger et al., 2013). Small animal PET studies of longitudinal design afford monitoring of the rate of β-amyloid accumulation, and present the possibility of testing interventions for attenuating plaque formation.

Preclinical brain PET imaging frequently suffer from shortcomings such as underpowered study groups, reader dependence of endpoints, varying approaches to data analysis, and inadequate blinding of investigators to treatment groups (Jucker, 2010). Automated template-based normalization of rodent brain to standard coordinates, in analogy to standard methods for analysis of human PET data, has the potential to minimize biases from reader dependence and imperfect blinding, although the reliability of such approaches has yet to be systematically investigated for preclinical Aβ-PET. In particular, the choice of the optimal template for automated spatial normalization of Aβ-PET images may be influenced by pathological features of the particular AD mouse model (Rohlfing et al., 2009). Since this issue has not hitherto been raised in preclinical Aβ-PET imaging, we planned to validate an automated, user-independent approach for spatial normalization by comparing binding results from readers at different training levels before and after normalization, with histopathological examination of fibrillar Aβ as the gold standard. Furthermore, we objected to study the influence of template selection at different pathology stages on the automated spatial normalization of mouse brain Aβ-PET images.

An additional point of contention in preclinical Aβ-PET concerns the method for image intensity scaling, with normalization either to the injected dose, or to tracer uptake in intracerebral reference regions. Just as in human PET studies with Aβ-PET tracer, the choice of reference regions is crucial for preclinical models, which have characteristic patterns of Aβ deposition. In human Aβ-PET imaging, the whole cerebellum and the cerebellar gray matter have been the preferred reference regions for most large scale quantitative investigations (Vandenberghe et al., 2010; Barthel and Sabri, 2011; Clark et al., 2011). However, recent human studies with fluorinated amyloid tracers have revealed longitudinal stabilization of standardized uptake value ratios (SUVR), with use of white matter or brain stem reference regions, this despite the ongoing accumulation of Aβ plaques as confirmed by histology (Landau et al., 2014, 2015; Brendel et al., 2015a; Chen et al., 2015). There has so far been no systematic comparison of scaling methods for mouse Aβ-PET imaging. Consequently, we aimed to compare different scaling methods and reference regions in a large series of Aβ studies with [^{18}F]-florbetaben (FBB) in an established AD mouse model, with regard to accuracy of the PET method in capturing longitudinal changes in Aβ-deposition, with terminal histological plaque quantitation serving as the gold standard. The overall aims of this study were to investigate if automated brain spatial normalization is beneficial for quantitation of preclinical Aβ-PET, and to identify an optimally performing method for intensity scaling.

MATERIALS AND METHODS

Animal Model and Study Design

All experiments were performed in compliance with the National Guidelines for Animal Protection, Germany, with approval of the local animal care committee of the Government of Oberbayern (Regierung Oberbayern), and overseen by a veterinarian. Anesthesia was performed with isoflurane 1.5%. Mice were killed by cervical dislocation in a state of deep narcosis.

The transgenic B6.PS2APP (line B6.152H) is homozygous for both the human presenilin (PS) 2, N141I mutation and the human amyloid precursor protein (APP) K670N, M671L mutation. The APP and PS2 transgenes are driven by mouse Thy-1 and mouse prion promoters, respectively. This line had been created by co-injection of both transgenes into C57Bl/6 zygotes (Richards et al., 2003). Homozygous B6.PS2APP mice show first appearance of plaques in the cortex and hippocampus at 5–6 months of age (Ozmen et al., 2009).

Aβ-PET scans (N = 114) were used from two studies wherein drug-naive longitudinal FBB-PET recordings were obtained in PS2APP mice (N = 37) at a short interval (8 and 9.5 months of age). Furthermore, we also used terminal Aβ-PET recordings (N = 40; range: 13–16 months; N = 24 from the longitudinal set and N = 16 from another historical investigation), in which histologically quantified terminal plaque load was measured. We defined the different ages for Aβ-PET imaging as "BL" for the

baseline at 8 months ($N = 37$ PS2APP mice), "FU" for the follow-up of the same group at 9.5 months ($N = 37$ PS2APP mice), and "TER" for the terminal Aβ-PET recordings obtained between 13 and 16 months of age ($N = 40$ PS2APP mice).

Radiochemistry

The [^{18}F]-florbetaben precursor (Piramal Imaging, Berlin) was radiolabeled by the method of Zhang et al. (2005), with slight modifications. This procedure is described elsewhere (Rominger et al., 2013), and yields a radiochemical purity exceeding 98% and specific activity of 50–90 GBq/μmol at the end of synthesis.

Amyloid Pet Acquisition and Reconstruction

Image acquisition and reconstruction followed a standardized protocol (Brendel et al., 2015b). Mice were anesthetized with isoflurane (1.5%, delivered via a mask at 3.5 L/min in oxygen) and received bolus injection of 10.1 ± 2.3 MBq of [^{18}F]-florbetaben in 150 μL of saline to a tail vein. Following placement in the tomograph (Siemens Inveon DPET), a single frame emission recording for the interval 30–60 min p.i. followed by a 15 min transmission scan was obtained using a rotating [^{57}Co] point source. The image reconstruction procedure consisted of an three-dimensional ordered subset expectation maximization (OSEM) with four iterations and 12 subsets followed by a maximum *a posteriori* (MAP) algorithm with 32 iterations. Scatter and attenuation correction were performed and a decay correction for [^{18}F] was applied. With a zoom factor of 1.0 and a128 × 128× 159 matrix, a final voxel dimension of 0.78 × 0.78 × 0.80 mm was obtained.

Image Analysis

Spatial Normalization

Aβ-PET images were first blinded to the reader by coding of the Aβ-PET files. Images were coregistered to a 3T magnetic resonance imaging (MRI) mouse brain template (Dorr et al., 2007) by a rigid manual fusion, using the PMOD FUSION tool (v. 3.4 PMOD Technologies, Zürich). The spatial normalization was independently performed by an expert (>1000 fusions), an experienced reader (∼150 fusions) as well as a novice reader who had been trained for 4 h over the course of 2 days. The expert fusion was repeated to assess test-retest variability (%) for operators with high training level.

All spatial normalized images of the expert reader were intensity scaled to the injected dose and multiplied by the individual body weight to give standardized uptake value (SUV) images. Then age-dependent groups ($N = 37$ or $N = 40$ images each) from PS2APP mice were averaged for the generation of three different templates defined at increasing stages of amyloid pathology (**Figure 1A**).

Subsequently, fused images from all readers were spatially normalized on all different templates by applying an automated nonlinear transformation, which removed the main differences in brain size and shape using the normalization algorithm in SPM5 (Wellcome Department of Cognitive Neurology, London, UK) implemented within the PMOD FUSION tool (V. 3.4 PMOD Technologies, Zürich). This algorithm was set to mouse brain dimensions using standardized settings (equal modality; nonlinear warping; 16 iterations; frequency cutoff 3; regularization 1.0; no thresholding). The procedure was tested with and without transient input smoothing by applying a 0.6 mm Gaussian to the image before initiation of warping operations. The calculated transformation matrix was saved and finally applied to the "raw" input image to avoid loss of resolution due to repeated image resampling.

Inter-Reader Analyses

For inter-reader analyses, Fleiss Kappa (κ) was calculated for TER results (SUV_{CTX} and $SUVR_{CTX/REF}$ as described below) from expert vs. experienced, experienced vs. novice, expert vs. novice, both before and after automated brain normalization. Furthermore, inter-reader variability (%) was calculated, and compared to the expert test-retest variability (%). For statistical testing of absolute differences for SUV_{CTX} and $SUVR_{CTX/REF}$ between different readers before and after brain normalization a permutation test was performed as described in Section Statistics below and was also used to test for significant differences between inter-reader variability (%) and expert test-retest variability (%).

Analysis of Template Influence on Automated Brain Intensity Normalization

To assess the impact of stage specific templates, TER results of the expert before brain normalization were compared with TER results after brain normalization to TER, FU, and BL templates by calculation of error-(%), with findings of the expert considered as the standard of truth. A paired *t*-test was used for statistical testing of significant alterations in SUV_{CTX} and $SUVR_{CTX/REF}$ (as described below) resulting from different templates.

Scaling

A total of five intensity scaling methods were performed, all using VOIs predefined in the final image space, which was identical for MRI and [^{18}F]-florbetaben templates. Beside calculation of frontal cortical SUV_{CTX}, we tested intensity scaling by four different reference regions (**Figure 1B**):

1. Whole cerebellum (CBL) with a volume of 65 mm^3.
2. Hindbrain white matter (WM), including high unspecific tracer retention areas (threshold-based) such as pons, midbrain, cerebellar peduncle, cranial hypothalamus and caudal thalamus, with a total volume of 67 mm^3.
3. Brainstem (BST), an oval shaped region extending from pons to midbrain, with a volume of 24 mm^3.
4. Whole brain as the global mean (GLM), with a volume of 525 mm^3.

As target regions two bilateral frontal cortex VOIs comprising 12 mm^3 each (**Figure 1A**), were employed for calculation of [^{18}F]-florbetaben cortex-to-reference $SUVR_{CTX/REF}$.

Longitudinal stability

Scaling methods were tested against each other by evaluating the longitudinal stability of the endpoint (SUV_{CTX} or $SUVR_{CTX/REF}$) over the brief 6 week interval from BL to FU in $N = 37$ animals. Pearson's coefficients of correlation (R) were calculated

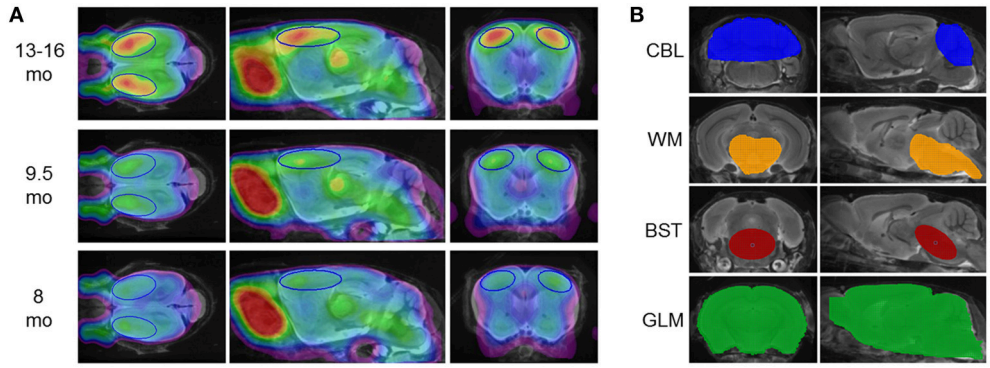

FIGURE 1 | (A) [^{18}F]-florbetaben PET templates at different pathology stages, deriving from mean findings in groups of PS2APP mice aged 8, 9.5, and 13–16 months. PET images are superimposed on an MRI-based mouse brain atlas (Dorr et al., 2007) for anatomical reference. The frontal cortical target VOI is depicted in blue. **(B)** Reference region VOIs are illustrated on the same MRI mouse atlas; from top to bottom: cerebellum (blue; CBL), hindbrain white matter (orange; WM), brainstem (red; BST), whole brain (green; GLM).

for SUV_{CTX} and $SUVR_{CTX/REF}$ values of the four different reference regions, given the assumption that the mouse model is characterized by a nearly linear progression of amyloidosis over time, as supported by findings from our previous study (Brendel et al., 2015b). The variance of BL and FU groups, expressed by SD-(%), was calculated as an indicator of intra-group stability. Effect sizes (Cohen's d) for the resulting differences between the two sequential Aβ-PET scans were calculated as an additional quality criterion in the longitudinal design.

Longitudinal regional analyses

To test the impact of different scaling methods for Aβ-PET on the detected differences in longitudinal data independently from the cortical target VOI, we assessed alterations in FBB-binding between BL and FU voxel-wise by statistical parametric mapping (SPM). We used SPM5 routines implemented in MATLAB (version 7.1), adapted from Sawiak et al. (2009) for mouse data. For SUV_{CTX} and each reference region approach, we performed a paired *t*-test for Aβ-PET images (FU vs. BL) of PS2APP ($N = 37$) mice, and thus assessed increases or decreases over 6 weeks of follow up.

Histochemical Analyses

Histochemical analyses were performed in a matching frontal cortex region of interest as the gold standard of amyloid burden, for evaluating reliability of frontal cortical SUV_{CTX} and four different $SUVR_{CTX/REF}$ results. The procedure followed a standardized protocol wherein cortical plaque load (%) was calculated for each animal (Brendel et al., 2015b). For correlation analyses of the terminal Aβ-PET estimates ($N = 40$) with plaque load (%), Pearson's coefficients of correlation (R) were calculated with and without brain normalization and for all different intensity normalization methods. Significant differences between correlation coefficients before and after spatial brain normalization, between different readers, and between different intensity normalization methods were assessed by an extended Fisher's transformation approach as described in Section Statistics.

Statistics

A permutation test was used to test for significance of not normally distributed differences between two readers before and after normalization and for the comparison of inter-reader variability (%) with test-retest variability (%) of the expert. Absolute values were used for these comparisons. For permutation testing, the results were pooled and a loop rearranging the pooled results into two groups (with 1 million repeats) was coded within Matlab 7.12.0. The originally observed results of difference between manually acquired and normalized data or of difference between test-retest expert variability (%) and inter-reader variability (%) were defined as target values. For every resampled pair the mean result was calculated and each mean result equal to or higher than the target value was counted automatically. Finally, the total count was set in relation to the number of repeats to obtain the *p*-value.

Significant differences between two dependent correlations with one variable in common (plaque load %) were assessed by an extended Fisher's transformation approach (Lee and Preacher, 2013). First, each correlation coefficient was converted into a z-score using Fisher's r-to-z transformation. Then, asymptotic covariance of the estimates was computed. Finally, these quantities were used in an asymptotic *z*-test. A threshold of $p < 0.05$ was considered to be significant for rejection of the null hypothesis in all statistical tests.

RESULTS

Spatial Normalization

Automated Brain Normalization Significantly Reduces Inter-Reader Variability

The intra-reader test-retest variability of $SUVR_{CTX/REF}$ for the expert reader was 1.4 ± 1.0% (range: 0.9–2.9% for different reference regions). Inter-reader agreement for $SUVR_{CTX/REF}$ was very high between the expert and the experienced reader without brain pre-normalization ($\kappa = 0.97 \pm 0.02$; inter-reader variability 1.4 ± 0.8%), indicating a very high reproducibility

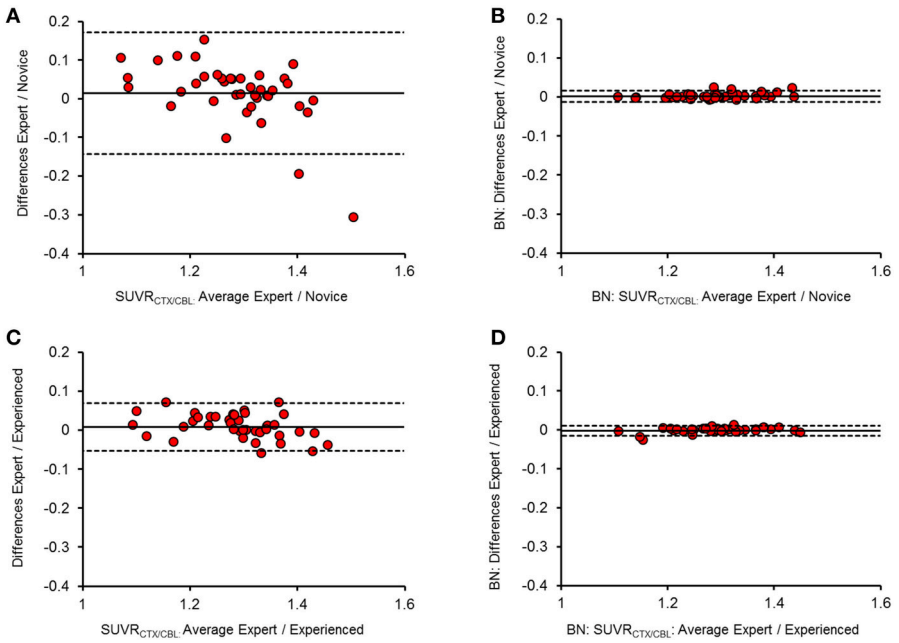

FIGURE 2 | Bland-Altman plots of the inter-reader $SUVR_{CTX/CBL}$ ($n = 40$) agreement before (A,C) and after (B,D) brain spatial normalization. Difference (y-axis) and mean (x-axis) between two readers are illustrated against each other, with the mean difference presented by the thick line and the upper (+1.96 SDs) and lower limits (−1.96 SDs) of agreement by the dashed lines. Panels **(A,B)** show the comparison between expert and novice reader, while **(C,D)** show the relation between expert and experienced reader.

when both readers are at a high training level without significant differences when compared to the expert test-retest variability (all p = n.s.). However, lower inter-reader agreement including some strong outliers occurred between novice reader and expert ($\kappa = 0.89 \pm 0.08$; inter-reader variability $3.0 \pm 1.8\%$; all $p < 0.01$), or novice and experienced reader ($\kappa = 0.88 \pm 0.06$; inter-reader variability $2.9 \pm 1.5\%$; all $p < 0.01$). Especially the agreement for $SUVR_{CTX/CBL}$ was lower in the latter two contrasts ($\kappa = 0.77/0.79$; inter-reader variability = 5.6%/5.2%) when only the manual PET-MRI fusions were compared. After automated spatial brain normalization, all κ values were ≥ 0.99 and the maximal inter-reader variability was 0.6%. All differences between readers were significantly lowered by the automated brain normalization procedure ($p < 0.001$ for all reference regions). Brain normalization without transient input smoothing (0.6 mm) during the automated coregistration process led to some instances of strong image distortions, and was therefore dismissed. Representative approximations of $SUVR_{CTX/CBL}$ between readers after brain spatial normalization are illustrated in Bland-Altman Plots (**Figure 2**) and all κ-values/%-variabilities are reported in **Table 1**.

Template Characteristics Influence Brain Normalization Results

FBB uptake in the TER scans was underestimated when spatially normalized to templates from BL and FU disease stages, under the assumption that the expert manual fusion serves as the standard of truth. This effect was most obvious with the cerebellum serving as the reference region (BL-template: $-0.6 \pm 2.1\%$, $p < 0.05$/FU-template: $-2.9 \pm 2.4\%$, $p < 0.001$; **Figure 3A**). With the stage specific TER template, low $SUVR_{CTX/REF}$ values tended to be overestimated, whereas high results were underestimated, but the mean error-(%) was only ±0.2%. Based on these findings, we attempted to quantify the bias deriving from the deviation of individual $SUVR_{CTX/REF}$ from the template $SUVR_{CTX/REF}$ by constructing a function defining the relationship between error-(%) and the deviation-(%) = (individual - $SUVR_{CTX/REF}$-template-$SUVR_{CTX/REF}$) / template - $SUVR_{CTX/REF}$*100. Using this function we estimated a bias of ±13.8% (linear regression: $R = -0.44$; $p < 0.01$) for $SUVR_{CTX/CBL}$(**Figure 3B**), meaning that an individual mouse with a 10% higher $SUVR_{CTX/CBL}$ compared to the template results gives on average a 1.38% lower result after brain intensity normalization. Respective bias was similarly high for $SUVR_{CTX/GLM}$ (±10.1%; linear regression: $R = -0.34$; $p < 0.05$), but distinctly lower for $SUVR_{CTX/WM}$ (±1.9%; linear regression: $R = -0.13$; p = n.s.; **Figure 3C**) and $SUVR_{CTX/BST}$ (±1.7%; linear regression: $R = -0.16$; p = n.s.). Absolute biases in $SUVR_{CTX/CBL}$ and $SUVR_{CTX/GLM}$ were significantly higher when compared to $SUVR_{CTX/WM}$ or $SUVR_{CTX/BST}$ (all $p < 0.001$).

Longitudinal Analysis

Intracerebral Reference Regions give Lower Variance and Higher Longitudinal Effect Sizes When Compared to SUV

Implausibly low longitudinal increases of FBB binding were obtained through generation of ordinary SUV_{CTX} estimates ($R = -0.12$, p = n.s.), which is explicable by the rather high relative standard deviations in the BL (15.9%) and FU (13.2%)

TABLE 1 | Inter-reader agreement.

	κ/inter-reader variability (%)			Test-retest variability
Reference	**Expert-experienced (κ/%)**	**Experienced-novice (κ/%)**	**Expert-novice (κ/%)**	**Expert (%)**
RAW FUSION				
CBL	0.95/2.6	0.79/5.2*	0.77/5.6*	2.9
WM	0.98/1.0	0.91/2.4**	0.93/2.1**	0.9
BST	0.99/0.9	0.94/2.0**	0.96/1.8**	0.9
GLM	0.95/1.2	0.88/2.1**	0.89/2.3**	0.9
MEAN ± SD	0.97 ± 0.02/1.4 ± 0.8	0.88 ± 0.06/2.9 ± 1.5**	0.89 ± 0.08/3.0 ± 1.8**	1.4 ± 1.0
BRAIN NORMALIZATION				
CBL	1.00/0.5	0.99/0.6	1.00/0.5	
WM	1.00/0.2	0.99/0.4	0.99/0.4	
BST	1.00/0.2	0.99/0.4	0.99/0.5	
GLM	1.00/0.2	0.99/0.5	0.99/0.4	
MEAN ± SD	1.00 ± 0.00/0.2 ± 0.1	0.99 ± 0.00/0.5 ± 0.1	0.99 ± 0.00/0.5 ± 0.1	

*Inter-reader agreement expressed by Fleiss κ and inter-reader variability (%) before and after brain normalization (BN) for all different reference regions. For the raw fusion the test-retest variability of the expert is given. *$p < 0.01$; **$p < 0.001$ for interreader-variability (%) vs. expert test-retest variability (%), permutation test.*

groups. Each of the four intracerebral reference regions stabilized the Aβ-PET $SUVR_{CTX/REF}$ estimates, and resulted in distinctly lower variance (2.3–4.6%), with highest agreement between BL and FU for $SUVR_{CTX/WM}$ ($R = 0.64$, $p < 0.001$). Highest effect sizes for the age-dependent increases were found with $SUVR_{CTX/WM}$ and $SUVR_{CTX/BST}$ ($d = 1.64$), which exceeded that for $SUVR_{CTX/CBL}$ ($d = 1.23$) and $SUVR_{CTX/GLM}$ ($d = 1.21$). Details of this analysis are provided in **Table 2**.

Global Mean Scaling Gives Physiologically Implausible Longitudinal Intensity Decreases in the Hindbrain

Voxel-wise analyses revealed a longitudinal progression of amyloidosis from BL to FU in the forebrain for all reference regions in 648,691 voxels (CBL), 662,374 voxels (WM), 612,517 voxels (BST), and 47,247 voxel (GLM) (all FDR-corrected; $p < 0.05$; **Figure 4A**). Together with the distinctly lower number voxels with temporally increasing SUVR to GLM scaling, 156,066 voxels in the hindbrain (pons, midbrain, and cerebellum) indicated an implausible decrease for SUVR from BL to FU (FDR-corrected; $p < 0.05$; **Figure 4B**). No amyloid or vascular pathology is known in these regions in PS2APP mice, nor were there any plausible physiological or pathophysiological explanations for a marked apparent decrease in the relative decrease in the hindbrain Aβ-PET signal in a 6 weeks' follow-up. No significantly changing voxels were found when performing SPM with raw SUV images.

Intensity Scaling by Intracerebral Reference Regions Gives Superior Agreement with Histology Compared to SUV, and is Further Improved by Automated Brain Spatial Normalization

The cortical plaque load (%) in $N = 40$ PS2APP aged 13–16 months mice was 10.8 ± 1.2%. The correlation between Aβ-PET and plaque load (%) was poor ($R \leq 0.34$, $p < 0.05$) for the case of plain SUV_{CTX} (**Figure 5A**), and consistent significantly lower when compared to any intensity scaling to intracerebral reference regions (all $p < 0.001$). $SUVR_{CTX/REF}$ estimates (**Figure 5B**) revealed a high correlation ($R \geq 0.66$, $p < 0.001$) with plaque load (%) in this homogeneous sample of PS2APP mice regardless of the operator training status, or application of automated brain spatial normalization. Without automated brain normalization, the correlation to histology of the manual coregistration by the novice reader was significantly lower ($R_{max} = 0.70$) when compared to the expert ($R_{max} = 0.78$; $p < 0.01$) or experienced reader ($R_{max} = 0.76$; $p < 0.05$). Application of spatial brain normalization harmonized this correlation between different readers ($R_{max} = 0.75$–0.76; no significant differences between readers). In this regard, manual coregistration by the novice reader was significantly improved by automated brain normalization (all reference regions: $p < 0.05$), whereas the changes for the expert and experienced reader did not show any significant alterations (all reference regions: p = n.s.). Scaling to WM or GLM ($R_{mean} = 0.75$) was slightly superior (p = n.s.) to BST ($R_{mean} = 0.74$) or CBL ($R_{mean} = 0.73$). All correlations are provided in **Table 3**.

Best Global Performance is Archived by Hindbrain White Matter Intensity Scaling

Based on the different analyses (brain normalization, group analysis, longitudinal assessment, and correlation with histology as the gold standard) we defined five categories, which need to be addressed when considering the optimal intensity scaling for [^{18}F]-florbetaben Aβ-PET imaging in mice (**Table 4**). (1) The impact of single animal results analyzed by templates used for automated brain normalization should be minimal, but this was not the case for cerebellar and global mean intensity scaling. (2) Variance in groups of mice should not be artifactually raised by the method, which was the case for raw SUV_{CTX}. (3) The effect sizes regarding longitudinal progression of amyloidosis

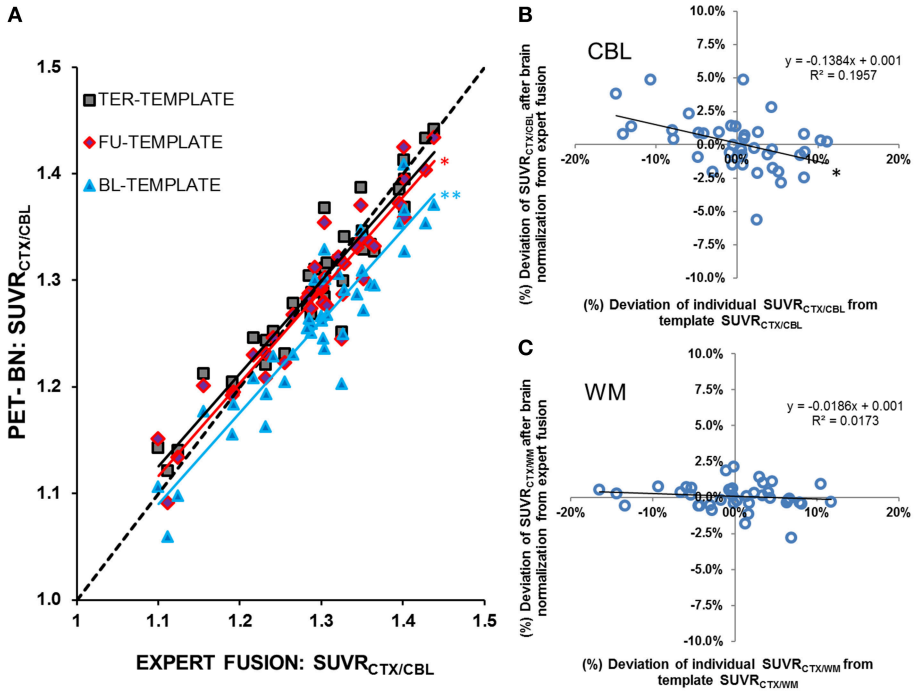

FIGURE 3 | (A) $SUVR_{CTX/CBL}$ from $N = 40$ PS2APP mice aged 13–16 months after brain spatial normalization to a stage-specific (high) tracer uptake template (TER-TEMPLATE, black-gray squares), an intermediate tracer uptake template (FU-TEMPLATE, red-purple diamonds) and a low tracer uptake template (BL-TEMPLATE, blue triangles). Lower uptake templates gave systematic underestimation of $SUVR_{CTX/CBL}$ after automated brain normalization when compared to expert fusion. With the stage-specific template, minor underestimations were observed for high $SUVR_{CTX/CBL}$ and *vice versa*. Dashed line represents the line of perfect identity ($R = 1$) between raw expert fusion and brain normalization). Significant differences (paired *t*-test) resulting from template mismatches vs. the stage specific TER-template are indicated by $^{*}p < 0.05$; $^{**}p < 0.001$. Relationships between (%)-deviations of individual $SUVR_{CTX/REF}$ from the template $SUVR_{CTX/REF}$ and the (%)-deviation of $SUVR_{CTX/REF}$ from the expert manual fusion after the brain normalization are illustrated for **(B)** the cerebellar and **(C)** the hindbrain white matter reference region. Significant correlation is indicated by $^{*}p < 0.01$.

TABLE 2 | Longitudinal 6-week follow-up.

	BL MEAN	BL SD (%)	FU MEAN	FU SD (%)	*d*	*R*
SUV_{CTX}	0.48	0.08 (15.9%)	0.50	0.07 (13.2%)	0.23	–0.12
$SUVR_{CTX/CBL}$	1.10	0.04 (3.6%)	1.16	0.05 (4.4%)	1.23	0.51
$SUVR_{CTX/WM}$	0.92	0.03 (3.1%)	0.98	0.04 (4.1%)	1.64	0.64
$SUVR_{CTX/BST}$	0.90	0.03 (3.6%)	0.96	0.04 (4.6%)	1.64	0.60
$SUVR_{CTX/GLM}$	1.06	0.02 (2.3%)	1.10	0.04 (3.4%)	1.21	0.63

Results from the longitudinal 6 week follow-up in (N = 37) PS2APP mice. Mean cortical FBB PET values and their SD are given for BL and FU scans for the different scaling methods together with the Cohen's effect size (d) and BL-FU correlation (R).

in the frontal cortical target region should be captured as best possible, which was the case for hindbrain white matter and brainstem intensity scalings. (4) Longitudinal results should not be affected by presence of amyloid pathology in the reference region, which was the case for the global mean intensity scaling. (5) Aβ-PET signal in single animals should correlate as best possible with the histological gold standard, which was the case for all intracerebral reference regions. There was trend toward better agreement for hindbrain white matter and global mean intensity scaling, compared to cerebellum or brainstem scaling. Thus, in summary the hindbrain white matter scaling performed best when considering the composite of factors.

DISCUSSION

We present a large-scale evaluation of automated spatial brain normalization and a systematic comparison of different intensity scaling methods for preclinical Aβ-PET imaging with FBB. Our established Aβ-PET methodologies were challenged by investigation of a homogeneous PS2APP data set, including a short-term longitudinal follow-up, and histologically validated gold standard results, all characterized by a rather narrow range of plaque burden; this bodes well for sensitive detection of treatment effects. Automated spatial brain normalization reliably harmonized the results of different

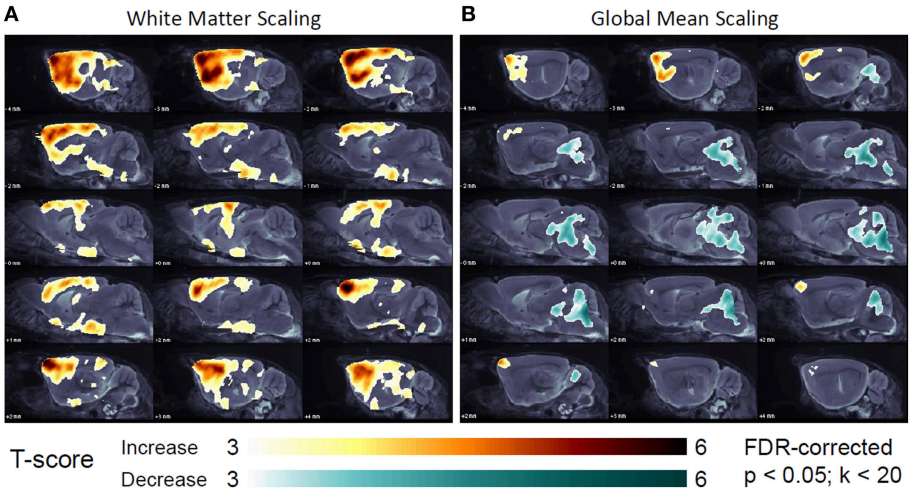

FIGURE 4 | Longitudinal changes in regional [^{18}F]-florbetaben uptake in the short-term 6 week follow-up, study of ($N = 37$) PS2APP mice after intensity scaling to the hindbrain white matter **(A)** and the global mean uptake **(B)** as assessed by SPM (FDR-corrected; $p < 0.05$; $k < 20$). T-contrasts expressing significant longitudinal increases (yellow-red) and decreases (turquois-green) are projected upon sagittal slices of the MRI mouse brain atlas.

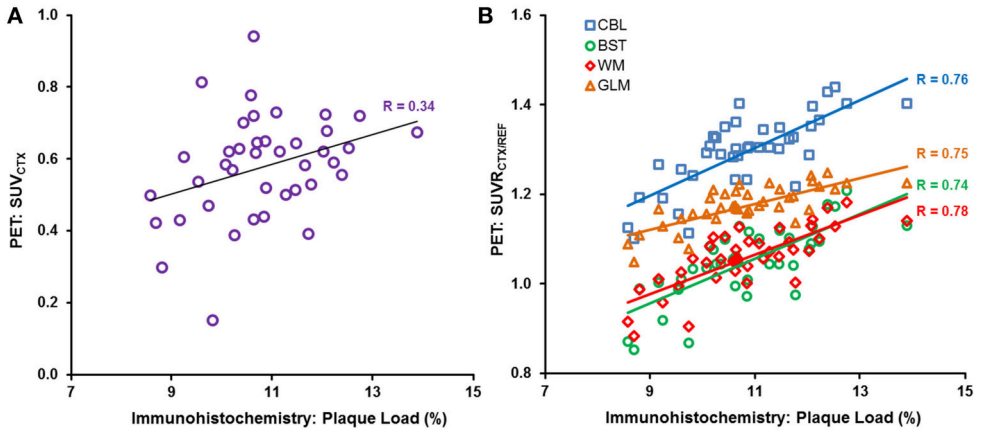

FIGURE 5 | Individual **(A)** SUV_{CTX} and **(B)** $SUVR_{CTX/REF}$ PET correlations (expert manual fusion) with gold standard plaque load (%), as assessed by histochemistry, in ($N = 40$) PS2APP mice aged 13–16 months, are illustrated for SUV_{CTX} (purple circles) and the different reference regions, i.e., cerebellum (CBL, blue squares), hindbrain white matter (WM, red diamonds), brain stem (BST, green circles), and global mean (GLM, orange triangle).

readers even if poorly trained, while the correspondence with histological gold standard assessments remained stable or even improved. Scaling by intracerebral reference regions ($SUVR_{CTX/REF}$) was distinctly superior to plain SUV_{CTX}, both with regard to longitudinal stabilization and agreement with histology. Global mean intensity scaling revealed a comparable correlation with histology when contrasted to reference regions demonstrably devoid of Aβ pathology, but this procedure impaired detection of longitudinal increases in Aβ in cortex, and returned physiologically implausible decreases in brain regions lacking Aβ burden. A hindbrain white matter reference was slightly superior to the cerebellar reference due, we suppose, to lesser bias from bone uptake and template differences.

Automated Brain Normalization

While small animal Aβ-PET studies experienced growing interest in the recent years the methodological tools used for their interpretation were rather heterogeneous. Spatial normalization has hitherto mostly been done on MRI templates (Poisnel et al., 2012; von Reutern et al., 2013), or with a hybrid PET-CT apparatus (Snellman et al., 2013). One previous investigation of this type used SPM-based automated brain normalization (Rojas et al., 2013), and in most studies, the tracer uptake was scaled to a cerebellum reference region (Maeda et al., 2007; Kuntner et al., 2009; Manook et al., 2012; Poisnel et al., 2012; Snellman et al., 2013), although some have employed plain SUV for their analyses (Waldron et al., 2015). However, with respect to the small effect sizes to brief follow-up in AD mice, and the susceptibility of

TABLE 3 | Histology agreement.

Reader	Expert		Experienced		Novice	
RAW/BN	**RAW**	**BN**	**RAW**	**BN**	**RAW**	**BN**
SUV_{CTX}	0.34**	0.34**	0.34**	0.34**	0.32**	0.31**
$SUVR_{CTX/CBL}$	0.76	0.75	0.76	0.74	0.66*	0.74
$SUVR_{CTX/WM}$	0.78	0.76	0.76	0.76	0.69*	0.75
$SUVR_{CTX/BST}$	0.74	0.74	0.74	0.73	0.70*	0.73
$SUVR_{CTX/GLM}$	0.75	0.76	0.76	0.76	0.70*	0.75

*Correlations (R) with plaque load (%) as assessed by histochemistry for expert, experienced and novice reader for the different scaling methods before (RAW) and after brain normalization (BN). Significant differences between correlation coefficients are indicated for SUV_{CTX} vs. any $SUVR_{CTX/REF}$ and for raw fusions vs. brain normalizations of the same reader *p< 0.05; **p< 0.001.*

TABLE 4 | Intensity scaling summary.

	Template affection	Variance	Longitudinal effect size	Pathology affection	Histology
SUV_{CTX}	o	–	–	o	–
$SUVR_{CTX/CBL}$	–	+	+	o	+
$SUVR_{CTX/WM}$	o	+	++	o	+(+)
$SUVR_{CTX/BST}$	o	+	++	o	+
$SUVR_{CTX/GLM}$	–	+	+	–	+(+)

Significant advantages (moderate: +, light green; large: ++, dark green)/disadvantages (–, light red) of different SUV_{CTX} and SUVR calculations are illustrated in five categories, which are deemed relevant for analysis of [^{18}F]-florbetaben measurements in the mouse brain. "o" indicate neutral condition; bracketed "+" indicate a trend to advantage. "Template affection" refers to results Section Template Characteristics Influence Brain Normalization Results. "Variance" refers to result Section Intracerebral Reference Regions give Lower Variance and Higher Longitudinal Effect Sizes When Compared to SUV. "Longitudinal effect size" refers to result Section Intracerebral Reference Regions Give Lower Variance and Higher Longitudinal Effect Sizes When Compared to SUV. "Pathology affection" refers to result Section Global Mean Scaling Gives Physiologically Implausible Longitudinal Intensity Decreases in the Hindbrain. "Histology" refers to result Section Intensity Scaling by Intracerebral Reference Regions Gives Superior Agreement with Histology Compared to SUV, and is Further Improved by Automated Brain Spatial Normalization.

our SUV_{CTX} results to methodological inaccuracies, it is crucial that Aβ-PET data be analyzed with robust, reliable and reader-independent strategies, so as to ensure accuracy of the study outcomes.

To our knowledge there have not been any studies systematically investigating the inter-reader variability as a limitation of small animal Aβ-PET studies, or indeed for any other classes of radioligand. Our investigations were able to show that manual coregistration of Aβ-PET images contributes substantially to variation of results between readers, especially when they have less experience. A further disadvantage of a manual approach arises from the blinding which is necessary for preclinical drug trials (Jucker, 2010). Thus, an experienced reader is usually able to visually identify animals with different extent of the Aβ pathology. So even if differing groups are blinded to the reader, the visual impressions of the images potentially influence the reader. The automated brain normalization diminishes the impact of these influences toward zero as $SUVR_{CTX/REF}$ values show nearly perfect inter-reader agreement after processing as inter-reader differences were significantly lowered by the method (**Figure 2**). Thus, the brain normalization brings about a pseudo-blinding for small animal Aβ-PET analysis, and guarantees minimization of inter-reader variance.

While aiming to improve the inter-reader agreement, the automated brain normalization method should not reduce the ultimate correlation between the PET endpoint with the histological gold standard of amyloid burden. Our results clearly indicate that correlation coefficients of PET results with plaque burden remain equal after brain spatial normalization for well-trained readers, whereas the agreement between PET and histology is significantly improved for less trained operators (**Table 3**): this is an important precondition for stable results in longitudinal or multicentre studies.

We also observed an effect of applying Aβ-PET templates at different pathology stages. Although this effect was never more than 2.9% of the group mean, this avoidable systematic error could potentially bias Aβ-PET outcomes in treatment studies with small effect sizes (Balducci et al., 2014; Brendel et al., 2015c). This bias of inappropriate templates is unsurprising, as automated brain normalization orientates mainly at edges and high uptake regions of the image (Gispert et al., 2003). High plaque burden in the forebrain results in a cortical hot-spot and sharper cortex-to-extracortical contrasts for Aβ-PET mouse brain images, which influences the quality of spatial normalization when this hot region is absent from the utilized template or *vice versa*. In practice, this mismatch tends to shrink the scaled PET image, leading to underestimation in mice with higher plaque burden than in the template and an overestimation in mice with lower plaque burden. Interestingly $SUVR_{CTX/WM}$ and $SUVR_{CTX/BST}$ suffered a lower bias (<2% relative to the deviation of the individual Aβ-PET image to its template) when compared to $SUVR_{CTX/CBL}$ and $SUVR_{CTX/GLM}$ (>10% relative to the deviation of the individual Aβ-PET to its template), supporting the preferred use of the WM and BST reference regions (**Figure 3**), with matching of stage/age. Furthermore, transient smoothing of the input image with a 0.6 mm filter proved indispensable to avoid strong distortions in the automated spatial normalization.

Intensity Scaling Methods

Variance of plain SUV_{CTX} was rather high in BL and FU groups of this investigation (15.9/13.2%), thus indicating inadequate intensity scaling of Aβ-PET images by this method. Well-known sources of error in the SUV_{CTX} calculation include paravenous leakage of the injectate, variability in brain perfusion, and imprecise measurement of radiotracer dosage. We typically calculate injected dose by well-counting syringes before and after tracer application, whereas measurement of the injected dose in a whole body VOI can be more precise (Rominger et al., 2013). However, our scanning configuration does not always capture the entire body of the mice. While SUV measurements are improved with arterial blood sampling, this is inherently linked with a high logistic and economic effort, scarcely feasible in a longitudinal setting. Our SUV_{CTX} findings were distinctly inferior to the several $SUVR_{CTX/REF}$ results, with respect both to longitudinal

and histological validation analyses. Thus, SUV methods are not to be recommended for preclinical Aβ-PET studies.

Having ascertained the need to make SUVR calculations, we need to identify the optimal reference region for intensity scaling. Since a whole brain VOI is easily obtained, scaling to the global mean brain uptake is convenient. Indeed we find a high correlation between $SUVR_{CTX/GLM}$ and the histological gold standard of Aβ accumulation. However, when large parts of the brain are affected by the amyloid pathology, the denominator for scaling is of course raised by the high tracer retention. This resulted in the spurious detection of declining relative FBB uptake in the hindbrain to follow-up at 6 weeks, an artifact that could mimic a real clearance of fibrillar Aβ in longitudinal interventional designs. Furthermore, global mean scaling attenuated the apparent cluster size and effect size for increases in Aβ in the longitudinal part of the study, relative to findings with scaling to reference regions expected to be devoid of Aβ pathology. Our findings are supported by earlier [^{18}F]-FDG-PET investigations of metabolic rate in human brain, in relation to artifactual findings arising as a consequence of global normalization (Borghammer et al., 2009). Scaling to [^{18}F]-FDG uptake in a reference cluster unaffected by pathology clearly improved the detection of zones of true hypometabolism in patients with AD or fronto-temporal dementia (Yakushev et al., 2009; Dukart et al., 2013). Thus, we are confident that scaling by reference regions devoid of plaque pathology should perform best for detection of Aβ in the present mouse study.

In most transgenic mouse models, the hindbrain remains relatively unaffected by Aβ plaque accumulation (Teipel et al., 2011), but due to the characteristically high retention of [^{18}F]-labeled Aβ tracers in white matter, the binding in hindbrain regions is quite heterogeneous. With regard to FBB-PET, we see low non-specific binding in the cerebellum (Rominger et al., 2013), which led to our adoption of cerebellum as a reference region in small animal Aβ-PET analysis for this and related ligands (Manook et al., 2012). While the cerebellum can serve as an accurate reference region, it remains vulnerable to spill-in from the overlying cranium and adjacent vascular structures (Mille et al., 2012). In addition, cerebellum VOIs are at risk for contamination from non-cerebral voxels, if the caudal border of the brain is not captured precisely. Together, these factors probably account for instances of false high and false low $SUVR_{CTX/CBL}$; resultant higher variance especially in longitudinal analyses of $SUVR_{CTX/CBL}$ are responsible for the lower correlation between BL and FU in the present longitudinal arm, as compared to the more precise findings with $SUVR_{CTX/WM}$ or $SUVR_{CTX/BST}$. While spill-over and imperfect capture of the caudal brain edges are less of an issue for human Aβ-PET, WM reference scaling seems to give more stable results to follow-up than does cerebellum scaling (Chen et al., 2015; Brendel et al., 2015a). Similarly, the highest effect size ($d = 1.64$) in the present 6-week longitudinal setting was observed for $SUVR_{CTX/WM}$ and $SUVR_{CTX/BST}$.

The whole point of Aβ-PET is to depict accurately the plaque load. We designed the present study to test the limits of sensitivity of the method, by examining reference tissue methods in a cohort of PS2APP mice with rather narrow inter-individual range in plaque load (8.6–13.9%). This is in comparison to the ten-fold range used in previous mouse studies of the correlation between Aβ-PET and histological plaque load (1.0–9.2%, 0.3–13.3%; Manook et al., 2012; Rominger et al., 2013). Results with all intracerebral reference regions correlated highly with the histological gold standard, although WM normalization gave a slightly higher correlation. The slight superiority of $SUVR_{CTX/WM}$ over $SUVR_{CTX/BST}$ can be explained by the larger volume, giving less statistical noise in the results. The slight superiority of $SUVR_{CTX/WM}$ over $SUVR_{CTX/CBL}$, attributed above to imperfect delineation of the caudal limit of the brain, is also demonstrated by the lower correlation of $SUVR_{CTX/CBL}$ by the novice reader with histology ($R = 0.66$); visual interpretation of caudal limit of the fusion images is a matter of skill-learning.

In summary, $SUVR_{CTX/WM}$ performed best for the detection of Aβ by PET in transgenic mice, which should prove advantageous in preclinical imaging studies of longitudinal design (**Table 4**). Thus, quantitation of [^{18}F]-florbetaben uptake in interventional trials, where accurate monitoring in single animals is mandatory, can be improved implementing hindbrain white matter intensity scaling, in conjunction with automated spatial normalization.

Limitations

As mentioned above, we did not use the best possible means to measure the injected FBB dose; we suppose that whole mouse VOIs would have propagated to better correlations of SUV_{CTX} with the histological gold standard. While our PS2APP mice are characterized by almost complete absence of Aβ pathology in the hindbrain, present findings are not translatable to mouse models, which may express relevant Aβ plaque burden in the reference regions tested in this paper. Thus, prior knowledge about the regional deposition of Aβ is indispensable for appropriate selection of the reference in preclinical Aβ-PET studies with FBB or related tracers.

Excessive reliance on automated methods for spatial normalization of mouse brain should be avoided. Although we did not detect any failures of the method, they might still occur, were artificial hot spots present in the image. Thus, we saw distinctly more cases of image distortions, especially in brains with more heterogenous FBB uptake, in the absence of transient input smoothing. As in all PET studies, it is important to visually control post-processed images for potentially failed spatial normalizations. In consideration of this issue, we first attempted automated brain normalization with larger templates (data not shown) encompasing adjacent extracerebral regions, so as to support a correction of effects of partial volume (Brendel et al., 2014). This approach yielded some excessive distortions of the brain, when the VOI extended to include sources in the neck or spine. We note that templates fulfilling the differing requirements for partial volume effect correction and automated brain normalization remain to be validated.

CONCLUSION

Automated spatial normalization of mouse brain can be applied to Aβ-PET studies with FBB, thus ensuring pseudo-blinding,

and by eliminating inter-reader variability due to differing skill learning. This improves the reproducibility of the endpoint, even if the reader is poorly trained. Intracerebral reference regions lacking Aβ pathology are necessary for accurate *in vivo* quantification of Aβ-PET with FBB; use of a hindbrain WM reference tissue gave the best performance predominately due to advantages in longitudinal designs. SUV_{CTX} generation and global mean scaling were distinctly inferior in performance to the intensity scaling by pathology-free intracerebral reference regions.

AUTHOR CONTRIBUTIONS

FO carried out the PET experiments, performed the data analysis, and drafted the manuscript; MB participated in the design of the study, contributed to global data analysis, performed the statistical analysis, and drafted the manuscript; AJ carried out the histological experiments, performed the histological data analysis, and drafted the manuscript; VK carried out the histological experiments, and performed the histological data analysis; AD performed statistical programming and analysis; FP carried out the PET experiments, and performed the PET data analysis; CF carried out the PET experiments, and performed the PET data analysis; FG carried out the radiochemistry; JC participated in the PET experiments and helped to draft the manuscript; KB participated in the design of the study and helped to draft the manuscript; CH participated in the design of the study and increased the intellectual content; PB participated in the design of the study and helped to draft the manuscript; JH conceived of the study, and participated in its design and coordination and drafted the manuscript; AR conceived of the study, and participated in its design and coordination, contributed to interpretation of the data and drafted the manuscript. All authors read and approved the final manuscript.

FUNDING

The study was financially supported by the SyNergy Cluster (Core 2 project). AJ was supported by the Foundation for Polish Science within the International PhD Project "Studies of nucleic acids and proteins—from basic to applied research," co-financed by European Union—Regional Development Fund (MPD/2009-3/2).

ACKNOWLEDGMENTS

A part of this paper originated from the doctoral thesis of FO. We thank Karin Bormann-Giglmaier and Rosel Oos for excellent technical assistance. Florbetaben precursor was kindly provided by Piramal Imaging. The authors acknowledge Inglewood Biomedical Editing for professional editing of the manuscript.

REFERENCES

Balducci, C., Mancini, S., Minniti, S., La Vitola, P., Zotti, M., Sancini, G., et al. (2014). Multifunctional liposomes reduce brain beta-amyloid burden and ameliorate memory impairment in Alzheimer's disease mouse models. *J. Neurosci.* 34, 14022–14031. doi: 10.1523/JNEUROSCI.0284-14.2014

Barthel, H., and Sabri, O. (2011). Florbetaben to trace amyloid-beta in the Alzheimer brain by means of PET. *J. Alzheimers Dis.* 26, 117–121. doi: 10.3233/JAD-2011-0068

Borghammer, P., Cumming, P., Aanerud, J., Förster, S., and Gjedde, A. (2009). Subcortical elevation of metabolism in Parkinson's disease–a critical reappraisal in the context of global mean normalization. *Neuroimage* 47, 1514–1521. doi: 10.1016/j.neuroimage.2009.05.040

Brendel, M., Delker, A., Rotzer, C., Boning, G., Carlsen, J., Cyran, C., et al. (2014). Impact of partial volume effect correction on cerebral beta-amyloid imaging in APP-Swe mice using [(18)F]-florbetaben PET. *Neuroimage* 84, 843–853. doi: 10.1016/j.neuroimage.2013.09.017

Brendel, M., Högenauer, M., Delker, A., Sauerbeck, J., Bartenstein, P., Seibyl, J., et al. (2015a). Improved longitudinal [(18)F]-AV45 amyloid PET by white matter reference and VOI-based partial volume effect correction. *Neuroimage* 108, 450–459. doi: 10.1016/j.neuroimage.2014.11.055

Brendel, M., Jaworska, A., Griessinger, E., Rotzer, C., Burgold, S., Gildehaus, F. J., et al. (2015b). Cross-sectional comparison of small animal [18F]-florbetaben amyloid-PET between transgenic AD mouse models. *PLoS ONE* 10:e0116678. doi: 10.1371/journal.pone.0116678

Brendel, M., Jaworska, A., Herms, J., Trambauer, J., Rötzer, C., Gildehaus, F. J., et al. (2015c). Amyloid-PET predicts inhibition of *de novo* plaque formation upon chronic gamma-secretase modulator treatment. *Mol. Psychiatry* 20, 1179–1187. doi: 10.1038/mp.2015.74

Chen, K., Roontiva, A., Thiyyagura, P., Lee, W., Liu, X., Ayutyanont, N., et al. (2015). Improved power for characterizing longitudinal amyloid-beta PET changes and evaluating amyloid-modifying treatments with a cerebral white matter reference region. *J. Nucl. Med.* 56, 560–566. doi: 10.2967/jnumed.114.149732

Clark, C. M., Schneider, J. A., Bedell, B. J., Beach, T. G., Bilker, W. B., Mintun, M. A., et al. (2011). Use of florbetapir-PET for imaging beta-amyloid pathology. *JAMA* 305, 275–283. doi: 10.1001/jama.2010.2008

Dorr, A., Sled, J. G., and Kabani, N. (2007). Three-dimensional cerebral vasculature of the CBA mouse brain: a magnetic resonance imaging and micro computed tomography study. *Neuroimage* 35, 1409–1423. doi: 10.1016/j.neuroimage.2006.12.040

Dukart, J., Perneczky, R., Förster, S., Barthel, H., Diehl-Schmid, J., Draganski, B., et al. (2013). Reference cluster normalization improves detection of frontotemporal lobar degeneration by means of FDG-PET. *PLoS ONE* 8:e55415. doi: 10.1371/journal.pone.0055415

Gispert, J. D., Pascau, J., Reig, S., Martínez-Lázaro, R., Molina, V., García-Barreno, P., et al. (2003). Influence of the normalization template on the outcome of statistical parametric mapping of PET scans. *Neuroimage* 19, 601–612. doi: 10.1016/S1053-8119(03)00072-7

Johnson, K. A., Minoshima, S., Bohnen, N. I., Donohoe, K. J., Foster, N. L., Herscovitch, P., et al. (2013). Appropriate use criteria for amyloid PET: a report of the amyloid imaging task force, the society of nuclear medicine and molecular imaging, and the Alzheimer's association. *J. Nucl. Med.* 54, 476–490. doi: 10.2967/jnumed.113.120618

Jucker, M. (2010). The benefits and limitations of animal models for translational research in neurodegenerative diseases. *Nat. Med.* 16, 1210–1214. doi: 10.1038/nm.2224

Kuntner, C., Kesner, A. L., Bauer, M., Kremslehner, R., Wanek, T., Mandler, M., et al. (2009). Limitations of small animal PET imaging with [18F]FDDNP and FDG for quantitative studies in a transgenic mouse model of Alzheimer's disease. *Mol. Imaging Biol.* 11, 236–240. doi: 10.1007/s11307-009-0198-z

Landau, S. M., Fero, A., Baker, S. L., Koeppe, R., Mintun, M., Chen, K., et al. (2015). Measurement of longitudinal beta-amyloid change with 18F-florbetapir

PET and standardized uptake value ratios. *J. Nucl. Med*. 56, 567–574. doi: 10.2967/jnumed.114.148981

Landau, S. M., Thomas, B. A., Thurfjell, L., Schmidt, M., Margolin, R., Mintun, M., et al. (2014). Amyloid PET imaging in Alzheimer's disease: a comparison of three radiotracers. *Eur. J. Nucl. Med. Mol. Imaging* 41, 1398–1407. doi: 10.1007/s00259-014-2753-3

Lee, I. A., and Preacher, K. J. (2013). *Calculation for the Test of the Difference between two Dependent Correlations with One Variable in Common*. Available online at: http://quantpsy.org

Maeda, J., Ji, B., Irie, T., Tomiyama, T., Maruyama, M., Okauchi, T., et al. (2007). Longitudinal, quantitative assessment of amyloid, neuroinflammation, and anti-amyloid treatment in a living mouse model of Alzheimer's disease enabled by positron emission tomography. *J. Neurosci*. 27, 10957–10968. doi: 10.1523/JNEUROSCI.0673-07.2007

Manook, A., Yousefi, B. H., Willuweit, A., Platzer, S., Reder, S., Voss, A., et al. (2012). Small-animal PET imaging of amyloid-beta plaques with [11C]PiB and its multi-modal validation in an APP/PS1 mouse model of Alzheimer's disease. *PLoS ONE* 7:e31310. doi: 10.1371/journal.pone.0031310

Mille, E., Cumming, P., Rominger, A., La Fougère, C., Tatsch, K., Wangler, B., et al. (2012). Compensation for cranial spill-in into the cerebellum improves quantitation of striatal dopamine D(2)/(3) receptors in rats with prolonged [(1)(8)F]-DMFP infusions. *Synapse* 66, 705–713. doi: 10.1002/syn.21558

Ozmen, L., Albientz, A., Czech, C., and Jacobsen, H. (2009). Expression of transgenic APP mRNA is the key determinant for beta-amyloid deposition in PS2APP transgenic mice. *Neurodegener. Dis.* 6, 29–36. doi: 10.1159/000170884

Poisnel, G., Dhilly, M., Moustie, O., Delamare, J., Abbas, A., Guilloteau, D., et al. (2012). PET imaging with [18F]AV-45 in an APP/PS1-21 murine model of amyloid plaque deposition. *Neurobiol. Aging* 33, 2561–2571. doi: 10.1016/j.neurobiolaging.2011.12.024

Richards, J. G., Higgins, G. A., Ouagazzal, A. M., Ozmen, L., Kew, J. N., Bohrmann, B., et al. (2003). PS2APP transgenic mice, coexpressing hPS2mut and hAPPswe, show age-related cognitive deficits associated with discrete brain amyloid deposition and inflammation. *J. Neurosci*. 23, 8989–9003.

Rohlfing, T., Sullivan, E. V., and Pfefferbaum, A. (2009). Subject-matched templates for spatial normalization. *Med. Image Comput. Comput. Assist. Interv*. 12(Pt 2), 224–231. doi: 10.1007/978-3-642-04271-3_28

Rojas, S., Herance, J. R., Gispert, J. D., Abad, S., Torrent, E., Jimenéz, X., et al. (2013). *In vivo* evaluation of amyloid deposition and brain glucose metabolism of 5XFAD mice using positron emission tomography. *Neurobiol. Aging* 34, 1790–1798. doi: 10.1016/j.neurobiolaging.2012.12.027

Rominger, A., Brendel, M., Burgold, S., Keppler, K., Baumann, K., Xiong, G., et al. (2013). Longitudinal assessment of cerebral β-amyloid deposition in mice overexpressing Swedish mutant β-amyloid precursor protein using 18F-florbetaben PET. *J. Nucl. Med*. 54, 1127–1134. doi: 10.2967/jnumed.112.114660

Sawiak, S. J., Wood, N. I., Williams, G. B., Morton, A. J., and Carpenter, T. A. (2009). Voxel-based morphometry in the R6/2 transgenic mouse reveals differences between genotypes not seen with manual 2D morphometry. *Neurobiol. Dis*. 33, 20–27. doi: 10.1016/j.nbd.2008.09.016

Schneider, L. S. (2013). Alzheimer disease pharmacologic treatment and treatment research. *Continuum (Minneap Minn)* 19, 339–357.

Snellman, A., Lopez-Picon, F. R., Rokka, J., Salmona, M., Forloni, G., Scheinin, M., et al. (2013). Longitudinal amyloid imaging in mouse brain with 11C-PIB: comparison of APP23, Tg2576, and APPswe-PS1dE9 mouse models of Alzheimer disease. *J. Nucl. Med*. 54, 1434–1441. doi: 10.2967/jnumed.112.110163

Teipel, S. J., Buchert, R., Thome, J., Hampel, H., and Pahnke, J. (2011). Development of Alzheimer-disease neuroimaging-biomarkers using mouse models with amyloid-precursor protein-transgene expression. *Prog. Neurobiol.* 95, 547–556. doi: 10.1016/j.pneurobio.2011.05.004

Vandenberghe, R., Van Laere, K., Ivanoiu, A., Salmon, E., Bastin, C., Triau, E., et al. (2010). 18F-flutemetamol amyloid imaging in Alzheimer disease and mild cognitive impairment: a phase 2 trial. *Ann. Neurol*. 68, 319–329. doi: 10.1002/ana.22068

von Reutern, B., Grünecker, B., Yousefi, B. H., Henriksen, G., Czisch, M., and Drzezga, A. (2013). Voxel-based analysis of amyloid-burden measured with [(11)C]PiB PET in a double transgenic mouse model of Alzheimer's disease. *Mol. Imaging Biol*. 15, 576–584. doi: 10.1007/s11307-013-0625-z

Waldron, A. M., Wyffels, L., Verhaeghe, J., Bottelbergs, A., Richardson, J., Kelley, J., et al. (2015). Quantitative muPET imaging of cerebral glucose metabolism and amyloidosis in the TASTPM double transgenic mouse model of alzheimer's disease. *Curr. Alzheimer Res.* 12, 694–703. doi: 10.2174/1567205012666150710104713

Yakushev, I., Hammers, A., Fellgiebel, A., Schmidtmann, I., Scheurich, A., Buchholz, H. G., et al. (2009). SPM-based count normalization provides excellent discrimination of mild Alzheimer's disease and amnestic mild cognitive impairment from healthy aging. *Neuroimage* 44, 43–50. doi: 10.1016/j.neuroimage.2008.07.015

Zhang, W., Oya, S., Kung, M. P., Hou, C., Maier, D. L., and Kung, H. F. (2005). F-18 stilbenes as PET imaging agents for detecting beta-amyloid plaques in the brain. *J. Med. Chem*. 48, 5980–5988. doi: 10.1021/jm050166g

Conflict of Interest Statement: KB is an employee of F. Hoffmann-La Roche; PB received consultant fees from GE and Piramal Imaging, and honoraria from Siemens; AR received consultant fees from Piramal Imaging and GE. The other authors declare that the research was conducted in the absence of any commercial or financial relationships that could be construed as a potential conflict of interest.

IVYSPRING INTERNATIONAL PUBLISHER

Theranostics

2018; 8(18): 4957-4968. doi: 10.7150/thno.27868

Research Paper

Efficacy of chronic BACE1 inhibition in PS2APP mice depends on the regional Aβ deposition rate and plaque burden at treatment initiation

Matthias Brendel[1], Anna Jaworska[2,3], Felix Overhoff[1], Tanja Blume[1,2], Federico Probst[1], Franz-Josef Gildehaus[1], Peter Bartenstein[1,4], Christian Haass[2,4,5], Bernd Bohrmann[6], Jochen Herms[2,4], Michael Willem[5], Axel Rominger[1,4,7]✉

1. Department of Nuclear Medicine, University Hospital, LMU Munich; Munich, Germany
2. DZNE – German Center for Neurodegenerative Diseases, Munich, Germany
3. Laboratory of Neurodegeneration, International Institute of Molecular and Cell Biology, Warsaw, Poland
4. Munich Cluster for Systems Neurology (SyNergy), Munich, Germany
5. Biomedical Center (BMC), Ludwig-Maximilians-University Munich, 81377 Munich, Germany
6. F. Hoffmann-La Roche, Basel, Switzerland
7. Department of Nuclear Medicine, Inselspital, University Hospital Bern, Bern, Switzerland.

✉ Corresponding author: Prof. Dr. Axel Rominger, Department of Nuclear Medicine, University Hospital Bern, Switzerland. Phone: +41 31 632 2610; Fax: +41 31 632 7663; E-Mail: axel.rominger@insel.ch

Received: 2018.06.13; Accepted: 2018.08.14; Published: 2018.09.09

Abstract

Beta secretase (BACE) inhibitors are promising therapeutic compounds currently in clinical phase II/III trials. Preclinical [^{18}F]-florbetaben (FBB) amyloid PET imaging facilitates longitudinal monitoring of amyloidosis in Alzheimer's disease (AD) mouse models. Therefore, we applied this theranostic concept to investigate, by serial FBB PET, the efficacy of a novel BACE1 inhibitor in the PS2APP mouse, which is characterized by early and massive amyloid deposition.

Methods: PS2APP and C57BL/6 (WT) mice were assigned to treatment (PS2APP: N=13; WT: N=11) and vehicle control (PS2APP: N=13; WT: N=11) groups at the age of 9.5 months. All animals had a baseline PET scan and follow-up scans at two months and after completion of the four-month treatment period. In addition to this longitudinal analysis of cerebral amyloidosis by PET, we undertook biochemical amyloid peptide quantification and histological amyloid plaque analyses after the final PET session.

Results: BACE1 inhibitor-treated transgenic mice revealed a progression of the frontal cortical amyloid signal by 8.4 ± 2.2% during the whole treatment period, which was distinctly lower when compared to vehicle-treated mice (15.3 ± 4.4%, $p<0.001$). A full inhibition of progression was evident in regions with <3.7% of the increase in controls, whereas regions with >10% of the increase in controls showed only 40% attenuation with BACE1 inhibition. BACE1 inhibition in mice with lower amyloidosis at treatment initiation showed a higher efficacy in attenuating progression to PET. A predominant reduction of small plaques in treated mice indicated a main effect of BACE1 on inhibition of *de novo* amyloidogenesis.

Conclusions: This theranostic study with BACE1 treatment in a transgenic AD model together with amyloid PET monitoring indicated that progression of amyloidosis is more effectively reduced in regions with low initial plaque development and revealed the need of an early treatment initiation during amyloidogenesis.

Key words: BACE1 inhibitor, transgenic AD mouse model, [^{18}F]-florbetaben PET, amyloid deposition rate

Introduction

Alzheimer's disease (AD) is the most common form of neurodegenerative dementia, and has an enormous impact on societies with aging populations [1]. The core histopathological features for diagnosis of AD consist of neurofibrillary tangles and amyloid plaques [2], which can now be assessed by molecular imaging *in vivo* [3, 4]. The principal component of amyloid plaques, the amyloid β-peptide (Aβ), is a

heterogeneous cleavage product of the β-amyloid precursor protein (APP). After initial ectodomain shedding of APP by the β-site amyloid precursor protein cleaving enzyme 1 (BACE1), which has many other known physiological substrates, the remaining APP C-terminal fragment (CTF-β) is subsequently cleaved by the intramembrane protease γ-secretase, thereby releasing free Aβ. Alternately, the smaller peptide fragment p3 is released following shedding by ADAM10. Additional fragments are formed via the η-secretase ectodomain shedding pathway, which is followed by a BACE1 or an ADAM10 cleavage to produce longer (Aη-α) or shorter (Aη-β) forms of the native Aη peptide [5]. However, the rate limiting step for production of the Aβ peptide is the activity of the β-secretase enzyme, which is widely considered to have a crucial role in the initiation of AD pathology. Current symptomatic therapeutic options for AD include acetylcholinesterase inhibitors [6] and NMDA receptor antagonists [7], both of which provide some transient amelioration of cognitive symptoms, but without any disease-modifying effects [8, 9]. With the advent of highly potent and BBB-permeable inhibitors of BACE1, this enzyme has emerged as a primary drug target for reducing Aβ deposition in the AD brain. Therefore, the development and *in vivo* characterization of BACE1 inhibitors as therapeutic agents is of highest interest, with the caveat that untoward side effects can occur because of the wide spectrum of identified BACE1 substrates, especially in the central nervous system [10]. Most of the hitherto available BACE1 inhibitors also block the activity of BACE2, a close homologue of BACE1, which may cause additional on-target side effects [11]. Nonetheless, several BACE1 inhibitors are in human clinical trials testing for efficacy and safety in individuals with pre-symptomatic or manifest AD [12]. However, these trials have not so far imparted cognitive improvement in AD patients, indicating the necessity of much earlier and sustained BACE1 inhibitor treatment to efficiently prevent the accumulation of Aβ in the brain [13].

Amyloid positron-emission-tomography (PET) has in recent years emerged as valuable tool for assessment of cortical amyloidosis *in vivo*, and has been designated as a gatekeeper for inclusion of patients in anti-amyloid treatment trials. For such trials it is crucial to determine the dose-response of BACE1 inhibition and to define the optimal stage of AD for initiation of effective intervention with specific BACE1 inhibitors [12]. By the same measure, Aβ-PET also serves as a non-invasive tool for monitoring the amyloid plaque burden in transgenic mice, yielding excellent correlations with histological or biochemical assessments [14-16]. In this regard, longitudinal preclinical trials of BACE1 inhibition using Aβ-PET as an endpoint are of great translational value, and are readily validated by *ex vivo* histological examinations. As in clinical studies, baseline Aβ-PET results can be used to construct comparable experimental animal groups, and to investigate preconditions for individual differences in the progression of pathology longitudinally [15].

Given this background, we aimed to apply a theranostic concept for monitoring by [^{18}F]-florbetaben Aβ-PET the progression of amyloidosis in living PS2APP mice treated for four months with the small molecule BACE1 inhibitor RO5508887 [17]. We used serial and regional PET analyses for identifying the determinants of efficacy of BACE1 inhibition. Multimodal histological and biochemical readouts obtained *post mortem* served to substantiate and extend the conclusions drawn from PET.

Methods

Study design

Groups of 26 female PS2APP-Swe (TG) and 22 female C57BL/6 (WT) mice were randomly assigned to either treatment (TG-BSI; WT-BSI) or vehicle (TG-VEH; WT-VEH) groups at the age of 9.5 months. A baseline [^{18}F]-florbetaben-PET scan (Aβ-PET) was performed at this time, followed by initiation of daily oral RO5508887 treatment or vehicle, for a period of four months. Follow-up Aβ-PET-scans were acquired after 10 weeks (at 11.5 months of age), and 18.5 weeks of treatment (at 13.5 months of age), whereupon the study was terminated. An additional pre-baseline PET scan at 8 months (-6 weeks) had been performed to investigate the natural longitudinal Aβ deposition rates in all mice prior to their randomization. Thus, each mouse underwent a total of four [^{18}F]-florbetaben-PET scans over a period of 18 weeks. After completing the final scan, mice were killed and the brains removed for histological and biochemical analyses. Dose-titration experiments had been conducted prior to the chronic treatment in a separate group of 24 PS2APP mice. **Figure 1** illustrates the study design.

Animals

All experiments were performed in compliance with the National Guidelines for Animal Protection, Germany, with approval of the local animal care committee (Regierung Oberbayern), and overseen by a veterinarian. The transgenic B6.PS2APP (line B6.152H) mouse is homozygous for both the human presenilin (PS) 2, N141I mutation and the human amyloid precursor protein (APP) K670N, M671L mutation. The APP and PS2 transgenes are driven by

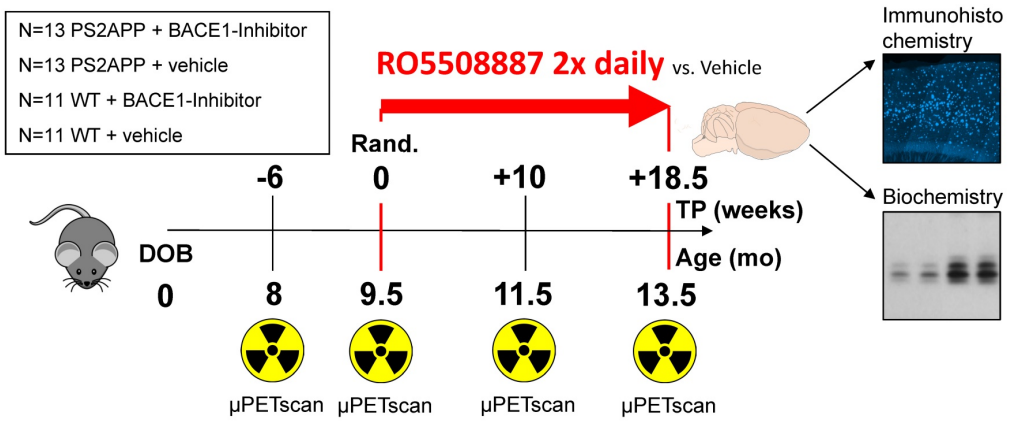

Figure 1. Illustration of the study design. PS2APP (TG) and WT mice were scanned by Aβ-PET starting at 8 months of age (Time-point (TP) -6). Treatment/vehicle randomization was realized after the 9.5 month scan (TP 0). Shortly after the terminal scan at 13.5 months (TP +18.5) all brains were split after perfusion and randomized hemispheres were used for terminal immunohistochemistry (methoxy-X04 plaque staining) and biochemistry analyses (protein assays).

mouse Thy-1 and mouse prion promoters, respectively. This line had been created by co-injection of both transgenes into C57BL/6 zygotes [18]. Homozygous B6.PS2APP mice show first appearance of amyloid plaques in the cortex and hippocampus at only five to six months of age [19].

BACE1 inhibitor

The previously evaluated BACE1 inhibitor RO5508887 was used at a defined dose of 100 mg/kg/d, which proved to be suitable in the chronic treatment arm of the same evaluation study using APPV717I transgenic mice [17]. Treatment was performed orally two times per day (11-13 h apart) per os (gavage). Acute *in vivo* treatment was performed for a dose finding in the PS2APP-Swe transgenic mouse model (N=24) with mutations causing increased BACE1 affinity and higher substrate turnover compared to normal APP, where RO5508887 proved to substantially block the enzyme at an acute dose of 30 mg/kg [17]. Therefore, the compound was administered once per os in PS2APP-Swe mice (60/90/120 mg/kg). For comparison, control PS2APP-Swe mice were treated with vehicle only (that is: 5% ethanol (VWR, Germany), 10% Solutol (MilliporeSigma, Germany) dissolved in sterile water). Brains were collected 2 and 4 h after acute treatment and stored at -80 °C until analysis. Two mice were used per time-point and dose/vehicle. DEA and RIPA lysates served to monitor the changes in BACE1-dependent APP processing affecting the levels of soluble Aβ as measured by Western blot analysis (**Figure S1**).

Aβ-PET

Aβ-PET image acquisition, reconstruction and analysis followed a standardized protocol, as previously published [14, 16, 20], with some refinements and adaptions as described in detail in Supplementary Material. After measuring tracer uptake in cerebral cortex and white matter templates, standardized-uptake-value-ratios ($SUVR_{CTX/WM}$) values were calculated for all groups of mice at each Aβ-PET scan timepoint. Individual longitudinal changes were calculated as a function of time (Δ%-$SUVR_{CTX/WM}$).

Regional deposition rates were assessed by voxel-wise PET analyses. To this end, mean parametric images ($SUVR_{WM}$) were calculated for the TG-BSI and TG-VEH groups at each time point (N =12-13 mice). The %-difference images were obtained by parametric image algebra in PMOD ((Timepoint-2 – Timepoint-1)/Timepoint-1 × 100%). Next, the %-difference map of vehicle-treated animals between baseline and terminal PET scan was used for defining volumes-of-interest (VOIs) depicting 2%-stepwise increments of Aβ deposition rate over the 18.5 weeks of treatment. Adjacent 2%-step VOIs were combined to define regions of low (2-10%) and high (>10%) amyloid deposition rates.

Biochemistry

Aβ extraction from brain and quantification

Brains were removed from the cranium and dissected into left and right hemispheres. One randomly selected hemisphere was snap-frozen by immersion in liquid nitrogen and stored at –80 °C. Soluble proteins were extracted with DEA buffer (50 mM NaCl, 0.2 % diethylamine, pH 10 + protease inhibitor (P8340, Sigma-Aldrich)). Membrane proteins were extracted with RIPA buffer (20 mM Tris-HCl (pH 7.5), 150 mM NaCl, 1 mM EDTA, 1 mM EGTA, 1% NP-40, 1% sodium deoxycholate, 2.5 mM sodium pyrophosphate + protease inhibitor). RIPA-insoluble material was dissolved in 70% formic acid. Quantification of Aβ was performed according to the manufacturer's protocol using the MSD®

MULTI-SPOT Human (6E10) Aβ Triplex Assay (Meso Scale Diagnostics, Rockville, USA) with a MSD SECTOR Imager 4200. Quantitative data were analyzed statistically by two-tailed Student's t-test (N =12 mice).

Protein analysis

Proteins were separated under denaturing conditions using discontinuous SDS-PAGE. Equal amounts of proteins denatured in Laemmli buffer were loaded onto the gel and 10 µL portions of the SeeBlue Plus2 Prestained Standard (Invitrogen) served as a molecular weight marker. Electrophoresis was performed in Tris-glycine buffer (25 mM Tris, 190 mM glycine in ddH_2O) using the Mini-PROTEAN system (BIORAD) on activated PVDF membranes. Low molecular weight proteins (< 20 kDa) were separated using precast gradient Tricine Protein Gels (10-20%, 1 mm, Novex) in Tris-tricine buffer using the XCell SureLock Mini-Cell system (Novex). After separation by SDS-PAGE, proteins were transferred onto membranes using the tank/wet Mini Trans-Blot cell system (BIORAD). CTFs, Aη and Aβ were detected after transfer on Nitrocellulose membranes (Protran BA85; GE Healthcare), while other proteins were blotted on PVDF (Immobilon-P, Merck Millipore). Upon completion of the transfer and prior to blocking, proteins transferred to nitrocellulose membranes were additionally denatured by boiling the membranes in PBS (140 mM NaCl, 10 mM Na_2HPO_4, 1.75 mM KH_2PO_4, 2.7 mM KCl in ddH2O, pH 7.4) for 5 min. After cooling to room temperature, the nitrocellulose membranes as well as the PVDF membranes were blocked in I-Block solution (0.2% Tropix I-Block (Applied Biosystems) in PBS-T (0.1% Tween20 in PBS) for 1 h at room temperature or overnight at 4 °C (with agitation). Transferred proteins were detected using immunodetection and enhanced chemiluminescence (ECL). First, blocked membranes were incubated with primary antibodies diluted in I-Block solution overnight at 4 °C (with agitation). After removal of the antibody, membranes were washed 3x in PBS-T buffer (10 min each, at room temperature, with agitation) and subsequently incubated with a horseradish peroxidase (HRP)-coupled secondary antibody (obtained from Santa Cruz Biochemicals). Secondary antibodies were diluted in I-Block solution and membranes were incubated for 1 h at RT (with agitation) followed by three washes in PBS-T. For ECL detection, membranes were incubated with HRP substrate (ECL, GE Healthcare or ECL Plus, Thermo Scientific) for 1 min at RT and signals were captured by exposure of X-ray film (Super RX Medical X-Ray, Fujifilm), which were subsequently developed using an automated film developer (CAWOMAT 2000 IR, CAWO). Signal intensities were quantified using ImageJ analysis software and plotted as relative differences of the treatment group compared to control.

Antibodies

DEA soluble protein was analysed for APP processing products with the following antibodies: 22C11 for detecting the APP N-terminus (used at 1 µg/mL, obtained from MilliporeSigma, Darmstadt, Germany), 6A1 for detecting sAPPβ-swe cleaved by BACE1 (used at 1 µg/mL; obtained from Tecan/ IBL International, Hamburg, Germany). 2D8 is an in-house rat monoclonal antibody against the N-terminus of Aβ, detecting also Aη-α (used at 2 µg/mL).

Histochemical analyses

Fibrillary β-amyloid plaques in brain specimens were stained with the fluorescent dye methoxy-X04 (0.01 mg/mL in PBS at pH 7.4 for 15 min) [21]. Full details are described in Supplementary Material. Plaque load was calculated as the summed area of all plaques relative to the frontal cortex area. Plaque density was calculated as the number of plaques relative to frontal cortex volume [20]. These analyses were performed by an operator blind to the Aβ-PET results.

Statistics

Group comparisons of VOI-based Aβ-PET results and biochemistry were performed with multivariate analysis of variance (MANOVA) using IBM SPSS Statistics (Version 23.0). Histology data (plaque load and plaque density) were compared between treated and untreated transgenic mice by multivariate analysis of covariance (MANCOVA) using Aβ-PET baseline estimates as a covariate. Treatment effects in low and high amyloid accumulating regions were compared with a *t*-test. For correlation analyses, Pearson's coefficients of correlation (R) were calculated. Plaque size distributions were compared with a Chi-square test followed by the Kolmogorov-Smirnov test with Prism V5.04 software (GraphPad Software, San Diego, CA, USA). A Shapiro-Wilk test was performed to verify normal distribution of sample values. A threshold of $p<0.05$ was deemed significant for rejection of the null hypothesis.

Results

Chronic BACE-I treatment effectively inhibits fibrillary Aβ deposition as monitored by PET

We applied a theranostic concept of longitudinal Aβ-PET during chronic BACE-1 inhibition in PS2APP

mice to study treatment effects over 18.5 weeks and to investigate the value of treatment monitoring. Multimodal readouts by terminal Aβ peptide level, and terminal plaque load to immunohistochemistry served for further characterization of the effect of chronic treatment with RO5508887 on amyloidosis in PS2APP mice.

Treatment and serial PET imaging proved well-tolerated, with only a single dropout in the TG-BSI group. All modalities revealed a significantly reduced progression of amyloidosis in TG-BSI mice when compared to the TG-VEH group. Particularly, PET revealed a significantly lower progression of amyloidosis as early as 10 weeks into the treatment regimen (+6.7% in BSI vs. +10.3% in VEH, $p < 0.05$) and an even greater effect at 18.5 weeks of treatment (+8.4% in BSI vs. +15.2% in VEH, $p < 0.001$; **Figure 2**). WT mice presented with stable PET values either in the treatment or the vehicle groups.

Terminal immunohistochemistry confirmed PET findings by the direct validation of fibrillary Aβ and indicated lower plaque load (-9.7%, $p < 0.05$; **Figure 3A**) as well as plaque density (-9.9%, $p < 0.05$; **Figure 3B**) in BACE1-treated TG mice when compared to TG vehicle controls. The major effect was observed on *de novo* plaque deposition, as the fraction of small plaques was apparently lower in the same contrast of treated versus control mice (**Figure 3C-D**).

Acute and chronic BACE1 treatment lowers Aβ deposition

Brains of the PSAPP2-swe transgenic mice were collected 4 h after the last BACE1 inhibitor or vehicle treatment to allow monitoring of both the steady-state enzyme activity after inhibitor application and the long-term effect of the chronic treatment. BACE1 inhibition results in reduction of the amyloidogenic pathway as indicated by lower levels of sAPP-β (Swe) and increased sAPP-α, while total sAPP remained unchanged. BACE1 inhibition resulted in a clear reduction of soluble Aβ and consequently an increase of Aη-α in the DEA fraction, which is enriched in soluble fragments, of the TG-BSI mice compared to TG-VEH controls 4 h after acute treatment (**Figures 4A-B**). Furthermore, soluble Aβ (DEA) and deposited Aβ (FA) were quantified by ELISA (**Figures 4C-D**). Compared to the TG-VEH group, we saw a 47% reduction of soluble Aβ40 and a 61% reduction of Aβ42, respectively, in the group treated with the BACE inhibitor RO550887 (**Figure 4C**). However, the TG-BSI animals showed only a slight reduction of Aβ40 levels (-10% in TG-BSI vs. TG-VEH, $p = 0.45$), but significantly reduced Aβ42 levels after chronic treatment over 18 weeks in the fraction of deposited Aβ (-40% in TG-BSI vs. TG-VEH, $p < 0.05$) (**Figure 4D**).

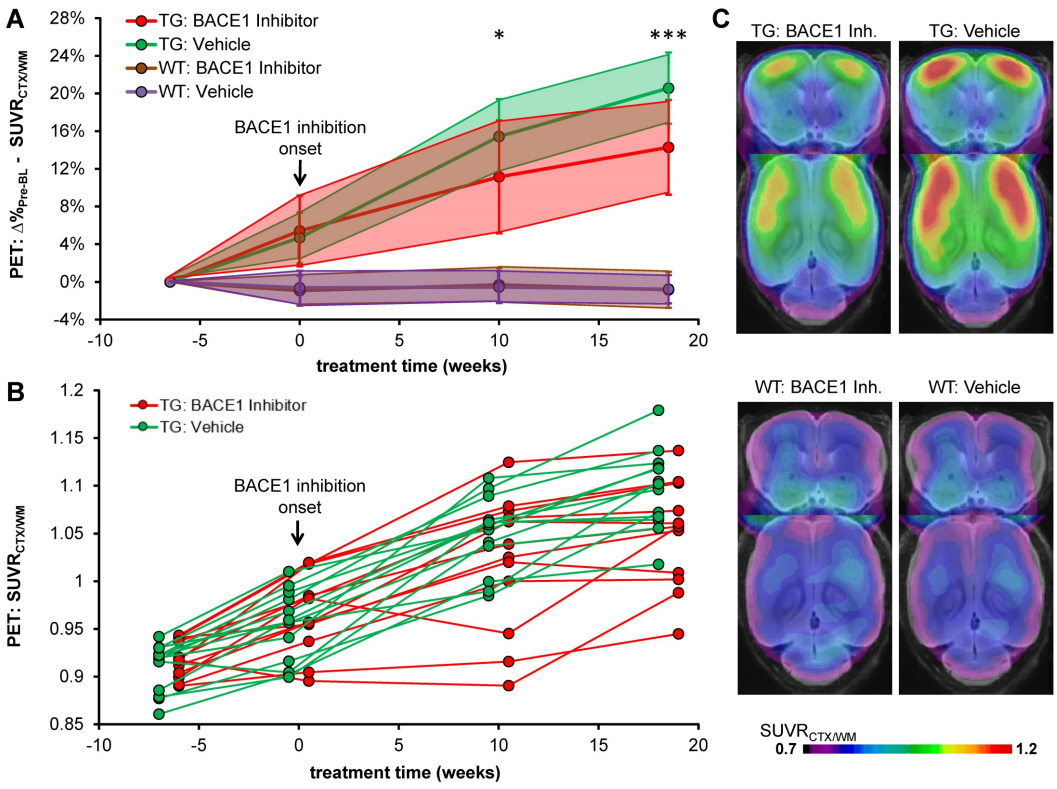

Figure 2. Longitudinal Aβ-PET imaging of BACE1 inhibition. (A) Plots show means (±SD) of the cortical amyloid signal relative to the baseline imaging for treated and vehicle groups of TG and WT mice. **(B)** Individual progression of the cortical amyloid signal in TG mice. **(C)** Signal intensities of the frontal cortical amyloid signal in TG and WT mice at the terminal Aβ-PET scan (18.5 weeks). Coronal and axial slices illustrate group averages upon a T1w MRI template. * $p < 0.05$; *** $p < 0.001$

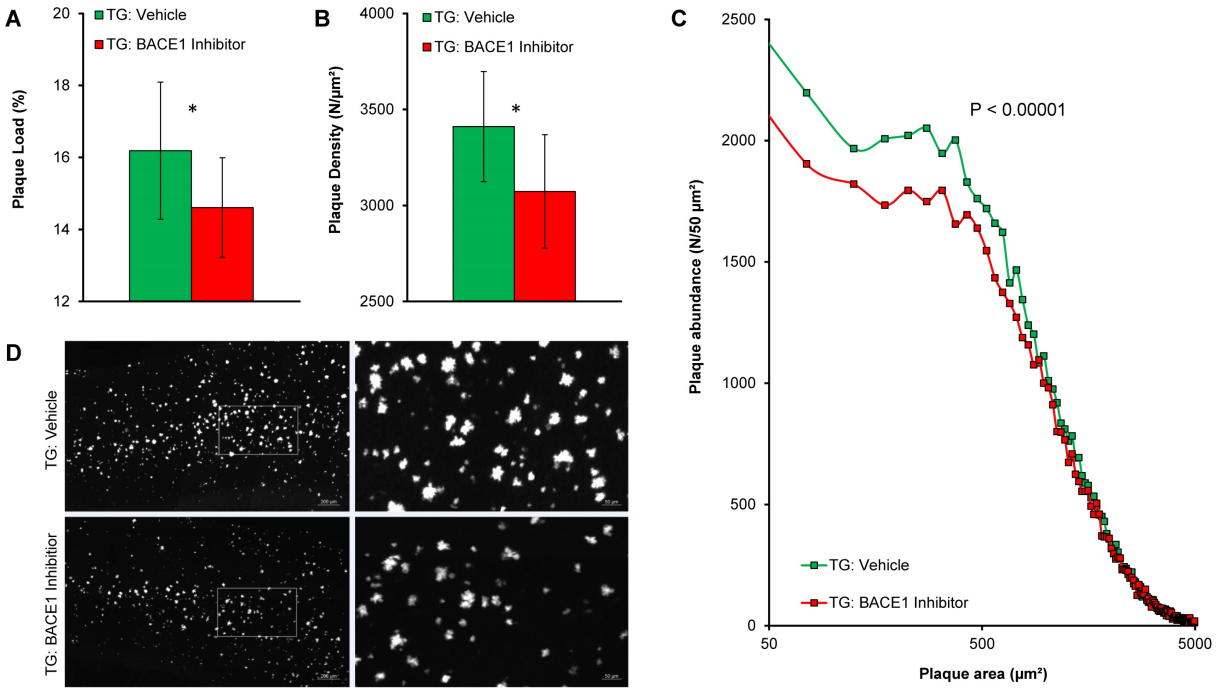

Figure 3. Immunohistochemical validation of Aβ-PET results. Plots show frontal cortical mean (±SD) of plaque load **(A)** and plaque density **(B)** by methoxy-X04 immunohistochemistry in TG-VEH (green) and TG-BSI (red) mice. **(C)** Histogram plotting of plaque size revealed significantly fewer small plaques in the TG-BSI animals (red) in comparison to the TG-VEH group (green), which was also explored in the visual analysis of sagittal cortical slices of methoxy-X04 staining **(D)**. Error bars indicate SD. * $p < 0.05$.

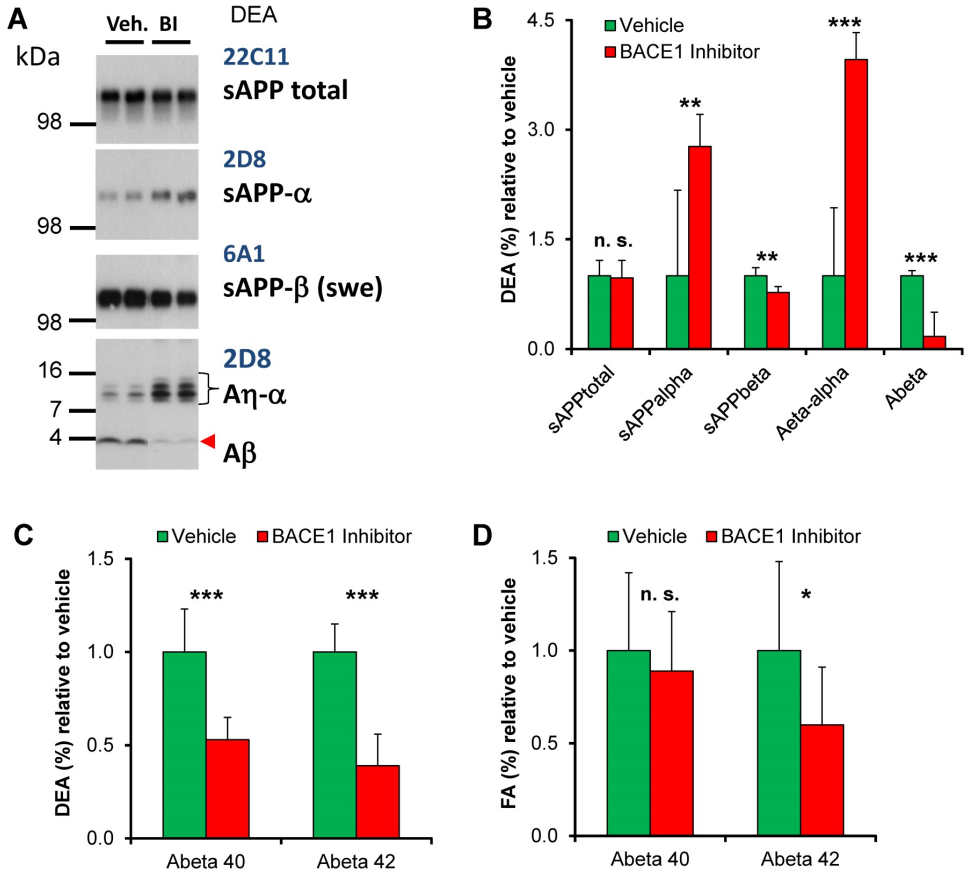

Figure 4. Biochemical analyses. (A) In Western blots, BACE1 inhibition was observed to result in reduction of the amyloidogenic pathway, as indicated by lowered levels of sAPP-β (Swe) and increased sAPP-α levels. The lower panel indicates that BACE1 inhibition caused reduced levels of soluble Aβ and an increase of Aη-α in brains of the TG-BSI mice compared to TG-VEH controls 4 h after acute treatment. **(B)** Quantification of APP processing products indicated significant increase for sAPP-α and Aη-α, but significant reduction for the BACE1-dependent products sAPP-β and Aβ, while total sAPP shedding remained unchanged (vehicle (n=6); BI/BACE inhibitor treated (n=5)). **(C)** Lower DEA levels of soluble Aβ40 and Aβ42 were observed in TG-BSI mice relative to TG-VEH controls. **(D)** Insoluble FA levels likewise indicated a significant reduction of Aβ42, but only a small tendency for reduced Aβ40 levels. Error bars indicate SD, * $p < 0.05$; ** $p < 0.005$; *** $p < 0.001$; n.s.= not significant.

In summary, all readouts and modalities indicated a significant chronic treatment effect by RO5508887 on progression of amyloidosis in PS2APP mice.

Effectiveness of chronic BACE1 inhibition treatment depends on regional Aβ deposition rates

In a separate analysis, we used the theranostic Aβ-PET approach to investigate regional longitudinal differences in amyloidosis during chronic treatment. We aimed to reveal possible relationships between the "naïve" regional deposition rate and the subsequent regional chronic treatment effect. Individual PET results in TG-VEH mice revealed the highest "naïve" regional increase in amyloidosis (Δ%-$SUVR_{WM}$) in the bilateral frontal cortex (primary somatosensory areas), followed by primary motor areas and auditory and visual cortices. Lower progression of amyloidosis was observed in temporal cortex areas (e.g., gustatory, insular), as well as in the bilateral thalamus and hippocampus (**Figure S2**).

Interestingly, we found a linear relationship ($R>0.99$; $p<0.001$) between the regional amyloid progression rate in TG-VEH, i.e., naïve progression, and the corresponding progression in TG-BSI mice (**Figure 5A**). This relationship indicated a threshold for regional deposition rate of 3.7% / 18.5 weeks in TG-VEH, below which complete blocking of further signal increase could be achieved with RO5508887 treatment of TG mice. A polynomial function could be fitted to a plot of the individual treatment effect relative to naïve progression in the TG-VEH group, thus revealing very high treatment effect in regions with low naïve progression, which declined to a trough, with only 40% attenuation of amyloidosis in those regions with naïve progression exceeding about 15% (**Figure 5B**). This finding was verified by voxel-wise mapping of the %-treatment effect, which showed the highest relative effect (nearly 100%) of BACE1 inhibition in brain regions with inherently low Aβ-accumulation (e.g., gustatory and insular areas, thalamus; **Figure 5C**).

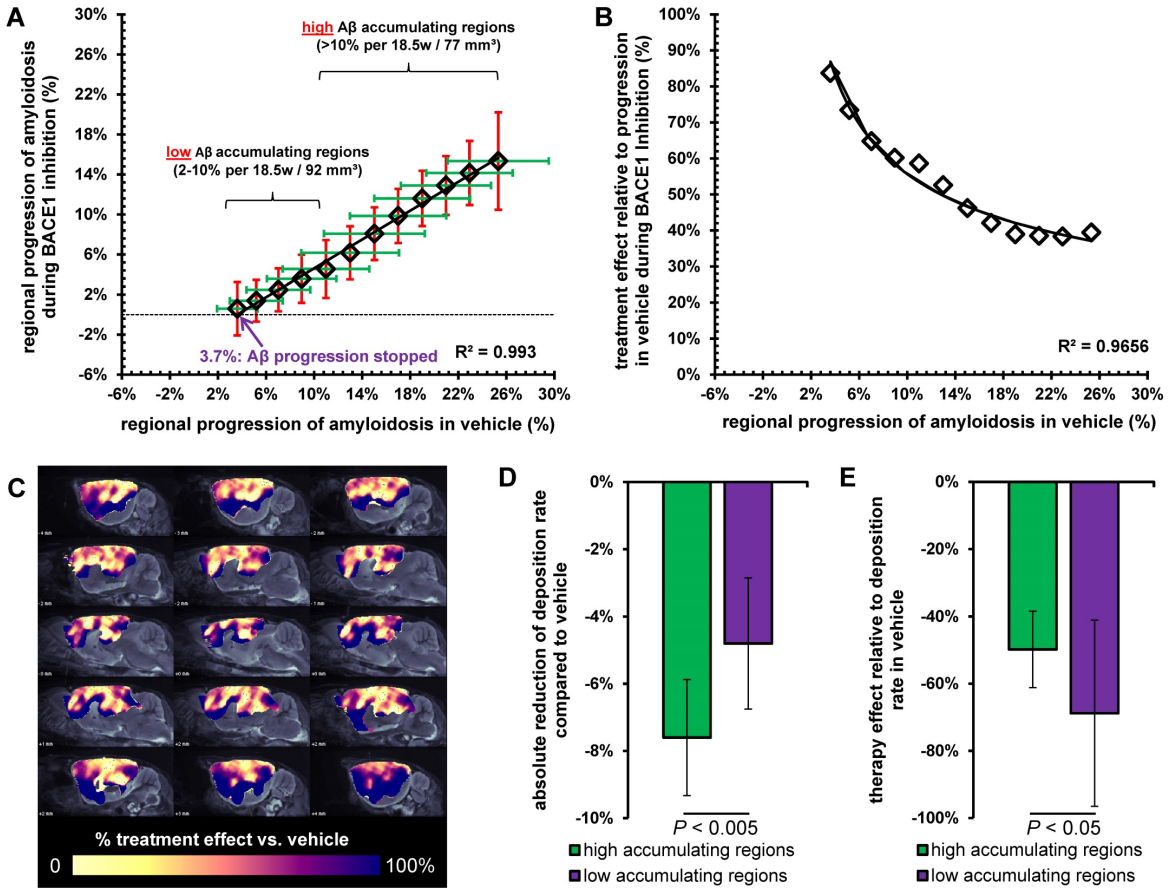

Figure 5. Analysis of high and low Aβ accumulating regions. (A) Progression of the Aβ-PET signal in TG-VEH (x-axis) against TG-BSI (y-axis) mice. Values were obtained from regions with equal Aβ accumulation in TG-VEH mice. Dotted line shows halted fibrillary Aβ accumulation (0%) in TG-BSI mice and the nearly linear correlation of single regions between TG-VEH and TG-BSI mice calculates a complete stop of further fibrillary Aβ accumulation in regions of ≤ +3.7% signal increase in TG-VEH. Low and high Aβ accumulating regions were defined by 2-10% and > 10% signal increase in TG-VEH mice over 18.5 months. **(B)** Consecutively, an exponential increase of the treatment effect in TG-BSI relative to TG-VEH mice was found with decreasing regional Aβ accumulation, as observed in drug-naïve TG mice. **(C)** A 3D analysis of the forebrain confirmed these findings by indicating the highest relative treatment effect in lateral neocortical brain regions with a low Aβ accumulation. The absolute reduction of the Aβ deposition rate was significantly larger in high Aβ accumulating regions **(D)**, whereas the relative therapy effect was significantly lower in high Aβ accumulating regions **(E)**.

Concerning the absolute reduction in Aβ deposition with treatment, we found a decrease of 7.6 ± 1.7% in high accumulating regions (≥ 10%; total volume: 77 mm³) and a lesser decrease of 4.8 ± 2.0% in low accumulating regions (<10%; total volume: 92 mm³; $p < 0.005$, **Figure 5D**). However, the relative treatment effect was significantly lower in high accumulating brain regions (49 ± 11%) when compared to brain regions with low accumulation, in which there was a relative treatment effect of 69 ± 28% ($p < 0.05$, **Figure 5E**). Kinetics of accumulation in individual animals to serial PET measurements in high and low Aβ accumulating regions are presented in **Figure S3**.

We find significant regional differences in the response to chronic BACE1 inhibition treatment, which is characterized by a linear relationship relative to vehicle treatment. Regions with more pronounced fibrillary Aβ deposition are characterized by greater resistance to BACE1 inhibition, whereas a 100% blocking was achieved in regions with low deposition rates, all relative to findings in the vehicle group. The finding of individual deposition rate thresholds for complete blocking of Aβ deposition by a theranostic concept might guide individual dose regimens for BACE1 inhibitors in future clinical studies. Optimal dosing for blockade in high accumulating regions must be assessed in the light of a possible trade-off between side effects and clinical efficacy.

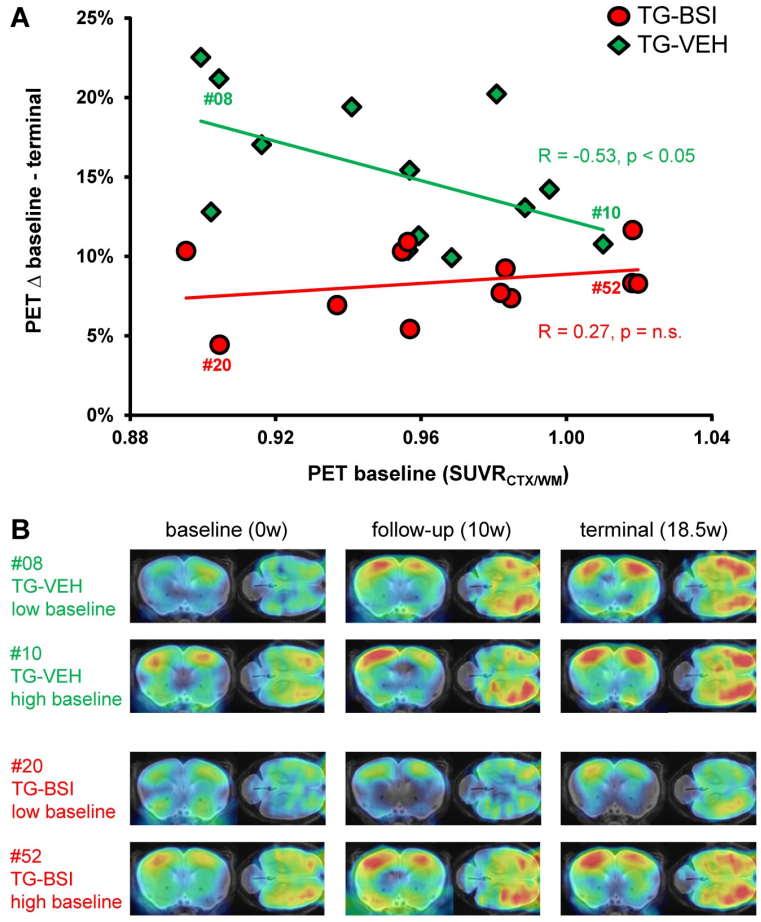

Figure 6. Treatment effect dependency from baseline amyloidosis. (A) Response prediction by means of Aβ-PET. The percentage increase from baseline to termination SUVR$_{CTX/WM}$ is depicted as a function of the individual baseline value. For the TG-BSI, a low baseline value predicted a lesser increase in amyloidosis during treatment, whereas TG-VEH mice with a low baseline value increased tremendously. The treatment effect in TG-BSI relative to TG-VEH was markedly lower when amyloidosis was already established. The correlations (R) between the percentage increase and the baseline value are indicated. **(B)** Aβ-PET signal intensities of individual exemplary mice for serial baseline, follow-up and terminal imaging time-points. The TG-BSI mouse with a low baseline (#20) indicates a very low Aβ accumulation whereas the TG-VEH mouse with a low baseline (#08) shows high Aβ accumulation. TG-BSI and TG-VEH with a high baseline show only minor differences in their sequential Aβ accumulation. Coronal and axial slices are illustrated upon a T1w MRI template.

BACE1 inhibition treatment is more effective during early amyloid build-up

The serial Aβ-PET design made possible an assessment of baseline plaque load in brains of individual mice prior to initiation of the treatment. We used this technique to predict differences in longitudinal fibrillary Aβ deposition from the baseline level, based on our earlier findings of such an association [15]. Indeed, present findings in TG-VEH mice indicated an inverse association between baseline Aβ burden and the relative increase from 9.5 to 13.5 months of age ($R = -0.53$, $p < 0.05$; **Figure 6A**). Thus, TG-VEH mice starting at a low baseline Aβ-level tended to catch up their initially delayed Aβ accumulation. TG-BSI mice revealed the highest treatment-related difference relative to the TG-VEH group when their initial Aβ-level was low, as the accelerated increase observed in vehicle animals was prevented, leading to a reversal in the direction of the correlation ($R = +0.27$, p = n.s.; **Figure 6A**). In those TG-BSI mice with high Aβ-levels to baseline PET, the treatment effect was hardly discernible from the TG-VEH group. Findings in representative mice with a nearly equal baseline amyloidosis are illustrated in **Figure 6B**. To confirm the "regular" inverse correlation between baseline Aβ-level and the subsequent deposition rate, we longitudinally imaged another vehicle-treated TG group (N=12), which confirmed the above results ($R_{BL/\Delta\%\text{-}BL\text{-}TER} = -0.58$, $p < 0.05$).

The finding that baseline PET results predict treatment efficacy indicates that therapeutic BACE1 inhibition should be obtained early in the pathology time course, as present amyloid deposits proved more resistant to later treatment initiation.

Discussion

In this adequately powered longitudinal PET study of cerebral amyloidosis in a transgenic AD mouse model we investigated regional effects of a chronic disease-modifying therapy based on BACE1 inhibition by applying a theranostic concept. The molecular imaging study entailed corroborative histopathological as well as biochemical analyses, thus encompassing three different readout modalities for monitoring amyloidogenesis.

Serial [^{18}F]-florbetaben Aβ-PET in PS2APP mice provides a robust method for monitoring anti-amyloid treatment effects

Serial Aβ-PET excellently captured the treatment effects of BACE1 inhibition versus vehicle and allowed *in vivo* assessment of the therapeutic target in individual mice. A recent study using a multi-tracer design succeeded in monitoring BACE1 effects in an amyloid mouse model using another Aβ-PET ligand ([^{18}F]-florbetapir), although the similarly altered signal in treated WT mice led the authors to conclude that the observed binding effects were not specific treatment effects on amyloid deposition [22]. In contrast, we found a highly stable background signal in WT mice in treatment and vehicle groups using the amyloid ligand [^{18}F]-florbetaben, which encourages the use of the mouse model in combination with the earlier-validated quantification method [16]. A recent PET study showed the ability to detect non-fibrillar Aβ forms *in vivo* during treatment of transgenic ArcSwe mice with another BACE1 inhibitor [23], whereas our PET ligand binds only fibrillary parts of the plaque. Future monitoring regimes could therefore entail dual PET with selective tracers to capture both components of amyloidosis during BACE1 inhibition.

Linear dependence of BACE1 inhibition treatment effect from Aβ deposition rates can be captured by individual serial imaging

In the present study with the BACE1 inhibitor RO5508887 at a daily dose of 100 mg/kg, we obtained only 49% attenuation of progression in brain regions with high Aβ deposition, suggesting that a higher dose might have been more efficacious. The APP-Swe transgenic mouse model, given its high rate of Aβ synthesis, presents a clear limitation arising from the need for relatively high inhibitor dosing. However, more recent data have indicated a dose-dependent impairment of synaptic plasticity and cognitive functions or reduced muscle spindle numbers in adult mice with chronic BACE1 inhibitor treatment, which could be attributed to impairing function of the BACE1 substrate Neuregulin-1 [24, 25]. Thus, there is need for caution in selecting dosage regimens for drugs targeting BACE1 aiming to achieve a therapeutic window with optimal trade-off between safety and efficacy. The current data provide evidence that regional efficacy of RO5508887 treatment linearly correlates with the regional naïve deposition rate revealed by Aβ-PET in vehicle-treated animals. Thus, prior knowledge of the individual Aβ deposition rate might inform the estimation of an optimal dosage of BACE1 inhibitor to slow or even arrest further progression of cortical fibrillary amyloidosis. This issue is even more important when considering the clinical finding that Aβ accumulation rates in amyloid-positive humans are very heterogeneous [26, 27]. Such a treatment design and combinatorial treatments together, e.g., with an Aβ immunotherapy strategy might require dosage titration of BACE1 inhibitors in individual patients according to their individual amyloidosis rates at initiation of therapy. Harkening back on the potential for cognitive side effects, it could well be that there are patients for whom the BACE1 inhibitor dosage predicted to be effective for slowing amyloidosis would bring an excessively high risk for adverse effects. On the other hand, some patients might require only low doses of BACE1 inhibitors, either because of their earlier disease stage, or an intrinsically lower Aβ progression. In this regard, recent detailed PET study of amyloid accumulation rates of humans with preclinical AD revealed a strong global and regional variation, which has major implications for anti-amyloid trials [28]. Our current findings of high and low amyloid accumulating regions in PS2APP mice are in line with the human findings, which emphasizes that our novel preclinical approach for dose-titration by considering amyloid deposition rates in multiple brain regions might be translatable to human investigations. Serial Aβ-PET therefore has the potential to serve as a readout for determining the individual dosage as well as for monitoring effectiveness of treatment in individual patients in the context of personalized medicine.

Early treatment initiation ensures high efficacy in BACE1 inhibition treatment

Current results constitute compelling evidence that efficacy of RO5508887 in individual TG mice receiving a predefined dose of the medication depends on their fibrillary individual Aβ levels at therapy initiation, as is revealed by baseline Aβ-PET. By selecting the present dose of 100 mg/kg/d RO5508887 on the basis of earlier findings [17] and by single dose validation in the current model, we observed a greater benefit in those mice having a relatively low plaque load at baseline, which matches

findings in our previous study with a gamma secretase modulator in Swedish mutant mice [15]. Thus, the relationship emerges as a general principle, irrespective of the molecular target in a treatment intervention. We now show that BACE1 inhibitor-treated mice with high and low baseline amyloid levels progressed equally, whereas the course in vehicle mice with low Aβ to baseline PET clearly had a more pronounced increase of amyloidosis between 9.5 and 13.5 months of age. This concept is coherent in the light of our immunohistochemistry findings, since the major impact of BACE1 treatment was clearly observed in lowering the fraction of small plaques. Thus, this treatment evoked the anticipated molecular effect on *de novo* plaque formation [17]. Findings of a recent chronic treatment study using a different BACE1 inhibitor and a different amyloid mouse model are in line with our terminal immunohistochemistry results as their images indicated a similar main treatment effect on small plaques [22]. In summary, we find that the present dosage of RO5508887 can substantially lower the progression of amyloidosis in those brain regions and in those individual animals with low pre-existing plaque load. Due to the logistic difficulty and cost of serial PET imaging, we only investigated one preselected dosage and only one starting age. However, higher doses and persistent inhibition achievable, e.g., by oral drug administration with food would be necessary if the treatment initiation were at a disease stage with established plaque deposition. It remains to be elucidated if sufficient RO5508887 doses for such cases can be administered without provoking treatment-limiting side effects. While our present results in a double transgenic β-amyloid mouse model are not immediately translatable to clinical AD, we provide compelling evidence that Aβ-PET can potentially inform a crucial decision for clinical AD trials: at what stage of AD should BACE inhibitors be administered? With precisely this in mind, cortical Aβ levels are being examined in current phase II/III trials of BACE inhibitors [12]. Very recently, two phase III trials with Lanabecestat were discontinued early as they would probably not have met their primary endpoints [29]. Full details on the reasons behind the decisions are not yet released, but there is a general opinion that BACE1 inhibitors are unlikely to be effective in individuals who already have symptoms of AD dementia [29]. Our current results of lesser efficacy in mice with established amyloidosis give the first PET-based *in vivo* evidence for this contention. It will be of enormous interest if the efficacy in human treatment indeed proves to be predictable from the state of cortical amyloidosis at initiation of treatment. The lack of behavioral testing in this study presents a limitation since we can make no claims about beneficial or detrimental effects on cognition in the treated mice.

Conclusion

We demonstrate that serial Aβ-PET in PS2APP mice provides a robust theranostic approach for monitoring BACE1 inhibition treatment effects in this adequately powered longitudinal study. Regional analyses indicated a linear dependence of treatment efficacy upon Aβ deposition rates in the vehicle-treated group. Serial Aβ-PET could therefore serve as a readout for titrating the optimal individual dosage as well as for monitoring treatment effectiveness in the context of personalized medicine. Finally, the correlation between baseline and the individual treatment effects in conjunction with terminal histological results revealed the need of an early BACE1 treatment initiation for prevention of *de novo* amyloidogenesis.

Abbreviations

Aβ: amyloid β-peptide; Aβ-PET: [^{18}F]-florbeta-ben β-amyloid positron-emission-tomography; AD: Alzheimer's disease; APP: β-amyloid precursor protein; BACE1: β-site amyloid precursor protein cleaving enzyme 1; BBB: blood brain barrier; CTF-β: C-terminal fragment; DEA: diethanolamine; ECL: enhanced chemiluminescence; FBB: [^{18}F]-florbetaben; HRP: horseradish peroxidase; MANOVA: multivariate analysis of variance; MANCOVA: multivariate analysis of covariance; MRI: magnetic resonance imaging; NMDA: N-Methyl-D-Aspartat; PET: positron-emission-tomography; PBS: phosphate buffered saline; PS: presenilin; PVDF: polyvinylidendifluorid; R: Pearson's coefficients of correlation; RT: room temperature; SD: standard deviation; SDS-PAGE: sodium dodecyl sulfate polyacrylamide gel electrophoresis; SUVR: standardized-uptake-value-ratio; TG: transgenic PS2APP-Swe mice; TG-BSI: treatment group of transgenic PS2APP-Swe mice; TG-VEH: vehicle group of transgenic PS2APP-Swe mice; TP: time-point; VOI: volume-of-interest; WT: C57BL/6 mice; WT-BSI: treatment group of C57BL/6 mice; WT-VEH: vehicle group of C57BL/6 mice.

Supplementary Material

Supplementary methods and figures.
http://www.thno.org/v08p4957s1.pdf

Acknowledgements

We thank Karin Bormann-Giglmaier, Rosel Oos, Heike Hampel and Veronika Müller for excellent

technical assistance. Florbetaben precursor was kindly provided by Piramal Imaging. We thank Jaroslaw Dzbek for help in data processing. We acknowledge Inglewood Biomedical Editing for professional manuscript editing.

Funding

The study was financially supported by the SyNergy Cluster (J.H., P.B., C.H., and A.R.) and by the European Research Council under the European Union's Seventh Framework Program (FP7/2007–2013)/ ERC Grant Agreement No. 321366-Amyloid (advanced grant to C.H.). A. J. was supported by the Foundation for Polish Science within the International PhD Project 'Studies of nucleic acids and proteins – from basic to applied research', co-financed from European Union - Regional Development Fund; MPD/2009-3/2.

Author contributions

MB: conceived of the study, performed manuscript writing, performed PET imaging and analyses; AJ: performed manuscript writing, performed immunohistochemical analyses; FO: performed PET imaging and analyses; TB: performed immunohistochemical analyses; FP: performed PET imaging and analyses; FG: performed radiochemistry analyses and synthesis of the tracer; PB: interpretation of PET imaging; CH: conceived the study and analyzed the biochemical results, interpretation of biochemical results; BB: conceived the study and analyzed the treatment results; JH: conceived the study and analyzed the immunohistochemical results, interpretation of immunohistochemical results; MW: conceived the study and analyzed the results and performed biochemical analyses, interpretation of biochemical results, performed manuscript writing; AR: conceived the study and analyzed the PET results; all authors drafted the work, revised it critically for important intellectual content, and approved the final version.

Conflicts of Interest

PB received speaking honoraria from Piramal Imaging. CH is an advisor of Hoffmann-La Roche. BB is an employee of Hoffmann-La Roche. AR received speaking honoraria from Piramal Imaging. All other authors declare no conflicts of interest.

References

1. Ziegler-Graham K, Brookmeyer R, Johnson E, Arrighi HM. Worldwide variation in the doubling time of Alzheimer's disease incidence rates. Alzheimers Dement. 2008; 4: 316-23.
2. Braak H, Braak E. Neuropathological stageing of Alzheimer-related changes. Acta Neuropathol. 1991; 82: 239-59.
3. Dubois B, Feldman HH, Jacova C, Hampel H, Molinuevo JL, Blennow K, et al. Advancing research diagnostic criteria for Alzheimer's disease: the IWG-2 criteria. The Lancet Neurol. 2014; 13: 614-29.
4. McKhann GM, Knopman DS, Chertkow H, Hyman BT, Jack CR, Jr., Kawas CH, et al. The diagnosis of dementia due to Alzheimer's disease: recommendations from the National Institute on Aging-Alzheimer's Association workgroups on diagnostic guidelines for Alzheimer's disease. Alzheimers Dement. 2011; 7: 263-9.
5. Willem M, Tahirovic S, Busche MA, Ovsepian SV, Chafai M, Kootar S, et al. eta-Secretase processing of APP inhibits neuronal activity in the hippocampus. Nature. 2015; 526: 443-7.
6. Sun X, Jin L, Ling P. Review of drugs for Alzheimer's disease. Drug Disov Ther. 2012; 6: 285-90.
7. Reisberg B, Doody R, Stoffler A, Schmitt F, Ferris S, Mobius HJ. Memantine in moderate-to-severe Alzheimer's disease. N Engl J Med. 2003; 348: 1333-41.
8. Herrmann N, Li A, Lanctot K. Memantine in dementia: a review of the current evidence. Expert Opin Pharmacother. 2011; 12: 787-800.
9. Dhillon S. Rivastigmine transdermal patch: a review of its use in the management of dementia of the Alzheimer's type. Drugs. 2011; 71: 1209-31.
10. Yan R, Vassar R. Targeting the beta secretase BACE1 for Alzheimer's disease therapy. Lancet Neurol. 2014; 13: 319-29.
11. Yan R, Fan Q, Zhou J, Vassar R. Inhibiting BACE1 to reverse synaptic dysfunctions in Alzheimer's disease. Neurosci Biobehav Rev. 2016; 65: 326-40.
12. Vassar R. BACE1 inhibitor drugs in clinical trials for Alzheimer's disease. Alzheimers Res Ther. 2014; 6: 89.
13. Egan MF, Kost J, Tariot PN, Aisen PS, Cummings JL, Vellas B, et al. Randomized trial of Verubecestat for mild-to-moderate Alzheimer's disease. N Engl J Med. 2018; 378: 1691-703.
14. Brendel M, Jaworska A, Griessinger E, Rotzer C, Burgold S, Gildehaus FJ, et al. Cross-sectional comparison of small animal [18F]-florbetaben amyloid-PET between transgenic AD mouse models. PloS One. 2015; 10: e0116678.
15. Brendel M, Jaworska A, Herms J, Trambauer J, Rotzer C, Gildehaus FJ, et al. Amyloid-PET predicts inhibition of de novo plaque formation upon chronic gamma-secretase modulator treatment. Mol Psychiatry. 2015; 20: 1179-87.
16. Overhoff F, Brendel M, Jaworska A, Korzhova V, Delker A, Probst F, et al. Automated spatial brain normalization and hindbrain white matter reference tissue give improved [(18)F]-Florbetaben PET quantitation in Alzheimer's model mice. Front Neurosci. 2016; 10: 45.
17. Jacobsen H, Ozmen L, Caruso A, Narquizian R, Hilpert H, Jacobsen B, et al. Combined treatment with a BACE inhibitor and anti-Abeta antibody gantenerumab enhances amyloid reduction in APPLondon mice. J Neurosci. 2014; 34: 11621-30.
18. Richards JG, Higgins GA, Ouagazzal AM, Ozmen L, Kew JN, Bohrmann B, et al. PS2APP transgenic mice, coexpressing hPS2mut and hAPPswe, show age-related cognitive deficits associated with discrete brain amyloid deposition and inflammation. J Neurosci. 2003; 23: 8989-9003.
19. Ozmen L, Albientz A, Czech C, Jacobsen H. Expression of transgenic APP mRNA is the key determinant for beta-amyloid deposition in PS2APP transgenic mice. Neurodegener Dis. 2009; 6: 29-36.
20. Rominger A, Brendel M, Burgold S, Keppler K, Baumann K, Xiong G, et al. Longitudinal assessment of cerebral beta-amyloid deposition in mice overexpressing Swedish mutant beta-amyloid precursor protein using 18F-florbetaben PET. J Nucl Med. 2013; 54: 1127-34.
21. Klunk WE, Bacskai BJ, Mathis CA, Kajdasz ST, McLellan ME, Frosch MP, et al. Imaging Abeta plaques in living transgenic mice with multiphoton microscopy and methoxy-X04, a systemically administered Congo red derivative. J Neuropathol Exp Neurol. 2002; 61: 797-805.
22. Deleye S, Waldron AM, Verhaeghe J, Bottelbergs A, Wyffels L, Van Broeck B, et al. Evaluation of muPET outcome measures to detect disease modification induced by BACE inhibition in a transgenic mouse model of Alzheimer's disease. J Nucl Med. 2017. 58: 1977-83
23. Meier SR, Syvanen S, Hultqvist G, Fang XT, Roshanbin S, Lannfelt L, et al. Antibody-based in vivo PET imaging detects amyloid-beta reduction in Alzheimer transgenic mice after BACE-1 inhibition. J Nucl Med. 2018. In press.
24. Filser S, Ovsepian SV, Masana M, Blazquez-Llorca L, Brandt Elvang A, Volbracht C, et al. Pharmacological inhibition of BACE1 impairs synaptic plasticity and cognitive functions. Biol Psychiatry. 2015; 77: 729-39.
25. Cheret C, Willem M, Fricker FR, Wende H, Wulf-Goldenberg A, Tahirovic S, et al. Bace1 and Neuregulin-1 cooperate to control formation and maintenance of muscle spindles. EMBO J. 2013; 32: 2015-28.
26. Brendel M, Hogenauer M, Delker A, Sauerbeck J, Bartenstein P, Seibyl J, et al. Improved longitudinal [(18)F]-AV45 amyloid PET by white matter reference and VOI-based partial volume effect correction. Neuroimage. 2015; 108: 450-9.
27. Villemagne VL, Burnham S, Bourgeat P, Brown B, Ellis KA, Salvado O, et al. Amyloid beta deposition, neurodegeneration, and cognitive decline in

sporadic Alzheimer's disease: a prospective cohort study. Lancet Neurol. 2013; 12: 357-67.
28. Guo T, Dukart J, Brendel M, Rominger A, Grimmer T, Yakushev I. Rate of β-amyloid accumulation varies with baseline amyloid burden: Implications for anti-amyloid drug trials. Alzheimers Dement. 2018. In press.
29. Burki T. Alzheimer's disease research: the future of BACE inhibitors. The Lancet. 2018. 391: 2486

7. Danksagung

Meinem Doktorvater, Herrn Professor Dr. med. Axel Rominger von der Klinik und Poliklinik für Nuklearmedizin der Universität Bern und meinem Betreuer, Herrn Dr. med. Matthias Brendel von der Klinik und Poliklinik für Nuklearmedizin der Universität München, danke ich für die Überlassung des Themas und der Betreuung dieser Arbeit.
Herrn Federico Probst danke ich für die stets freundschaftliche und produktive Zusammenarbeit bei der Durchführung und Auswertung der Experimente. Dr. Andreas Delker und PD Dr. Guido Böning danke ich für die physikalische und statistische Beratung.
Weiterhin danke ich Rosel Oos und insbesondere Karin Bormann-Giglmaier für die exzellente methodische und technische Unterstützung und die hervorragende Zusammenarbeit bei der Durchführung der Experimente.
Für das Ermöglichen des Studiums und die stetige Unterstützung gilt mein tiefster Dank meinen Eltern, Herrn Dr. Ulrich Overhoff und Frau Gabriele Apel-Overhoff.
Ganz besonders möchte ich mich bei meiner Frau Viktoria bedanken, ohne Ihre tägliche Unterstützung wäre diese Arbeit nicht möglich gewesen.

LMU LUDWIG-MAXIMILIANS-UNIVERSITÄT MÜNCHEN

Promotionsbüro
Medizinische Fakultät

MMRS MUNICH MEDICAL RESEARCH SCHOOL

Eidesstattliche Versicherung

Overhoff, Felix

Name, Vorname

Ich erkläre hiermit an Eides statt,

dass ich die vorliegende Dissertation mit dem Titel

Etablierung einer standardisierten Analyse longitudinaler Aβ PET Scans zur effektiven Evaluation der BACE-Inhibition im transgenen Alzheimer-Mausmodell

selbständig verfasst, mich außer der angegebenen keiner weiteren Hilfsmittel bedient und alle Erkenntnisse, die aus dem Schrifttum ganz oder annähernd übernommen sind, als solche kenntlich gemacht und nach ihrer Herkunft unter Bezeichnung der Fundstelle einzeln nachgewiesen habe.

Ich erkläre des Weiteren, dass die hier vorgelegte Dissertation nicht in gleicher oder in ähnlicher Form bei einer anderen Stelle zur Erlangung eines akademischen Grades eingereicht wurde.

Bonn, 02.05.2021

Ort, Datum

Felix Overhoff

Unterschrift Doktorandin bzw. Doktorand